Seba Susan

Analysis of EEG Signals in Spatial, Spectral and Temporal Domains for Classification

Delhi Technological University

Document Details

Submission ID

trn:oid:::27535:108049143

Submission Date

Aug 12, 2025, 3:41 PM GMT+5:30

Download Date

Aug 12, 2025, 3:48 PM GMT+5:30

File Name

copy of thesis for plag.pdf

File Size

2.2 MB

123 Pages

30,725 Words

172,660 Characters

10% Overall Similarity

The combined total of all matches, including overlapping sources, for each database.

Filtered from the Report

- Bibliography
- Small Matches (less than 10 words)

Exclusions

- 4 Excluded Sources

Match Groups

163 Not Cited or Quoted 9%
Matches with neither in-text citation nor quotation marks

21 Missing Quotations 1%
Matches that are still very similar to source material

0 Missing Citation 0%
Matches that have quotation marks, but no in-text citation

0 Cited and Quoted 0%
Matches with in-text citation present, but no quotation marks

Top Sources

8% Internet sources
5% Publications
5% Submitted works (Student Papers)

Integrity Flags

1 Integrity Flag for Review

Replaced Characters
41 suspect characters on 19 pages
Letters are swapped with similar characters from another alphabet.

Our system's algorithms look deeply at a document for any inconsistencies that would set it apart from a normal submission. If we notice something strange, we flag it for you to review.

A Flag is not necessarily an indicator of a problem. However, we'd recommend you focus your attention there for further review.

Match Groups

- **163** Not Cited or Quoted 9%
  Matches with neither in-text citation nor quotation marks
- **21** Missing Quotations 1%
  Matches that are still very similar to source material
- **0** Missing Citation 0%
  Matches that have quotation marks, but no in-text citation
- **0** Cited and Quoted 0%
  Matches with in-text citation present, but no quotation marks

Top Sources

8% Internet sources
5% Publications
5% Submitted works (Student Papers)

Top Sources

The sources with the highest number of matches within the submission. Overlapping sources will not be displayed.

1	Internet	
www.researchgate.net		1%
2	Internet	
discovery.researcher.life		<1%
3	Internet	
www.mdpi.com		<1%
4	Internet	
mdpi-res.com		<1%
5	Internet	
ntnuopen.ntnu.no		<1%
6	Internet	
www.frontiersin.org		<1%
7	Submitted works	
Universiti Teknologi Petronas on 2022-03-08		<1%
8	Internet	
digital.library.unt.edu		<1%
9	Publication	
Arti Anuragi, Dilip Singh Sisodia, Ram Bilas Pachori. "Automated Alcoholism Dete...		<1%
10	Internet	
arxiv.org		<1%

11 Submitted works

University of Technology, Sydney on 2024-06-09 <1%

12 Internet

lrcdrs.bennett.edu.in <1%

13 Internet

academic.oup.com <1%

14 Internet

www.science.gov <1%

15 Publication

Virender Kumar Mehla, Amit Singhal, Pushpendra Singh. "An Efficient Classificati... <1%

16 Internet

www.processregister.com <1%

17 Internet

essay.utwente.nl <1%

18 Internet

peerj.com <1%

19 Submitted works

Rose-Hulman Institute of Technology on 2024-07-06 <1%

20 Publication

Garima Chandel, Ashish Sharma, Sonia Bajaj, Saweta Verma. "Computer Based De... <1%

21 Submitted works

University of Essex on 2025-03-21 <1%

22 Internet

www.fundacionineco.org <1%

23 Submitted works

University of Melbourne on 2020-11-08 <1%

24 Publication

Wajid Mumtaz, Pham Lam Vuong, Likun Xia, Aamir Saeed Malik, Rusdi Bin Abd Ra... <1%

25 Internet

ebin.pub <1%

26 Submitted works

Yeshwant Rao Chavan College of Engineering on 2019-05-10 <1%

27 Publication

Arti Anuragi, Dilip Singh Sisodia. "Alcohol use disorder detection using EEG Signal... <1%

28 Submitted works

University of Technology, Sydney on 2017-05-24 <1%

29 Internet

doctorpenguin.com <1%

30 Internet

etd.aau.edu.et <1%

31 Internet

github.com <1%

32 Publication

Behnam Latifi, Ali Amini, Ali Motie Nasrabadi. "Siamese based deep neural netwo... <1%

33 Publication

Sai Kiran Oruganti, Dimitrios A Karras, Srinesh Singh Thakur, Janapati Krishna Ch... <1%

34 Internet

www.medrxiv.org <1%

35 Internet

biomed.bas.bg <1%

36 Publication

Khumukcham Robindro Singh, Nazrul Hoque, Arnab Kumar Maji, Sabyasachi Mon... <1%

37 Submitted works

University of Lincoln on 2021-10-17 <1%

38 Internet

ieee-dataport.org <1%

39 Internet
publish.kne-publishing.com <1%

40 Internet
repositorium.sdum.uminho.pt <1%

41 Internet
www.ijcaonline.org <1%

42 Publication
Juan L. Lopez Marcano, Martha Ann Bell, A. A. Louis Beex. "EEG channel selection ... <1%

43 Submitted works
Queen Mary and Westfield College on 2023-05-10 <1%

44 Publication
Sazzli Kasim, Sorayya Malek, JunJie Tang, Xue Ning Kiew, Song Cheen, Bryan Liew,... <1%

45 Submitted works
University of Nevada Reno on 2018-12-19 <1%

46 Publication
Vikram Shenoy Handiru, A. P. Vinod, Cuntai Guan. "A novel supervised locality sen... <1%

47 Internet
web.archive.org <1%

48 Publication
Danyal Mahmood, Humaira Nisar, Rab Nawaz, Vooi Voon Yap, Chi-Yi Tsai. "Attenti... <1%

49 Internet
academic-accelerator.com <1%

50 Internet
ui.adsabs.harvard.edu <1%

51 Submitted works
Cranfield University on 2013-01-07 <1%

52 Publication
Mesut Şeker, Mehmet Siraç Özerdem. "Dementia rhythms: Unveiling the EEG dyn... <1%

53 Submitted works

University of London External System on 2024-03-24 <1%

54 Submitted works

University of Ulster on 2018-01-22 <1%

55 Internet

research.usq.edu.au <1%

56 Publication

Davidson, Haleigh Brielle. "Neural Signatures of ADHD: A Fast Periodic Visual Sti... <1%

57 Submitted works

Federal University of Technology on 2019-05-02 <1%

58 Submitted works

Jacobs University, Bremen on 2023-05-16 <1%

59 Submitted works

National University of Singapore on 2012-04-05 <1%

60 Publication

Nilima Salankar, Saeed Mian Qaisar, Paweł Pławiak, Ryszard Tadeusiewicz, Moha... <1%

61 Submitted works

The Hong Kong Polytechnic University on 2006-02-14 <1%

62 Submitted works

University of East London on 2021-09-09 <1%

63 Submitted works

Veermata Jijabai Technological Institute on 2023-10-21 <1%

64 Publication

Xiao Lei Zhang, Henri Begleiter, Bernice Porjesz, Ann Litke. "Reflection of working... <1%

65 Publication

Yongkoo Park, Wonzoo Chung. "Optimal Channel Selection Using Correlation Coe... <1%

66 Publication

Zhengqing Miao, Meirong Zhao. "Time–space–frequency feature Fusion for 3-cha... <1%

67 Internet
dspace.mit.edu <1%

68 Internet
fastercapital.com <1%

69 Internet
jjcit.org <1%

70 Submitted works
Erasmus University of Rotterdam on 2025-02-28 <1%

71 Submitted works
Karl Landsteiner Privatuniversität für Gesundheitswissenschaften GmbH on 2023... <1%

72 Publication
Nitesh Singh Malan, Shiru Sharma. "Time window and frequency band optimizati... <1%

73 Publication
Samar Bouazizi, Hela Ltifi. "Enhancing accuracy and interpretability in EEG-based ... <1%

74 Submitted works
Sim University on 2015-05-08 <1%

75 Submitted works
Universiti Teknologi Malaysia on 2019-08-26 <1%

76 Internet
documents.mx <1%

77 Internet
download.bibis.ir <1%

78 Internet
en-materials.tau.ac.il <1%

79 Internet
lib.buet.ac.bd:8080 <1%

80 Internet
ouci.dntb.gov.ua <1%

81 Internet

pubmed.ncbi.nlm.nih.gov <1%

82 Internet

www.collectionscanada.ca <1%

83 Internet

www.standardsmedia.com <1%

84 Publication

"Neural Information Processing", Springer Science and Business Media LLC, 2024 <1%

85 Submitted works

Anna University on 2024-04-25 <1%

86 Publication

Bapat, Kumar Rajmani. "Enhanced EEG Emotion Recognition: A Hybrid Stacked En... <1%

87 Submitted works

CSU, San Jose State University on 2025-04-27 <1%

88 Submitted works

City University on 2008-10-15 <1%

89 Publication

E. Sathiya, T. D. Rao, T. Sunil Kumar. "Gabor filter-based statistical features for AD... <1%

90 Submitted works

Istanbul Bilgi University on 2022-10-05 <1%

91 Publication

Kayhan Latifzadeh, Nima Gozalpour, V. Javier Traver, Tuukka Ruotsalo, Aleksandr... <1%

92 Publication

Lecture Notes in Computer Science, 2013. <1%

93 Publication

Syeda Noor-Ul-Huda Safder, Muhammad Usman Akram, Muhammad Najam Dar, ... <1%

94 Submitted works

Thapar University, Patiala on 2025-02-28 <1%

95 Submitted works

Universiti Teknologi Malaysia on 2025-07-02 <1%

96 Submitted works

University of Malaya on 2023-06-26 <1%

97 Internet

dspace.knust.edu.gh <1%

98 Internet

edoc.site <1%

99 Internet

export.arxiv.org <1%

100 Internet

ia801005.us.archive.org <1%

101 Internet

ijsrset.com <1%

102 Internet

thescholarship.ecu.edu <1%

103 Internet

www.ijraset.com <1%

104 Publication

"Advances in Digital Health and Medical Bioengineering", Springer Science and B... <1%

105 Publication

"Brain Informatics and Health", Springer Science and Business Media LLC, 2016 <1%

106 Publication

"Machine Learning: ECML 2004", Springer Science and Business Media LLC, 2004 <1%

107 Publication

Fengwei Sun, Zhi Kong, Yun Tang, Jihui Yang, Gengdi Huang, Yu Liu, Wentao Jiang... <1%

108 Submitted works

JIS University on 2025-04-30 <1%

109 Submitted works

Juntendo University on 2023-06-20 <1%

110 Publication

Krishna Kant Singh, Akansha Singh, Jenn-Wei Lin, Ahmed A. Elngar. "Deep Learnin... <1%

111 Publication

Kritiprasanna Das, Ram Bilas Pachori. "Electroencephalogram Based Motor Imag... <1%

112 Submitted works

Manipal University on 2023-06-26 <1%

113 Publication

N.P. Guhan Seshadri, Sneha Agrawal, Bikesh Kumar Singh, B. Geethanjali, V. Mah... <1%

114 Submitted works

Sheffield Hallam University on 2024-01-22 <1%

115 Publication

Shuaibin Wang, Jinglong Wu, Deyu Zhang, Dingjie Suo, Tianyi Yan. "An Algorithm ... <1%

116 Submitted works

Turun yliopisto on 2019-10-14 <1%

117 Submitted works

Universiti Kebangsaan Malaysia on 2016-02-01 <1%

118 Submitted works

University of Birmingham on 2016-01-06 <1%

119 Submitted works

University of Hull on 2023-05-03 <1%

120 Publication

Xinzhi Ma, Weihai Chen, Zhongcai Pei, Jingmeng Liu, Bin Huang, Jianer Chen. "A T... <1%

121 Internet

catalog.libraries.psu.edu <1%

122 Internet

digitalcommons.odu.edu <1%

123 Internet

dokumen.pub <1%

124 Internet

lup.lub.lu.se <1%

125 Internet

nozdr.ru <1%

126 Internet

repository.essex.ac.uk <1%

127 Internet

utq.edu.iq <1%

128 Internet

www.iece.org <1%

Chapter 1

Introduction

This chapter presents an overview of the research, outlining the formulated problems and the underlying motivation that guided the study in its chosen direction. The scope of the work is discussed to provide context and establish the foundation for conducting the research. Additionally, the identified research gaps, research objectives, key contributions, and thesis outline are highlighted. Subsequent chapters present detailed experimental procedures and results, along with comprehensive discussions that substantiate the findings.

1.1 Introduction

Electroencephalography (EEG) has long been established as a critical non-invasive technique for monitoring and understanding brain activity. Due to its high temporal resolution and relative ease of use, EEG is extensively applied in clinical diagnosis, cognitive neuroscience, and brain-computer interface systems. Despite its widespread use, accurately interpreting EEG signals remains a significant challenge because of the inherent complexity, variability, non-linear and non-stationary nature of brain electrical activity [57][113][121]. Two methods are used to record the electrical activity of neurons: an invasive method and a non-invasive method. Electrodes are placed inside the scalp of the brain through surgery in an invasive method, and in non-invasive methods, electrodes are placed on the scalp of the brain to record the signals.

The recorded EEG signal can be divided into frequency sub-bands using Fast Fourier Transform (FFT), and each frequency sub-band has different functional characteristics. The most widely used frequency sub-bands and their approximate spectral boundaries are delta (1–3 Hz), theta (4–7 Hz), alpha (8–12 Hz), beta (13–30 Hz), and gamma (30–100 Hz). Typically, delta band is associated with deep sleep, theta band with drowsiness, alpha band with relaxed wakefulness, beta band with alertness, and the gamma band with higher cognitive processing. EEG signals are extensively used to extract features that serve as neurophysiological biomarkers for analyzing brain function. These features play a crucial role in the detection and classification of various brain disorders, such as alcohol use disorder (AUD) and attention-deficit/hyperactivity disorder (ADHD), by capturing abnormal neural activity patterns associated with each condition. To analyze the frequency characteristics of the EEG signal, spectral features such as band frequency, absolute and relative power of sub-bands, spectral entropy, factor dimensions, etc., have been used in [83][84][120]. Temporal features capture the variations in amplitude of the signal, such as the shape of the waveforms or a pattern of transience over time. These have most often been used in time-domain descriptions such as Hjorth parameters, variance, skewness and other higher-order statistics.

Feature selection is a critical step in designing a generalized framework for brain signal classification. It identifies the most relevant features that improves the performance of the classification models. Statistical techniques like t-tests and Analysis of Variance (ANOVA) are used to rank features based on their statistical significance. Similarly, for dimensionality reduction, Principal Component Analysis (PCA) is a well-known technique to reduce the number of variables while retaining most of the information in EEG signals. Ensemble-based Filtering methods, as used in this research, utilize majority voting schemes on different statistical ranking methods, to determine the most discriminative features. Greedy Wrapper algorithms like Sequential Forward Selection (SFS), are used to iteratively build an optimal feature subset. Recent advancements in EEG classification include deep learning frameworks that capture spatial, spectral, and temporal dependencies in neural signals. CNN-based models like EEGNet [133] are valued for their efficiency and flexibility in BCI applications, whereas hybrid models

such as CNN-LSTM improve temporal pattern modeling. Together, these architectures represent a significant shift toward unified and transferable EEG models for a wide range of clinical and cognitive tasks.

1.2 Research Gaps

We conducted a literature survey on EEG signal feature extraction and classification in temporal, spectral, and spatial domains, and have enumerated some research gaps in the current state of the art on EEG signal classification. Though the studies conducted in literature have been extensive, and many valuable achievements have been made, a few research gaps have been identified:

- There is a lack of targeted research on generalizable discriminative Quantitative EEG feature subsets. The generalization capability of existing Quantitative EEG features is less across multiple brain disorders.
- Inter-channel connectivity and other spatial aspects of EEG signals remain underutilized in existing methods for capturing brain activity patterns.
- Existing research often treats statistical, spatial, temporal, and spectral EEG features in isolation, with limited efforts to develop unified frameworks that comprehensively integrate these dimensions.

1.3 Problem Definition

Traditionally, the diagnosis of brain disorders relies on subjective clinical assessments and behavioral observations, which are often prone to inconsistency and misdiagnosis. While EEG provides objective data on brain function, there has been a significant gap in creating a systematic framework to analyze this complex, high-dimensional data. Specifically, the challenge has been to identify a minimal, yet highly discriminative, subset of Quantitative EEG (QEEG) features that not only achieves high classification accuracy for a single disorder but is also proven to be effective and generalizable across multiple distinct neurological conditions. The research done in this thesis aims to solve this problem by providing an end-to-end framework for EEG classification that is generalizable across multiple brain disorders. This research fills

the previously identified research gaps by proposing a comprehensive framework that integrates multi-domain feature extraction with advanced feature selection techniques to create a reliable and generalizable diagnostic tool. The key research objectives addressed in this thesis are summarized below.

1.3.1 Research Objectives

OBJECTIVE 1: Statistical analysis of EEG signals to identify discriminative Quantitative EEG feature subsets that are generalizable across multiple brain disorders.

OBJECTIVE 2: Design a novel framework to measure Functional Connectivity from EEG signals to capture complex brain patterns for improved disorder classification.

OBJECTIVE 3: To determine a subset of relevant features from temporal, spectral, and spatial analysis of EEG signals for improved classification.

1.4 Contributions of the Thesis

This thesis aims to identify a subset of EEG features that can serve as reliable biomarkers for EEG signal classification. Additionally, it proposes a generalized framework pipeline designed for identifying brain dysfunctions. Furthermore, a novel framework is presented for capturing functional connectivity between different brain regions. The research is structured around three primary objectives, as outlined in Section 1.3.1. Each of these objectives is systematically addressed and presented as part of the thesis contributions detailed below.

OBJECTIVE 1: *Statistical analysis of EEG signals to identify discriminative Quantitative EEG feature subsets that are generalizable across multiple brain disorders.*

We present a systematic approach for the statistical analysis of EEG signals,

demonstrating how to identify a highly discriminative subset of Quantitative EEG (QEEG) features that can be used to identify various brain disorders. In this objective, we introduce a unique set of twenty seven QEEG features that are used to classify behavioral and neurological disorders. This methodology is proven to be generalizable, as it is applied successfully across multiple brain disorders, specifically ADHD and AUD.

OBJECTIVE 2: *Design a novel framework to measure Functional Connectivity from EEG signals to capture complex brain patterns for improved disorder classification.*

To address this problem, we propose a novel framework that utilizes QEEG features based on the band-specific absolute values of inter-electrode correlations, serving as a measure of brain functional connectivity for diagnosing AUD and ADHD. Specifically, the Pearson product-moment correlation coefficient is calculated between time-series signals recorded from pairs of EEG electrodes across five frequency sub-bands. To reduce the dimensionality of the concatenated features from these sub-bands, we introduce an ensemble feature selection method that integrates both filter and wrapper techniques.

OBJECTIVE 3: *To determine a subset of relevant features from temporal, spectral, and spatial analysis of EEG signals for improved classification*

This objective proposes a novel diagnostic framework that quantifies behavioral and neurological disorder ability through spectral, power and connectivity QEEG pooled across temporal, spectral and spatial dimensions of an EEG signal evoked by visual stimuli; the generalizability of this approach is proved using a subject-wise data splitting strategy. The spectral features represent the frequency characteristics of the EEG signal, while power features represent the amplitude characteristics. Connectivity refers to the inter-hemispheric brain region connectivity, which is measured using

averaged correlation and coherence statistics computed between all possible channel pairs in the left and right hemispheres. Ensemble-based feature selection is then employed for the selection of optimal features from the concatenated feature list. To further train the model, different machine learning algorithms are utilized to classify the EEG data and achieve good classification accuracy.

1.5 Outline of the Thesis

This thesis is divided into six chapters, as discussed below.

1. **Chapter 1: Introduction**

   This chapter provides an introduction to the thesis, outlining the problem statement, research gaps and the motivation behind our research. We also detail the key contributions and present a roadmap for the rest of the thesis.

2. **Chapter 2: Literature Survey**

   In this chapter, we present an overview of the state-of-the-art methods employed in EEG signal classification. In the first section of this chapter, we discuss the temporal, spatial and spectral domain features, followed by hybrid approaches. Furthermore, we discuss various feature reduction techniques employed in EEG signal classification to reduce the framework's complexity. This is followed by an in-depth analysis of state-of-the-art machine learning algorithms used for EEG signal classification, concluding with a summary of findings.

3. **Chapter 3: Statistical analysis of EEG signals to identify discriminative Quantitative EEG feature subsets that are generalizable across multiple brain disorders.**

   This chapter introduces a set of twenty-seven QEEG features that

form a discriminative subset, demonstrating generalizability across multiple brain disorders. The study emphasizes the value of a comprehensive feature set that includes power, spectral, and functional connectivity measures to effectively capture the diverse neurological patterns associated with conditions such as AUD and ADHD. Each EEG signal is segmented into five frequency bands, from which the twenty-seven QEEG features are extracted for classification. These features are then employed by machine learning techniques—Support Vector Machine (SVM), k-Nearest Neighbors (kNN), Random Forest (RF), and Artificial Neural Network (ANN)—for the diagnosis of ADHD and AUD.

4. **Chapter 4: Design a novel framework to measure Functional Connectivity from EEG signals to capture complex brain patterns for improved disorder classification.**

   In this chapter, the framework's core innovation is its reliance on linear monotonic inter-electrode associations as a primary set of QEEG features. By systematically computing the absolute value of the Pearson product-moment correlation coefficient between pairs of EEG electrodes across multiple frequency sub-bands, we were able to create a highly comprehensive map of brain functional connectivity. This approach captures a detailed picture of how different brain regions interact, providing a rich feature space for subsequent analysis. A critical component of the framework is its robust feature selection methodology. To manage the high dimensionality of the data, an ensemble-based approach was implemented, combining statistical filter methods with a greedy wrapper algorithm. This process was essential for identifying a concise, optimal subset of features with maximum predictive power. The strategic reduction in features not only prevented overfitting but also significantly improved the classification model's

efficiency and accuracy.

5. **Chapter 5: To determine a subset of relevant features from temporal, spectral, and spatial analysis of EEG signals for improved classification**

   This chapter presents a novel framework designed to extract the twenty-seven QEEG features defined in Research Objective 1 from spectrally and spatially filtered EEG signals that have been preprocessed using sub-time segmentation. A filter bank is developed to decompose the 0–100 Hz frequency range into ten sub-bands. Subsequently, a spatial filtering technique is applied to select six spatially filtered channels for feature extraction. To reduce feature dimensionality and retain the most relevant features for classification, we introduce an ensemble-based feature selection approach that combines multiple selection techniques. The proposed framework is evaluated on various datasets associated with different brain disorders to assess its generalizability and effectiveness.

6. **Chapter 6: Conclusion**

   This chapter summarizes the key findings and main contributions of the thesis. Along with that, future research directions are also discussed in this chapter.

Chapter 2

Literature Survey

This chapter provides a comprehensive review of the existing literature on the analysis and classification of electroencephalography (EEG) signals. The primary focus of this survey is to explore the various methods and techniques that have been employed to extract and utilize features from EEG data in the spatial, spectral, and temporal domains. The goal of this review is to establish a foundational understanding of the current state of research, identify key methodologies, and pinpoint existing gaps in the literature that this thesis aims to address. This chapter reviews the literature on EEG signal analysis by focusing on three key domains: spatial, spectral, and temporal. We will examine methods used to capture the topographical distribution of brain activity, such as Common Spatial Pattern (CSP), which helps in separating different brain states. The review will also cover techniques that analyze the signal's frequency components, including Power Spectral Density (PSD) and Wavelet Transforms, to quantify activity within specific brainwave bands. Finally, we will explore state-of-the-art methods for analyzing the EEG signal, statistical measures and models for various brain disorders.

EEG signals represent the electrical activity of the brain recorded from electrodes placed on the scalp using standardized electrode placement systems such as the ten-twenty electrode system [82]. These signals contain valuable information about brain function and can be analyzed using various signal processing techniques to

extract meaningful features for clinical applications [118]. The complexity of EEG signals necessitates sophisticated processing methods to extract relevant information while minimizing noise and artifacts [39, 107]. The field of EEG signal processing has evolved significantly, with researchers developing various approaches to analyze brain signals in different domains [72, 80, 114]. Modern EEG analysis platforms such as EEGLAB [20, 41] and FieldTrip [111] have facilitated advanced signal processing and analysis. This survey reviews the literature by processing domain and methodology, offering insights into current research trends.

2.1 Literature Survey on Domain-Specific EEG Features: Temporal, Spectral, and Spatial

2.1.1 Temporal Domain Features

The temporal domain focuses on extracting features directly from the raw time series EEG signal. This approach has been a key research area for various brain disorders, such as AUD and ADHD classification. Statistical features extracted from the time domain have proven effective for various neurological and psychiatric applications. Multiple studies have demonstrated the effectiveness of time-domain statistical features for diagnosis of alcoholic EEG signals [16-17,117,131]. These studies utilized features such as mean, standard deviation, skewness, and kurtosis to characterize the temporal properties of EEG signals. The attention continuity measure has been identified as a significant nonlinear feature for detecting ADHD in children in [8]. This temporal feature captures the sustained attention capabilities by analyzing the continuity of attention-related patterns in EEG signals over time. Several other studies have also explored similar temporal domain features for detecting ADHD. [21, 47, 93,122].

Nonlinear analysis techniques have gained prominence in temporal domain EEG processing [57,116,121]. These methods capture the complex, nonlinear dynamics of brain activity that may not be apparent through conventional linear analysis. The application of nonlinear features has shown promise in various clinical applications, including ADHD diagnosis and alcoholism detection [2, 9, 10]. Recurrence plot

analysis and other nonlinear methods have been applied to understand the complex temporal dynamics of brain signals [102]. These approaches provide insights into the deterministic and stochastic components of EEG signals.

Several studies have examined temporal dynamics in various neuropsychiatric conditions. For autism spectrum disorder, temporal features have been examined in multiple studies [18, 36, 37, 48]. The temporal variability of brain connections has been studied in ADHD and bipolar disorder in [12], revealing distinct patterns in these conditions. For epilepsy detection, temporal domain features have been widely utilized [23, 79]. Temporal domain analysis encounters several challenges, such as sensitivity to artifacts [94, 107], susceptibility to noise, and the requirement for careful preprocessing [39]. The interpretation of temporal features can be complex, particularly when dealing with multi-channel EEG recordings where temporal relationships between different brain regions must be considered.

2.1.2 Spectral Domain Features

Spectral analysis examines the frequency components of EEG signals, which is vital for understanding rhythmic brain activity. Spectral domain analysis examines the frequency content of EEG signals, typically focusing on specific frequency bands associated with different brain states and pathological conditions. The traditional EEG frequency bands include delta (0.5-4 Hz), theta (4-8 Hz), alpha (8-13 Hz), beta (13-30 Hz), and gamma (>30 Hz) [118]. Multiple studies have utilized frequency band analysis for various applications [30-35] [58, 97, 98]. The theta/beta ratio has been extensively studied as a biomarker for ADHD diagnosis. Arns et al. [11] conducted a comprehensive meta-analysis of a decade of EEG theta/beta ratio research in ADHD, establishing the clinical significance of this spectral measure. The elevated theta/beta ratio in ADHD patients reflects the imbalance between slow-wave (theta) and fast-wave (beta) activities in the brain. The absolute and relative power of an EEG signal have been used as features for AUD diagnosis, with t-tests and Principal Component Analysis (PCA) used for feature selection [83]. Power spectral density (PSD) analysis quantifies the distribution of signal power across different frequency components. This

technique has been widely used in neuropsychiatric applications [50,60, 95]. Frequency domain features were also introduced utilized in [49] for ADHD classification. Studies have shown that PSD features can effectively characterize different brain states and pathological conditions. Spectral features have been used for early detection of Alzheimer's disease [68, 74, 99, 103-105], with studies showing characteristic changes in spectral power distributions. Spectral analysis has been used for sleep stage classification in [27, 45, 130] and drowsiness detection in [40, 46]. Multiple studies have utilized spectral features for emotion recognition from EEG [95, 124]. Spectral coherence analysis examines the functional connectivity between different brain regions by measuring the correlation between frequency components of EEG signals from different electrodes. Tcheslavski and Gonen [119] investigated alcoholism-related alterations in the spectrum, coherence, and phase synchrony of the topographical electroencephalogram, revealing significant changes in spectral connectivity patterns. Similar approaches have been used in other studies examining brain connectivity [5, 12, 125].

Anuragi et al. [9] utilized Fourier-Bessel series expansion based empirical wavelet transform for automated alcoholism detection. The continuous wavelet transform has been applied for alcoholism diagnosis [123], and flexible analytical wavelet transform has shown promise in alcohol use disorder detection [10]. Wavelet-based approaches have been extensively used for seizure detection [53, 63, 87, 88]. These studies have demonstrated the effectiveness of wavelet transforms in capturing the time-frequency characteristics of epileptic seizures. Wavelet techniques have been applied to ADHD detection and analysis [84], providing better time-frequency resolution compared to traditional Fourier-based methods.

Spectral analysis of each band and approximation entropy (ApEn) were utilized in [113] to analyze the EEG signal of adolescents with ADHD, with results showing significantly lower ApEn in ADHD patients over the right frontal regions. Spectral entropy was utilized in [108] to find the abnormal patterns in the EEG signal for brain disorder classification.

2.1.3 Spatial Domain Features

Spatial domain analysis examines the distribution of brain activity across different scalp locations. The spatial domain focuses on the relationships and interactions between different EEG channels, effectively treating the brain as a network. This domain is valuable for analyzing how activity is distributed and connected across the brain. Brain topographical mapping provides insights into the spatial patterns of neural activity and can reveal region-specific abnormalities in neurological and psychiatric conditions [50, 132]. The Common Spatial Pattern (CSP) algorithm is a widely used spatial filtering technique that identifies the most discriminative EEG channels by maximizing the variance of EEG signals from one class while minimizing the variance from another class. TaghiBeyglou et al. [116] applied CSP along with nonlinear analysis of filter-banked EEG for ADHD diagnosis in children. CSP has also been applied in brain-computer interface applications [90, 112, 128] and motor imagery classification [100, 128].

Spatial domain analysis extends to brain network connectivity studies. Aydın et al. [5] compared domain-specific connectivity metrics for estimating brain network indices in boys with ADHD. The authors explored correlation, phase, and coherence measures for brain region connectivity analysis in boys undergoing treatment for ADHD. While ANOVA was used for feature selection, the classification was achieved using logistic regression. Barttfeld et al. [12] examined functional connectivity and temporal variability of brain connections in adults with ADHD and bipolar disorder, revealing distinct spatial connectivity patterns. Brain connectivity has been studied in autism spectrum disorder [62, 106], showing altered connectivity patterns compared to typical development. Wang et al. [125] investigated disrupted brain network efficiency and decreased functional connectivity in multi-sensory modality regions in male patients with AUD.

Optimal channel selection is crucial for effective spatial domain analysis. Bavkar et al. [13, 14] developed approaches for rapid screening of alcoholism using optimal

channel selection, demonstrating that careful selection of EEG channels can significantly improve classification performance while reducing computational complexity. Other studies have addressed channel selection for various applications [93, 94], showing the importance of spatial optimization in EEG analysis. Bavkar et al. [14] further utilized EMD domain statistical features combined with harmony search algorithm for optimal EEG channel selection in alcoholism screening. Kumar et al. [84] applied empirical mode decomposition for ADHD identification.

Brain symmetry indices provide valuable spatial information about hemispheric differences in brain activity. Van Putten [132] introduced the revised brain symmetry index, which has applications in various neurological conditions where hemispheric asymmetry is a characteristic feature. Spatial features have been used for Parkinson's disease detection [19, 22, 83], showing characteristic spatial patterns associated with the condition. Spatial analysis has been applied to cognitive workload assessment [25, 92], revealing spatial patterns associated with different levels of mental effort.

2.1.4 Hybrid Approaches

Hybrid approaches combine features from multiple domains (e.g., temporal, spectral, and spatial) to create more robust and accurate classification models. Hybrid domain analysis combines features from multiple domains to provide a more comprehensive characterization of EEG signals. This approach leverages the complementary information available in different domains to improve classification accuracy and robustness. Time-frequency analysis techniques, for instance, provide simultaneous temporal and spectral information. These methods are particularly valuable for analyzing non-stationary EEG signals where frequency content varies over time.

Multi-domain approaches combining temporal, spectral, and spatial analysis provide superior performance compared to single-domain methods, as proved in the past studies [9, 10, 14, 116, 121]. Wang et al. [124] developed a spatial-temporal feature fusion neural network for EEG-based emotion recognition, demonstrating the effectiveness of combining spatial and temporal information in a unified framework.

Similar approaches have been used in other applications as well [26, 54, 91, 100]. Hybrid approaches often incorporate multimodal information, combining EEG with other neuroimaging modalities or physiological signals. This integration provides a more comprehensive understanding of brain function and can improve diagnostic accuracy [51,69]. Multiple studies have used hybrid approaches for BCI Brain-Computer Interface applications [70, 71, 81, 112, 128], combining different signal processing techniques for improved performance. Hybrid methods have also been extensively used for epilepsy detection [38, 44, 79], combining multiple feature types for robust seizure identification.

2.2 Feature Selection for Advanced EEG Analysis

Feature selection methods aim to identify a compact subset of features that reduces redundancy while enhancing relevance to the target variable. These techniques typically rely on filter-based and wrapper-based approaches. Statistical filter-based methods for feature selection examine the relevance and redundancy of features based on statistical measures. These methods are computationally efficient and provide insights into the discriminative power of individual features [52, 93]. Wrapper-based methods evaluate feature subsets by training and testing machine learning models. While computationally intensive, these methods often provide superior feature subsets tailored to specific classification algorithms [52, 93].

Embedded methods incorporate feature selection within the model training process. These approaches are particularly relevant for neural networks and other complex models where feature importance can be learned during training [70, 71, 100]. Various other techniques have also been explored such as Independent Component Analysis [41, 94], manifold learning [56], and sparse representation [90] for dimension reduction in EEG. Multiple studies have addressed feature selection for alcoholism detection [13, 14], demonstrating the effectiveness of optimal feature selection in improving classification performance. Feature selection has been applied to epilepsy detection [63, 65, 79, 85, 87, 88, 89], helping to identify the most discriminative features for seizure classification. Agrawal et al. [4] conducted a

comprehensive survey of metaheuristic algorithms for feature selection, covering one decade of research (2009-2019). These algorithms, including genetic algorithms, particle swarm optimization, and harmony search, have been successfully applied to EEG feature selection problems. The harmony search algorithm has been specifically applied to EEG channel selection for alcoholism screening [14], demonstrating the effectiveness of metaheuristic approaches in optimizing feature subsets.

2.3 Classification Techniques for EEG Feature-Based Analysis

As machine learning models become more complex, ensuring interpretability of results becomes increasingly important [96], particularly in clinical applications where understanding the decision-making process is crucial. Support Vector Machines have been widely used for EEG classification due to their effectiveness in high-dimensional spaces and ability to handle non-linear relationships through kernel functions. SVM approaches have been applied to ADHD and alcoholism detection [6][93][109], demonstrating effectiveness in identifying ADHD patterns. SVM has been extensively used for seizure detection [85, 89], providing robust classification performance. SVM has been applied to various other conditions, including autism [42, 43, 67], Parkinson's disease [19, 22], and emotion recognition [75, 78]. k-NN has been used in various EEG classification tasks [50, 64, 65], providing simple but effective classification. Tree-based methods have been applied in multiple studies [15, 19, 22], offering interpretable classification models. Bayesian approaches have been used in some EEG classification studies [64, 65], providing probabilistic classification outputs. Ensemble methods combine multiple classifiers to improve overall performance. Susan et al. [115] evaluated heterogeneous ensembles with boosting meta-learner, demonstrating the potential of ensemble approaches in EEG classification tasks. Other ensemble approaches have been used in various studies [28, 88, 115]. Acharya et al. [3] developed a deep CNN for automated detection and diagnosis of seizure using EEG signals, achieving high accuracy in seizure detection tasks. Other CNN-based seizure detection studies include [25,28,79, 86]. CNN approaches have been applied to ADHD detection [47, 59], showing promise in automated ADHD diagnosis. CNNs have been

used in various other applications [29, 77, 100, 101], demonstrating their versatility in EEG signal processing. LSTM networks have been used for emotion recognition [54, 91], effectively capturing temporal patterns in emotional states. RNN variants have been applied to various EEG classification tasks [28, 54, 91], showing effectiveness in handling sequential data. EEGNet, a pre-train model was used in [133] to diagnosis the ADHD in children. Hybrid architectures combining CNNs and LSTMs have been used in multiple studies [28, 54, 91], leveraging both spatial and temporal feature learning capabilities. Some studies have incorporated attention mechanisms to focus on relevant parts of the EEG signal [124], improving classification performance. Multiple studies have developed specialized BCI classification systems [70, 71, 81, 90, 112, 128], incorporating domain-specific knowledge and requirements. Real-time classification has been addressed in several studies [40, 46, 51, 70, 71, 127], focusing on low-latency processing for practical applications. Multi-class classification approaches have been developed for various applications [79, 81], handling multiple categories of brain states or conditions.

Belete and Huchaiah [15] investigated grid search in hyperparameter optimization of machine learning models, providing insights into systematic approaches for optimizing classifier performance. Similar optimization approaches have been used in other studies [15, 52]. Proper validation strategies are crucial for reliable performance estimation in EEG classification tasks. The choice of cross-validation method can significantly impact the reliability of reported results, as addressed in multiple studies [15, 52, 64, 65]. The lack of standardized protocols for EEG data collection, preprocessing, and analysis makes it difficult to compare results across different studies and laboratories [82, 118]. Establishing standardized procedures would facilitate better comparison and validation of results. High-quality, labeled EEG datasets are essential for developing robust classification systems. Several studies have contributed datasets [103, 108, 120], but more comprehensive and diverse datasets are needed. Translating research findings into clinical practice remains challenging. Studies need to demonstrate not only technical accuracy but also clinical utility and practical implementation feasibility [1, 69, 96].

Chapter 3

Statistical analysis of EEG signals to identify discriminative Quantitative EEG feature subsets that are generalizable across multiple brain disorders

This chapter presents the statistical techniques to identify reliable and broadly applicable quantitative EEG (QEEG) features that can help distinguish between different brain disorders. Instead of limiting the analysis to a single domain, we identify subsets of QEEG features spanning the spectral, spatial, and temporal domains, to identify features that work across multiple neurological issues. This could lead to more accurate diagnoses and make clinical processes more efficient. Unlike traditional methods targeting a single disorder, this broader approach is designed to improve how practical and adaptable these diagnostic tools are in real-world healthcare.

Brain disorders are inherently complex, and understanding them requires a careful and statistically sound approach to interpreting high-dimensional EEG data. Since raw EEG signals are often noisy and filled with information that may not directly relate to the diagnostic objective, extracting and selecting the right features becomes essential. This chapter presents a systematic process of deriving a rich set of QEEG features that can help to effectively diagnose multiple brain disorders, specifically AUD and

ADHD. These include spectral power across standard frequency bands (delta, theta, alpha, beta, gamma), coherence measures that capture functional connectivity between brain regions, and a variety of temporal and spatial characteristics—all aimed at building a diagnostic framework that is both robust and generalizable. EEG signals are analyzed to extract power, spectral, and functional connectivity features across five frequency bands, which are used for the diagnosis of brain disorders. Four feature selection methods: ANOVA, Chi-square, Gini Index and Information Gain ratio are used to rank the QEEG features based on their relative importance to the classification task. A majority voting scheme is used to select the most prominent features for classification. We conducted experiments on benchmark AUD and ADHD datasets to demonstrate that our proposed framework outperforms state-of-the-art approaches in terms of classification performance.

3.1 Proposed QEEG Feature Set and Extraction Framework

The proposed framework for QEEG feature extraction is depicted in Figure 3.1. In the first step, the EEG is decomposed into delta (0.5-4 Hz), theta (4-7 Hz), alpha (7-13 Hz), beta (13-30 Hz) and gamma (30-100 Hz) frequency bands using a filter bank. Each sub-band is subsequently employed to extract power [63], spectral [123], and connectivity [106][120] features, as outlined in Table 3.1. A majority voting feature selection technique reduces the input vector dimension for classification. The proposed majority voting scheme uses the ensemble feature ranking method to select the most important features for classification. We used ANOVA, Chi-square test, Information Gain Ratio and Gini index (GI), four ranking strategies to give a rank to all the features and the top-*k* most significant features are selected for the classification task. The selected features are classified by Support Vector Machine (SVM), k-Nearest Neighbour (kNN), Random Forest (RF) and Artificial Neural Network (ANN) classifiers.

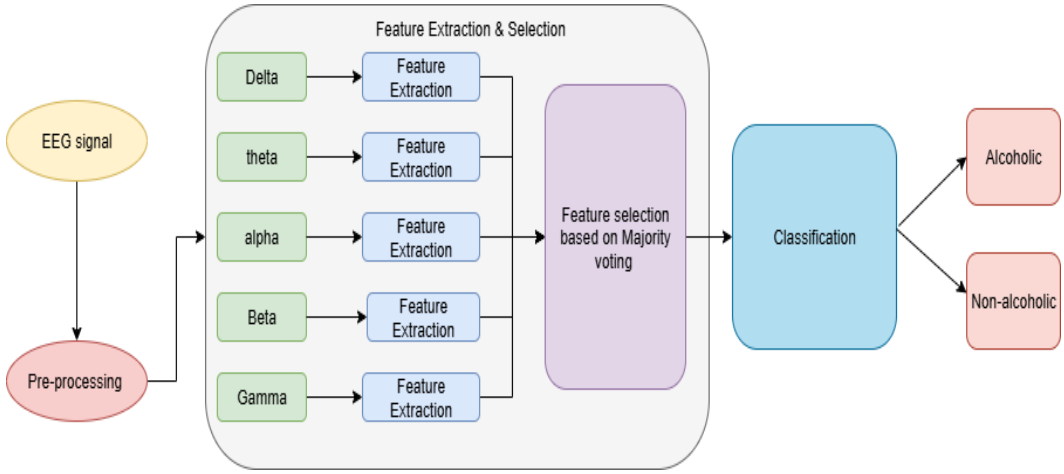

Figure 3.1: Proposed Framework for QEEG Feature Extraction.

Table 3.1: Details of the proposed QEEG feature set introduced in this study. [Notations: x denotes the EEG signal in time-domain, e denotes the signal envelope, w denotes the time window, SD denoted standard deviation, p denotes probability, n denotes the number of samples, X denotes the EEG signal in frequency-domain, DFT denotes Discrete Fourier Transform, K denotes the number of frequency bins, PSD is Power Spectral Density, the presence of a bar indicates the mean], along with citations of usage in previous works. For the formulae, we have adopted the variables used in the NEURAL toolbox [9]]

S.No	QEEG feature	Formula	Description
F1 (Power)	ATP (Amplitude Total power)	AP= $\frac{1}{N}\sum_{i=1}^{n} abs(X_i)^2$	Amplitude power in the time domain: average power of EEG signal over time, which reflects the overall strength of neural activity
F2 (Power)	ASD	ASD= $\sqrt{\frac{\sum_{i=1}^{n}(x_i-\bar{X})^2}{n-1}}$	Standard deviation in the

	(Amplitude Standard Deviation)		time domain: captures both fast and slow variability of EEG signal amplitude over time
F3 (Power)	ASKW (Amplitude Skewness)	ASKW= $\frac{\sum_{i=1}^{n}(x_i - \bar{X})^3}{(N-1) \times SD^3}$	Skewness in the time domain: asymmetry in the distribution of EEG signal's amplitude over time
F4 (Power)	AKR (Amplitude Kurtosis)	AKR= $\frac{\sum_{i=1}^{n}(x_i - \bar{X})^4}{(N-1) \times SD^4}$	Kurtosis in the time domain: extremity of deviations in the EEG signal, such as spikes or bursts
F5 (Power)	AEM (Amplitude Envelop Mean)	AEM=$\sum_{i=1}^{n} \frac{e_i}{n}$	Mean of signal envelope: average amplitude of the EEG signal envelope over time, which captures dynamic fluctuations in signal strength

			over time
F6 (Power)	AESD (Amplitude Envelop SD)	AESD= $\sqrt{\frac{\sum_{i=1}^{n}(e_i - \bar{e})^2}{n-1}}$	Standard deviation of signal envelope: captures only slow modulation changes over time
F7 (Power)	REM (rEEG Mean)	$REM_i = \sum_{\forall l} r_i[l]/L$ where, r(l) denotes the peak-to-peak signal voltage in a short-time windowed segment controlled by parameter l; l is the number of window segments	Mean value of peak-to peak signal voltage: mean of difference between the maximum peak and minimum trough across different time windows
F8 (Power)	REMD (rEEG Median)	REMD = Median (r[l])	Median value of peak-to peak signal voltage: mean of difference between the maximum peak and minimum trough across different time windows

F9 (Power)	RESD (rEEG SD)	RESD= $\sqrt{\frac{\sum_{i=1}^{n}(r-\bar{r})^2}{n-1}}$	Standard deviation of peak-to peak signal voltage: SD of difference between the maximum peak and minimum trough across different time windows
F10 (Power)	RELM (rEEG Lower margin)	R_{lower}= percentile (x, 0.05)	Lower margin (5th percentile) of peak-to-peak signal voltage: value below which 5% of all peak-to-peak voltage readings fall
F11 (Power)	REUM (rEEG upper margin)	R_{upper}= percentile (0.95, x)	Upper margin (95th percentile) of peak-to peak signal voltage: value above which only 5% of all peak-to peak voltage readings fall
F12 (Power)	REW (rEEG width)	R_{width}=$R_{upper} - R_{lower}$	Upper margin – lower margin:

			inter-percentile range of peak-to-peak voltage excluding outliers
F13 (Power)	RCOV (rEEG Coefficient of variance)	$RCOV = \frac{RESD}{REM}$	Coefficient of Variation: ratio of SD to mean of peak-to-peak voltage
F14 (Power)	REASY (rEEG Asymmetry	$R_{Asym} = \frac{R_{upper} - R_{median}) - (R_{mediam} - R_{lower})}{R_{upper} - R_{lower}}$	Asymmetry about the median: symmetry of distribution around the median
F15 (Spectral Distributio n)	SPAP (Spectral absolute power)	$AP_i = \sum_{\forall k} \lvert X_k \rvert^2 / K$	Absolute power in the spectral domain: Total power in specific EEG frequency bands
F16 (Spectral Distributio n)	SPRP (Spectral relative power	$RP = AP / AP_{Total}$	Relative power in the spectral domain: Ratio of power in specific EEG frequency bands to the total power across all bands

F17 (Spectral Distribution)	SPF (Spectral Flatness-Winner Entropy)	SPF=$\frac{exp(\sum_{\forall x} \log PSD[K]/K)}{\sum_{\forall x} \log PSD\ [k]/k}$	Spectral flatness: ratio of geometric mean of power spectral density to its arithmetic mean
F18 (Spectral Distribution)	SPD (Spectral Difference)	SPD=$\sum_{\forall x} \lvert PSD_n^k - PSD_{n+1}^k \rvert$	Spectral difference: difference between power spectral densities over time
F19 (Spectral Distribution)	SPE (Spectral Entropy-Shannon entropy)	SPE=$-\frac{\sum_{\forall k} \overline{PSD}[k] \log \overline{PSD}[k]}{log\ k}$ where, $\overline{PSD}$ is the normalized power spectral density equal to PSD divided by total PSD across frequencies	Spectral entropy: disorder of power distribution across frequencies
F20 (Spectral Distribution)	SPEF (Spectral Edge Frequency)	SPEF= $\underset{\forall f}{\text{argmin}}(SPRP(f) - SPRP(0.5) \geq 0.95)$	Spectral edge frequency: frequency below which 95% of total spectral power lies
F21 (Spectral Distribution)	FD (Fractal dimension)	$FD = log(n)/\left[log\left(\frac{dm}{L}\right) + \log(n)\right]$ where, L is the length of the signal and dm is the diameter	Katz fractal dimension: roughness or complexity of the time series
F22 (Spectral	PEEN (Permutation	PEEN= $-\sum_{j=1}^{m!} p(j) log\ p(j)$	Permutation entropy:

Distribution)	Entropy)	where, j denotes each permutation and m is the length of the ordinal samples in the range of 3 to 7	irregularity of the time series
F23 (connectivity)	BSI (Brain symmetry index	BSI=$\frac{1}{F}\sum_{k=f1}^{f2}\left\lvert\frac{PSD_{left}(K)-PSD_{right}(k)}{PSD_{left}(K)+PSD_{right}(k)}\right\rvert$ *PSD is power spectral density (averaged over channels in the left and right hemispheres); F is the frequency range equal to f2−f1	Measures symmetry between left and right hemispheres
F24 (connectivity)	CORR (Correlation)	CORR= $\underbrace{Median}_{\forall\, channel\ pairs}\ [Correlation(c_1, c_{2)}]$ *correlation is pearson correlation; (c_1,c_2) is a channel pair	Median of correlation of signal envelope between all possible channel pairs
F25 (connectivity)	COHM (Mean coherence)	COHM= $\underbrace{median}_{\forall(c_1,c_2)}\frac{1}{F}\sum_{k=f_1}^{2}\frac{\lvert PSD_{(C1,C2)}(k)\rvert^2}{PSD_{(C1,C1)}(k)\times PSD_{(C2,C2)}(k)}$ *PSD is power spectral density; F is the frequency range equal to f2−f1; (c_1,c_2) is a channel pair	Median of mean coherence over all possible channel pairs
F26 (connectivity)	COHMX (Connectivity coherence max)	COHMX= $\underbrace{median}_{\forall(c_1,c_2)}\left[\underbrace{max}_{\forall k}\left(\frac{\lvert PSD_{(C1,C2)}(k)\rvert^2}{PSD_{(C1,C1)}(k)\times PSD_{(C2,C2)}(k)}\right)_{\forall k}\right]$ *PSD is power spectral density; (c_1,c_2) is a channel pair.	Median of maximum coherence over all possible channel pairs
F27 (connectivity)	COHFMX (Frequency of maximum coherence)	COHFMX= $\underbrace{median}_{\forall(c_1,c_2)}\left[\underbrace{argmax}_{\forall k}\left(\frac{\lvert PSD_{(C1,C2)}(k)\rvert^2}{PSD_{(C1,C1)}(k)\times PSD_{(C2,C2)}(k)}\right)_{\forall k}\right]$ *PSD is power spectral density; (c_1,c_2) is a channel pair.	Median of the frequency of maximum coherence over all possible channel pairs

3.2 Quantitative EEG Feature Selection by Majority Voting for Alcohol Use Disorder Detection

This section describes the identified QEEG features and explores their diagnostic value in the context of Alcohol Use Disorder (AUD). We extract power, spectral, and connectivity features listed in Table 3.1, 8640 in all, from the five frequency bands across 64 EEG channels. To reduce the complexity of the classification model, the top-3000 significant features are identified using a majority vote amongst different feature selection and ranking methods: - ANOVA, chi-square test, Gini Index and Information gain ratio. Experiments on a benchmark AUD dataset prove that our method performs better than the state of the art. Among all classifiers, the highest accuracy is 98.65%, which was obtained using the ANN classifier for the proposed method.

3.2.1 Pre-Processing

QEEG feature extraction involves the application of mathematical programs to transform the raw EEG into frequency bands [120]. First, a low-pass filter at a cut-off of 30 Hz is used, and then the EEG signal is down-sampled at 128 Hz. The resultant EEG is divided into delta (0.5-4 Hz), theta (4-7 Hz), alpha (7- 13Hz), beta (13-30Hz) and gamma (30-100 Hz) frequency bands. Before extracting the features, all the electrodes were arranged in a common reference montage (CAR) and bipolar montage.

3.2.2 Feature Extraction

For further analysis, the twenty seven features listed in Table 3.1 are extracted from five frequency sub-bands across the 64 electrodes. Fourteen power features are extracted as listed from F1 to F14 in Table 3.1. Eight spectral features from F15 to F22 are derived from the spectral domain. The EEG signal is converted into the frequency domain using the Fast Fourier transformation, for frequencies ranging from 0.5 to 100 Hz at a resolution of 0.5 Hz. Five connectivity features from F23 to F27 are extracted

from each frequency band for every channel. A total of 8640 features are extracted in this manner from the five frequency bands pertaining to the 64 EEG channels.

3.2.3 Feature Selection

For finding the most important QEEG features that aid in AUD diagnosis, an ensemble of feature ranking methods is used. The following feature ranking techniques constitute our proposed ensemble:

- ANOVA: Analysis of variance (ANOVA) is a statistical model that determines the statistical difference between the independent groups.
- Chi-square test: The chi-square test finds the relationship among categorical data. It is a statistical hypothesis test that estimates the features that are dependent on each other.
- Information Gain Ratio: Information gain ratio is the reduction in uncertainty. It is the ratio of information gain and the attribute's intrinsic information.
- Gini index (GI): Gini index is a feature selection method that measures the inequality or discrimination level of the features within a class.

3.2.4 Classification

In our experiments, we have used four different classifiers to distinguish alcoholic and non-alcoholic EEG data. The four classifiers are Support Vector Machines (SVM), k-Nearest Neighbor (KNN), Random Forest (RF), and Artificial Neural Network (ANN). SVM classifies the data based on the margin maximization concept. KNN is a non-parametric classification algorithm that uses similarity measures to classify new cases among already stored available instances. RF is a non-linear ensemble classifier that contains N number of decision trees. Each decision tree has a different set of hyper-parameters on a sub-sample of a dataset. ANN is a complex adaptive classification system that can change its internal structure based on adjusting the weight of a connection. For the experiments and result analysis, we used MATLAB R2019a version.

3.2.5 Dataset

EEG data of alcoholic and non-alcoholic subjects were obtained from the University of California (UCI)[1]. The EEG data is extracted from 64 electrodes, which are placed on the scalps of the subjects. The electrode position on the subject's scalp was located using the American Electroencephalographic Association standard. EEG signals of 120 subjects were recorded when they were shown 90 images of various objects. Each subject completed 120 trials for various stimuli. The signals have a resolution of 12 bits, and the EEG signals are measured at a frequency rate of 256 Hz for 32 seconds. After removing trails that had unwanted eyes and noise artifacts, the EEG recordings of each class were obtained. In this study, we used the "large dataset" version in the database, which contains separate training and testing data sets. This version contains 300 samples belonging to 10 alcoholic individuals and 300 samples belonging to 10 control individuals in the training set, and likewise in the testing set. Two independent cohorts–validation (V) and cross-validation (CV) are used in the study, to test the generalization ability of the proposed approach. The validation cohort corresponds to the training set (600 samples), and the cross-validation cohort corresponds to the testing set (600 samples). Figure 3.2 (a) shows a single electrode signal of an alcoholic subject, and 3.2(b) shows a single electrode signal of a control subject.

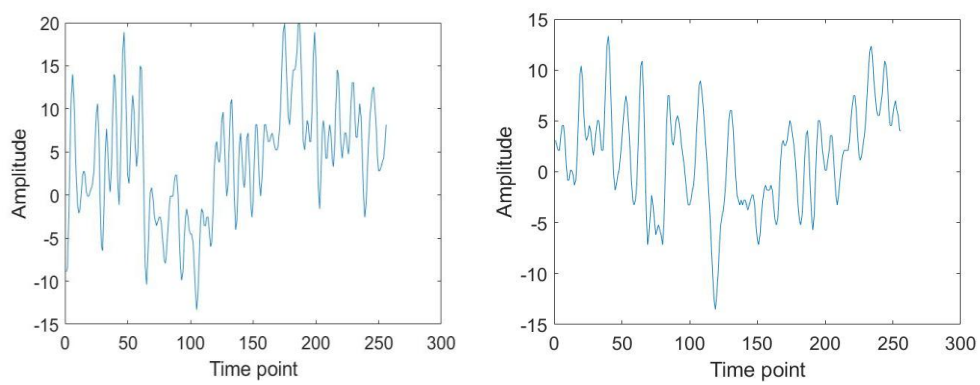

(a) (b)

Figure 3.2: EEG signals (a) Control signal (b) Alcoholic Signal

3.2.6 Results and analysis

This section describes the main findings of our work. Extensive experiments are carried out to evaluate the proposed QEEG features for the classification of alcoholic and non-alcoholic EEG signals. In our analysis, the feature vector contains 8640 features that were derived from five frequency bands pertaining to the 64 EEG channels and ranked individually by different feature selection and ranking methods such as ANOVA, information gain ratio, Chi-square and Gini index feature selection methods. Each feature selection method assigns a score to each feature according to its criteria. Majority voting is now performed among the four feature ranking methods. After that, we select the top 50, 500, 1000, 1500, 2000, 2500, 2867, 3000, 3500, 4000 and 4500 features selected by majority voting technique for classification. We find that before and after 3000 features, there is no noticeable change in accuracy scores. So the top-3000 highly ranked features are selected for the classification. We compare our results with those of [18][63][83],[90] and [120], which are state-of-the-art methods for QEEG classification. Table 3.2 summarizes the classification performance using all four classifiers (KNN, SVM, RF, and ANN) for all methods. The proposed method gives the maximum accuracy of 98.65% (CV) using ANN classifier. The other classifiers like kNN, SVM, RF achieve accuracy of 96.10%, 95.43%, and 93.56% (CV) respectively.

Table 3.2 Performance of various methods for alcoholism diagnosis shown for validation (V) on the test data and cross-validation (CV) on the train data.

Author name & Year	Classifier	Accuracy (V)	Accuracy (CV)	Feature extraction	Feature selection	No. of EEG channels
Mumtaz et al. (2016) [83]	kNN	75.74%	74.64%	Absolute power, Relative power	t-test and principal component analysis	64
	SVM	84.32%	85.15%			
	RF	79.37%	78.77%			
	ANN	86.47%	84.20%			
Toole et al. (2017) [120]	kNN	96.20%	94.90%	Amplitude, rEEG, connectivity, burst and inter-burst intervals, and spectral QEEG	-	64
	SVM	96.53%	95.33%			
	RF	93.40%	93.05%			
	ANN	94.88%	92.88%			

Park et al. (2017) [90]	Ensemble classifier	71.61%	71.26%	CSP	Mutual information-based feature selection	6
Bhatti et al. (2019) [18]	Radial basis function neural networks	75.48%	75.90%	CSP	Sequential backward floating selection	6
Huang et al. (2020) [63]	kNN	71.95%	72.50%	QEEG + All sub-bands	-	64
	SVM	80.69%	80.10%			
	RF	77.56%	76.46%			
	ANN	83.66%	82.60%			
Proposed Method	kNN	95.12%	96.10%	QEEG + All sub-bands	Majority-voting	64
	SVM	94.90%	95.43%			
	RF	92.80%	93.56%			
	ANN	98.28%	98.65%			

We find that, among the top-3000 features, the maximum number of features are selected from the theta frequency band. Figure 3.3 plots the number of selected features associated with the 64 electrodes for the top-3000 selected features. We observe from Figure 3.4 that the maximum selected features are associated with the FP1, FP2, AF1 and AF2 electrodes, proving that the left and right frontal lobes are the brain regions that are affected the most in AUD, as illustrated in Figure 3.4. Our result demonstrates that the frontal lobe is the most vulnerable brain region in an alcoholic subject.

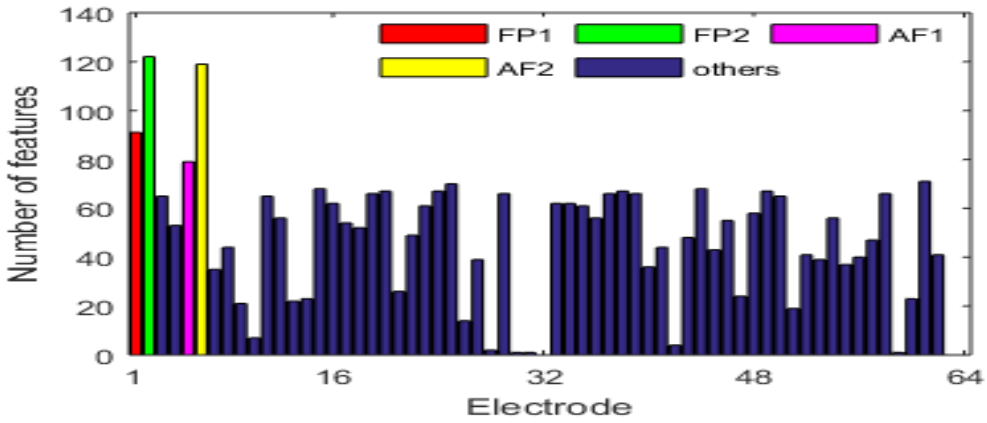

Figure 3. 3 Selected features from different electrodes

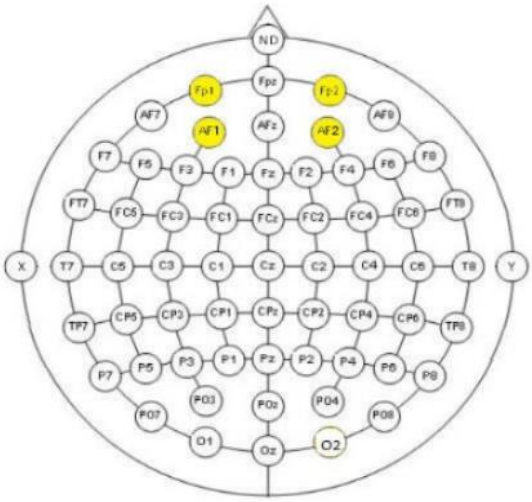

Figure 3.4 The four electrodes associated with the maximum number of selected features (FP1, FP2, AF1, and AF2) are shown highlighted in yellow.

3.3 Computer-Added Diagnosis Framework for ADHD Detection using Quantitative EEG

This section describes the identified QEEG features and explores their diagnostic value in the context of Attention Deficit Hyperactivity Disorder (ADHD). A 19-channel EEG signal from a benchmark ADHD dataset[2] is used to extract the power, spectral and functional connectivity features from five frequency bands to diagnose ADHD in children.

3.3.1 Pre-Processing

The EEG signal is upsampled at 256 Hz sampling frequency in the preprocessing stage. Then the signal is filtered using a bandpass filter to generate five frequency bands corresponding to delta (δ: 0–3 Hz), theta (θ: 4–7 Hz), alpha (α: 8–12 Hz), beta (β: 13–30 Hz), and gamma (γ: 30–100 Hz) [101]. The time series was segmented into 1-second segments for each subject, and the number of segments is varied because each child takes a different time to perform the task. The topographic map represents the activity across the scalp. Figure 3.5 displays the band-wise topographic maps of an ADHD

participant and a healthy participant. In this representation, the blue colour across the scalp represents less activity, and the red colour represents high activity.

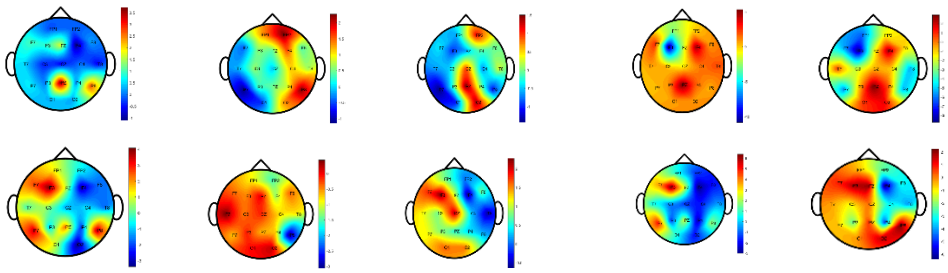

Figure 3.5 Topographic map of ADHD and healthy participants. ADHD band-wise topographic map displayed from (a) to (e) and the healthy participant band-wise topographic map displayed from (f) to (j). The blue colour represents less activity, and the red colour represents high activity across the scalp.

3.3.2 Feature Extraction

In this step, for each frequency band, we extract the twenty seven QEEG features (given in Table 3.1) for ADHD classification. The EEG signal is converted into the frequency domain using the Fast Fourier transformation (FFT) for frequencies ranging from 0 to 100 Hz at a resolution of 0.5 Hz. Then all the features are extracted from each of the sub-bands for the 19 EEG channels.

3.3.3 Feature Selection

In the proposed framework, we used the ensemble feature ranking method to select the most important features for classification. We used ANOVA, Chi-square test, Information Gain Ratio and Gini index (GI), four ranking strategies to give a rank to all the features. A majority voting scheme, similar to that used by the authors in their previous experiment, is used to determine the most significant 600 features for ADHD diagnosis.

3.3.4 Classification

In our experiments, four classifiers are used to predict the diagnostic accuracy. The four classifiers are Support Vector Machines (SVM), k-Nearest Neighbor (KNN), Random Forest (RF), and Artificial Neural Network (ANN). SVM classifies the data based on the margin maximization concept. KNN is a non-parametric classification algorithm that uses similarity measures to classify new cases among already stored available instances. RF is a non-linear ensemble classifier that contains N number of decision trees. Each decision tree has a different set of hyper-parameters on a sub-sample of a dataset. ANN is a complex adaptive classification system that can change its internal structure based on adjusting the weight of a connection. For the experiments and result analysis, we used MATLAB R2019a version.

3.3.5 Results and Discussions

This section summarizes the findings of this study. A comprehensive evaluation has been conducted to evaluate the proposed framework for classifying ADHD and healthy EEG data. The accuracy of the proposed method and state-of-art methods are summarized in Table 3.3. Using the Random Forest classifier, we achieved the best accuracy of 81.92% for the proposed method.

Table 3.3 Performance of various methods for ADHD diagnosis shown for 10-fold cross-validation on the train data.

Study	EEG Channels	Features	Feature extraction	Feature selection method	Classifier	Accuracy (%)
Arns et al. [11]	1	Theta/Beta Ratio	Cz electrode	-	kNN SVM RF ANN	78.12±2.90 63.58±1.67 53.95±3.40 58.99±2.10
Mumtaz et al. [83]	19	Absolute power,	All sub-bands	t-test and PCA	kNN SVM RF	69.16±2.63 73.31±3.87 72.20±4.63

		Relative power			ANN	69.90±1.92
Toole et al. [120]	19	Spectral, Amplitude, peak-to peak voltage features	All sub-bands	-	kNN SVM RF ANN	73.68±3.60 76.02±2.83 81.46±2.77 81.38±2.00
Huang et al. [63]	19	Absolute power, Relative power, Permutation Entropy	All sub-bands	-	kNN SVM RF ANN	71.01±.3.59 68.57±.4.10 73.38±.3.95 63..92±2.06
Park et al. [90]	6	-	Sub-band CSP	MIBIF	kNN SVM RF ANN	78.77±3.75 56.64±1.91 77.78±3.70 79.34±4.89
Vahid et al. [133]	19	-	-	-	EEGNet (deep)	77.14±0.81
Proposed method	19	Spectral, Amplitude, peak-to-peak voltage, Connectivity	All sub-bands	Majority voting scheme	kNN SVM RF ANN	77.20±0.08 76.83±0.39 81.92±023 77.21±2.30

Our feature vector comprises of 2565 features derived by extracting the twenty seven features (Table 3.1) from five frequency bands across 19 EEG channels. The derived features are ranked separately using Information gain, Chi-square, ANOVA and GI feature selection techniques. Next, the feature ranks are averaged to yield the top-600 discriminative features that are passed as the input to an array of classifiers. We performed ten-fold (split the data into 80-20 ratio) cross-validation to train the model. The k-value determines the number of nearest neighbors in KNN. We used k=8 and the Manhattan function to calculate the distance. We used an RF classifier having 500 trees of depth 8 with six nodes in each subtree. For SVM, we employed an RBF kernel with a penalty value of 10 and an eps of 0.1. We use a rectifying linear unit activation function (ReLU) and two hidden layers with 90 and 10 neurons, respectively, in the

ANN classifier. The Adam optimizer, which is a stochastic gradient-based optimizer, is used with 100 iterations. Table 3.3 presents the findings of the proposed technique for all four classifiers (KNN, SVM, RF, and ANN) in terms of accuracy, F1-score, precision, and recall. We compare our findings to those of [11][63][83], [90][120] and [133], which are state-of-the-art techniques for EEG classification.

We also determine the band-wise number of features shortlisted in the top-600 selected features for EEG classification. When we carefully examine the results, it is revealed that delta, alpha and gamma bands are equally important for ADHD classification, among all the bands, as we observe in Figure 3.6. Similarly, we also compute the participation of each electrode in the top-600 selected features for classification. Figure 3.7 displays a detailed analysis of the electrode participation for classification. The feature count for a pair of electrodes in bipolar montage is incremented by one for both electrodes, for visualization purposes only.

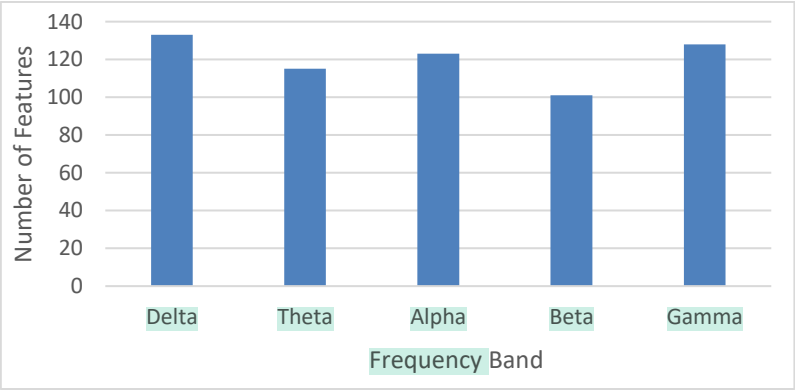

Figure 3.6. Number of features belonging to the five frequency bands in the top-600 feature subset.

Though all the 19 electrodes contribute to the shortlisted set of features for classification, FP2, O2, F7 and F8 are slightly more important, as observed from Figure 3.7. In a previous work [66], it was asserted that for the eyes open resting state, the frontal and central region, especially electrode FP2, shows some significant activity, while for the eye closing state, the O1 electrode shows significant changes. On similar lines, both the frontal and parietal regions are implicated in ADHD and involve brain networks and attention. This evidence indicates that our framework is informative and gives an accurate analysis. Our work has some limitations, though,

such as it requires a fixed setup where the number of bands is fixed. We may try adaptive sub-bands with more advanced features in future.

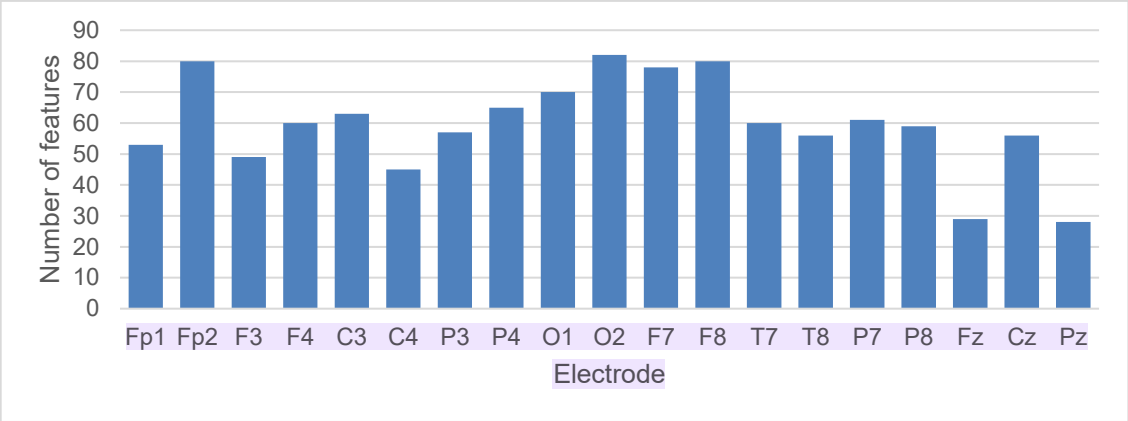

Figure 3.7 The number of features associated with different electrodes in the top-600 feature subset

We also tried to find out the more affected part of the brain in ADHD children by examining a reduced feature set comprising the top-100 ranked features. Figure 3.8 displays the electrodes contributing to the maximum number of features in the reduced feature set. The O2, P8 and T7 electrodes are related to the right occipital region, right parietal lobe and the left temporal lobe, respectively. Two electrodes are selected from the frontal lobe: F7, associated with the left frontal region, and FP2, associated with the right frontal lobe. Our findings reveal that the brain's frontal, parietal, and occipital areas discriminate between ADHD and children, resulting in accurate EEG signal classification.

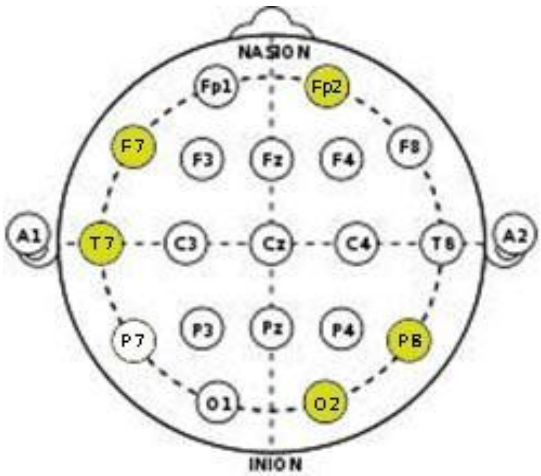

Figure 3.8. The most discriminative electrodes for ADHD detection.

3.4 Conclusion

This chapter conducted a comprehensive statistical analysis of EEG signals with the objective of identifying discriminative Quantitative EEG (QEEG) feature subsets that are generalizable across multiple brain disorders. The chapter identifies a set of twenty seven QEEG features extracted from the temporal, spectral and spatial domains, that can be used as biomarkers for brain disorder classification. A wide range of QEEG features are identified, including those related to amplitude features that reflect the signal's power and envelope characteristics, with rEEG features that provide additional nonlinear metrics of brain activity. The next features are spectral features that capture the frequency distribution of the EEG signal. Functional Connectivity features measure the coherence and correlation between different brain regions. The research successfully demonstrates that a multi-domain approach to feature extraction, combined with rigorous statistical feature selection, can produce highly effective and robust diagnostic models. By examining both AUD and ADHD datasets, this chapter highlighted the importance of a diverse feature set that is generalizable across multiple brain disorders.

Another contribution of this chapter is the critical role of feature selection in identifying a truly discriminative subset of features. The use of multiple feature ranking methods, such as ANOVA, Chi-square, Gini Index, and Information Gain ratio, in conjunction with a majority voting scheme, proved to be a powerful strategy. This ensemble approach effectively filtered out irrelevant and redundant features, thereby reducing model complexity and preventing overfitting. The results consistently showed that the selected feature subsets, though smaller, led to improved classification performance across various classifiers (SVM, KNN, Random Forest, and ANN). In summary, the statistical analysis and feature selection frameworks presented in this chapter are highly generalizable. They provide a robust methodology for identifying a concise, yet highly informative, subset of QEEG features that can be used for the computer-aided diagnosis of multiple brain disorders. This approach sets the stage for designing efficient and accurate diagnostic systems that are not tied to a single disorder or feature type.

Chapter 4

Design a novel framework to measure Functional Connectivity from EEG signals to capture complex brain patterns for improved disorder classification

One of the most promising directions in EEG analysis is the characterization of brain functional connectivity, which refers to the statistical relationships between spatially distinct brain regions. Functional connectivity patterns can reveal how brain areas interact and synchronize, which often becomes disrupted in pathological conditions.

This chapter introduces a novel framework for extracting functional connectivity as a QEEG feature, employing a generalized pipeline that captures connectivity patterns from EEG data recorded across different brain disorders using scalp electrodes positioned over distinct brain regions. Rather than focusing on a specific disease category, the proposed approach is evaluated using datasets from two distinct neurological conditions, AUD and ADHD, emphasizing its versatility and adaptability. This study presents linear monotonic inter-electrode correlation features calculated across individual frequency bands, which capture the brain's functional organization and enhance classification performance when employed as QEEG

features.

To extract the features, EEG data is decomposed into five frequency bands (delta, theta, alpha, beta, and gamma), each reflecting different functional aspects of brain activity. Within each band, the absolute value of the Pearson correlation coefficient is computed between all possible electrode pairs, capturing both the strength and direction-independent connectivity. This results in a high-dimensional feature space that reflects the topographical and spectral organization of brain connectivity. To reduce the dimension of such a large feature set, an ensemble-based feature selection strategy is employed. Statistical filters such as ANOVA and Chi-square tests are used to rank features according to their discriminative power, followed by a wrapper method—greedy forward selection—that refines the final feature subset in the context of classification performance. This two-stage selection process not only reduces computational complexity but also enhances generalization by eliminating irrelevant or redundant features. To assess the effectiveness of the selected QEEG connectivity features, four machine learning classifiers—Support Vector Machine (SVM), k-Nearest Neighbors (KNN), Artificial Neural Network (ANN), and Random Forest (RF) are applied. The classification pipeline is rigorously validated using both cross-validation on training data and evaluation on unseen test data. Notably, the SVM classifier consistently delivers superior performance, achieving near-perfect accuracy on both datasets.

In summary, this chapter introduces a data-driven framework that quantifies EEG-based functional connectivity through a novel band-wise correlation feature set. It systematically integrates signal decomposition, statistical filtering, feature selection, and classification to offer a clinically meaningful and computationally efficient approach to EEG-based disorder detection. By demonstrating strong performance across datasets associated with different brain disorders, the proposed method sets a foundation for developing generalized diagnostic tools using EEG as a primary modality.

4.1 Proposed Method

A systematic overview of the proposed method is given in Figure 4.1. In the first step, noise artifacts are removed from the alcoholic and non-alcoholic EEG signals. Each electrode signal is transformed into the frequency domain by employing FFT transformation and decomposed into five frequency sub-bands [delta (δ: 0.5–4 Hz), theta (θ: 4–7 Hz), alpha (α: 7–13 Hz), beta (β: 13–30 Hz), and gamma (γ: 30–100 Hz)]. Further, signals are recovered in the time domain using inverse FFT on each sub-band and passed onto the next step for feature extraction. The absolute value of the Pearson product-moment correlation coefficient is computed between all possible pairs of the EEG channels in each of the five sub-bands. A symmetric correlation matrix for each sub-band generates a unique feature set. These features are compiled across the five frequency sub-bands and get a feature vector. ANOVA and Chi-square are employed to rank the features based on their relative importance; the two feature ranks are then averaged, and a wrapper algorithm (greedy forward selection) is employed to derive the *K* top-most ranked features, where *K* was determined after ten-fold cross-validation on the train set. The most significant *K* features are then given as input to the four classifiers: SVM, RF, ANN and KNN to classify the EEG signals. The next section describes the mathematical formulation of the signal decomposition and correlation computation in more detail.

4.1.1 Signal Decomposition

Let an EEG signal be denoted by $\{x(n, m),\ 1 \le n \le N \text{ and } 1 \le m \le M\}$, where *n* is the sample number or time-stamp, *N* is the total number of samples, *m* is the channel index, and *M* is the total number of EEG channels or electrodes. The task undertaken is to classify the EEG signals of alcoholic and non-alcoholic subjects, recorded while performing a visual identification task. The EEG signal is transformed into the frequency domain using Fast Fourier Transform (FFT) as shown in equation (4.1).

$$x(k,m) = \sum_{n=0}^{N-1} x(n,m) e^{-j\frac{2\pi}{N}kn} \qquad k=0,1,2,\ldots,N-1 \tag{4.1}$$

Where x (k, m) is the magnitude spectrum calculated with the frequency resolution of 0.5 Hz. The spectrum is decomposed into five sub-bands: delta (δ: 0.5–4 Hz), theta (θ : 4–7 Hz), alpha (α : 7–13 Hz), beta (β : 13–30 Hz), and gamma (γ: 30–100 Hz). For the bth sub-band of the mth channel, a resynthesized EEG signal is obtained by applying inverse fast Fourier transform (IFFT) as shown in equation (4.2).

$$x_b(m) = \frac{1}{N}\sum_{k=0}^{N-1} x_b(k,m)e^{j\frac{2\pi}{N}kn} \qquad \text{where, k, n=0,1,2,.,.,N-1} \qquad (4.2)$$

Here, $X_b(.)$ is a spectrum obtained by selecting frequency bins corresponding to band b and corresponding complex conjugates for real-valued signal resynthesis.

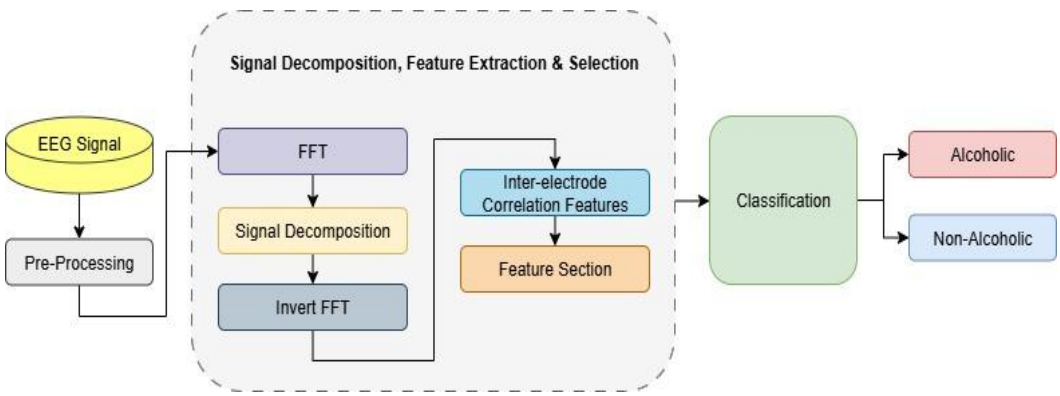

Figure 4.1. Proposed methodology framework

4.1.2 Band-wise inter-electrode correlation features

In this step, the inter-electrode correlations for each sub-band are calculated. Pearson's correlation coefficient is the most commonly used statistical measure to find the linear relationship between two or more variables and represents how these variables co-vary. It is a single-value measure of association between two or more variables with a sense of direction. The value of the correlation coefficient (r) varies in the range [-1, +1]. The inter-electrode correlation matrix C_b is computed for each sub-band b= 1, 2, ...,5, using equations (4.3) and (4.4). Each element of this matrix $C_b(i, j)$ is the Pearson's correlation coefficient representing the pair-wise association of

electrodes i and j, where i, j=1,2, ..., M in the sub-band b, where b=1, 2, ..., 5.

$$C_b(i,j) = \begin{pmatrix} r_b(1,1) & \dots & r_b(1,M) \\ \dots & r_b(i,j) & \dots \\ r_b(M,1) & \dots & r_b(M,M) \end{pmatrix} \tag{4.3}$$

Here, C_b is the correlation matrix of sub-band b. The (absolute value of) Pearson's correlation coefficient $r_b(i,j)$ between two variables i and j that represent EEG channels in our case, is given by

$$\frac{N(\sum x_b(i)x_b(j)) - (\sum x_b(i))(\sum x_b(j))}{\left([N\sum x_b(i)^2 - (\sum x_b(i))^2][N\sum x_b(j)^2 - (\sum x_b(j))^2]\right)^{0.5}} \tag{4.4}$$

where $x_b(m)$ is the EEG data for m^{th} channel and band b. The sign of the correlation coefficient $r_b(i,j)$ indicates the direction of the association, and it is found that it does not affect the relationship strength between the EEG channels. Hence, only the absolute value of Pearson's correlation coefficient is used as the QEEG feature. If the variables are completely uncorrelated, then $r_b(.)$=0, while perfect association is indicated by $r_b(.)$=1. For all auto-correlation pairs (i=j), $r_b(.)$=1, indicating the perfect correlation of the channel with itself. Furthermore, the correlation matrix is symmetric across the primary diagonal due to the commutative property of correlation. So, the diagonal and lower triangular values are removed from the correlation matrix C_b to obtain unique band-wise inter-electrode correlation features. For each sub-band, we obtain a feature vector F_b by linearizing the upper triangular values of the matrix C_b. The feature vectors of all five sub-bands b=1, 2,…, 5 are further concatenated to generate a super vector SV, which is given as input to the feature selection and classification stage.

4.1.3 Feature selection

This section proposes an ensemble feature selection method. This approach uses two filter selection methods to find the most discriminative features: ANOVA and Chi-square. ANOVA is a statistical approach for discriminating the features based on

variance across the means. We used one-sided ANOVA with a 0.05 significance level. In the Chi-square filter method, the selected features exhibit the strongest statistical association with the target as indicated by the highest Chi-square statistic. It compares every feature with target variables and finds a relationship between the feature and the target. Both ANOVA and Chi-square filter methods provide a rank for all the features. We take the average of ANOVA and Chi-square ranks, and in this manner provide a rank to all the features. A greedy forward feature selection wrapper algorithm now finds the top-*K* ranked features. The following steps are implemented to perform ensemble feature selection involving two filter methods (ANOVA and Chi-square) and one wrapper method (greedy forward selection).

Step 1. Extract all correlation features and concatenate across sub-bands.

Step 2. Apply ANOVA and Chi-square filter methods and average the ranks for all features.

Step 3. Calculate the rank for each feature based on the average rank obtained from ANOVA and Chi-square. Rank 1 corresponds to the most significant feature, and so on.

Step 4. Use the greedy forward feature selection wrapper method to find the K-most significant features.

i. Start with an empty set.
ii. Select the most important feature starting with rank 1.
iii. Train and validate the model to calculate the average 10-fold validation accuracy.
iv. Add the next important feature from the ranked list.
v. Repeat steps iii and iv until all features are processed.

Step 5. Calculate the maximum value of the average validation accuracy. If multiple maxima are found, select the one with the least K number of features.

The K-most significant features are selected by ten-fold cross-validation on the training set with an 80:20 train: validation split. Here, K is the feature rank corresponding to the maximum validation accuracy after ten-fold cross-validation.

4.1.4 Classification

To analyze the discriminative ability of the proposed QEEG features, we employed four different classifiers in this work, namely: - Support Vector Machine (SVM), Random Forest (RF), Artificial Neural Network (ANN) and K-Nearest neighbor (KNN). SVM calculates the hyperplane that classifies the data into different classes by maximizing the margin between the classes in a higher-dimensional space. We used the RBF kernel with the regularization parameters C=30 and Gamma=0.1. The next classifier is kNN, a distance-based and non-parametric learning technique. This method makes predictions by comparing a given data point to the *k* most similar data points in the training set and assigning the class label that is most common among those *k* neighbours. RF is an ensemble learning-based method that creates multiple decision trees. It combines the predictions of all the decision trees to make a final decision. The number of decision trees is set to 500. The maximum number of attributes to consider when looking for the best split is defined as 11. The maximum depth of each tree is set to 7. An Artificial Neural Network (ANN) is another classification algorithm comprising layers of interconnected neurons that process data and make predictions. The ANN has two hidden layers, the first with 130 neurons and the second with 40 neurons. Adam optimizer is used to train the ANN. It is an adaptive algorithm that regulates the learning rate for each parameter during training. The last parameter, ReLU, specifies the activation function used in the neurons of the ANN. The hyperparameters of the four classifiers are also detailed in section 4.2.1. The algorithm for the proposed methodology is given next.

4.1.5 Algorithm

ALGORITHM 1 Computation of absolute inter-electrode correlation and classification process

Input: Raw EEG signal
Output: Predicted class of EEG signal-alcoholic or non-alcoholic
Step 1: Remove noisy artifacts
Step 2: Band-wise decomposition of EEG signals
2.1 FFT analysis

2.2 Extract *delta(δ), theta(θ), alpha(α), beta(β),* and *gamma*(γ) sub-bands.
2.3 IFFT synthesis

***Step 3*:** Correlation matrix computation
3.1 Calculate the correlation matrix C_b for each sub-band for channels using Eq. (4.3)
3.2 Remove diagonal values
3.3 Remove lower triangular values

***Step 4*:** Feature vector fusion across sub-bands
4.1 Linearize the absolute values in the matrix to form the 2016-dimensional feature vector
4.2 Concatenate the feature vectors of each sub-band and construct a feature super-vector SV= [F_δ, F_θ, F_α, F_β, F_γ]

***Step 5*:** Feature selection
5.1 Rank features using both ANOVA and Chi-square
5.2 Calculate the average of the two ranks for each feature in super-vector
5.3 Select *K* most important features for the classification using the greedy forward feature selection wrapper method

***Step 6*:** Classification
6.1 Train SVM, RF, ANN and KNN classifiers
6.2 Use the trained models to predict whether the test input signal is alcoholic or non-alcoholic EEG

End

4.2 Experimental Analysis

All the experiments are conducted using the "large" version of the AUD dataset described in Chapter 3, which contains 10 alcoholic and 10 non-alcoholic subject data. The train and test folders contain 600 samples each. The computer system used for the experiments is an Intel(R) Core (TM) i5-8265U CPU 1.80 GHz with 8 GB RAM with Windows 10 Professional K 64bit. MATLAB R2019a version software is used for the experiments and analysis. This section delves into the performance of the proposed band-wise inter-electrode QEEG features for AUD classification, with comparisons to existing EEG-based features, on the same benchmark dataset.

As the first step, we pre-process the EEG alcoholic and non-alcoholic signals to remove noisy artifacts, and then we transform each electrode signal into the frequency domain by employing FFT transformation using equation (4.1), and then we decompose the EEG into five frequency sub-bands using FFT. Since we use the five frequency sub-bands: delta (δ: 0.5–4 Hz), theta (θ: 4–7 Hz), alpha (α: 7–13 Hz), beta

(β: 13–30 Hz), and gamma (γ: 30–100 Hz), the corresponding frequency bins for each band are set to [1, 8], [8, 14], [14, 26], [26, 60] and [60, 200]. Further, inverse FFT (IFFT) was applied to each sub-band using equation (4.2), and the sub-band was passed onto the next step for feature extraction. IFFT was calculated for the entire signal at once without overlap. Then, find the band-wise inter-electrode correlation features, as per the procedure explained in the algorithm in Section 4.1.3. ANOVA and Chi-square are employed for feature selection to reduce the feature dimension; the two feature scores are then averaged, and a new rank is assigned to all the features. A greedy forward feature selection method selects the top-*K* ranked features. The most significant *k* features were given as input to the four classifiers: SVM, RF, ANN and kNN whose hyperparameters are shown in Table 4.1, to classify the alcoholic EEG signal.

Table 4.1 Hyperparameters of different classifiers

S.No	Classifiers	Parameters	Values
1	SVM	Regularization parameter (L2 penalty) Kernel function RBF kernel coefficient (gamma)	30 RBF 0.1
2	kNN	Number of nearest neighbors Metric kernel	6 Manhattan Distance
3	RF	Number of decision trees Maximum number of attributes to consider when looking for the best split Maximum depth of individual decision tree Minimum number of records at a leaf node	500 11 7 5
4	ANN	Hidden layers Activation function Optimizer Maximum iterations	[130, 40] ReLu Adam 200

4.2.1 Experiments on Alcohol Use Disorder (AUD Dataset)

This section used the benchmark alcoholic and non-alcoholic EEG data, which is available online. The dataset belongs to the UCI machine learning repository and is freely available for research (UCI, 2018). A total of 122 participants were shown 90 pictures of diverse objects, and their EEG signals were collected. The subjects were shown either a single stimulus or two stimuli comprising pictures from the 1980 Snodgrass and Vanderwart picture sets; the two pictures/stimuli shown to the subject were either in the 'matched' or 'unmatched' condition. Each participant completed 120 trials for a variety of stimuli. Every single trial yielded a 64 ×256 matrix that represents 64 channels and 256 time points. The EEG signals are measured at a sampling frequency of 256 Hz for 32 seconds. All electrodes are positioned according to the 10–20 electrode scheme [118]. Several artifacts, such as eye blinking and body movements (>73.3 microvolts), have been removed from the baseline during EEG recording. The EEG signals were split into four sections, each of eight seconds (2048 samples) duration. A sample of alcoholic and non-alcoholic EEG signals in amplitude is represented in Figure 4.2 (a). The temporal representation of the EEG signal is in Figure 4.2 (b), in which the x-axis represents the all-channel index and the y-axis represents the time. A display of a magnitude spectrum of 64 channels is shown in Figure 4.2 (c).

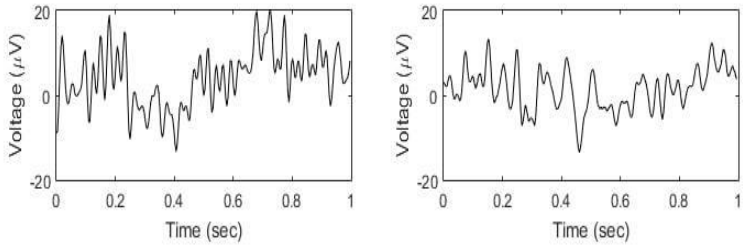

(a)

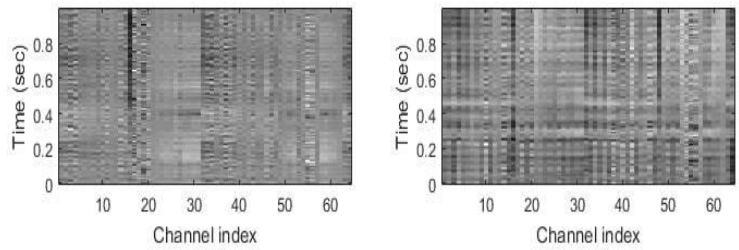

(b)

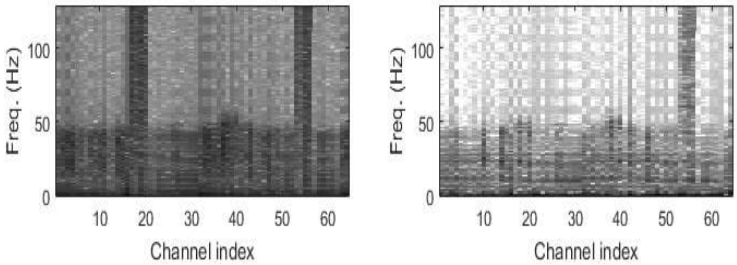

(c)

Figure. 4.2. Representation of alcoholic and non-alcoholic EEG signal in terms of (a) amplitude (b) temporal domain and (c) frequency domain

In AUD dataset we have 64 channels and 256 time points. The absolute value of the Pearson product-moment correlation coefficient is computed between all possible pairs of the 64 EEG channels in each of the five sub-bands. A 64×64 symmetric correlation matrix for each sub-band generates 2016 unique features. These features are compiled across the five frequency sub-bands to yield a feature vector of 10080 dimensions. ANOVA and Chi-square are employed to rank the features based on their relative importance; the two feature ranks are then averaged, and a wrapper algorithm (greedy forward selection) is employed to derive the *K* top-most ranked features, where *K* was determined to be 492 after ten-fold cross-validation on the train set. The most significant 492 features are then given as input to the four classifiers: SVM, RF, ANN and KNN to classify the alcoholic EEG signals.

This section compared the classification accuracy of the proposed band-wise inter-electrode QEEG features with existing QEEG features and discussed the main findings of the proposed framework. Table 4.2 lists the proposed and existing methods' classification accuracy on the open-source benchmark alcoholic and non-alcoholic

EEG dataset. The cross-validation results were obtained by swapping the train and test sets. The proposed method achieves 100% accuracy with the support vector machine classifier and 99.20%, 98.94% and 97.20% accuracies with kNN, ANN, and RF classifiers, respectively. The second-best results are obtained by [9] with 97.85%(V) accuracy using ANN, and the third-best results are obtained by [120] with 96.53% (V)accuracy using SVM. The cross-validation results follow the same trend, with SVM achieving the highest accuracy of 99.58%. The experimental results establish the discriminative ability of the proposed QEEG features for distinguishing between alcoholic and non-alcoholic subjects.

Table 4.2 Performance of various methods for alcoholism diagnosis shown for validation (V) on the test data and cross-validation (CV) on the train data.

Author and year	Classifier	Accuracy (V)	Accuracy (CV)	Features
Mumtaz, Vuong, Xia, Malik and Rashid, 2016 [83]	KNN	75.74%	74.64%	Absolute power, Relative Power
	SVM	84.32%	85.15%	
	RF	79.37%	78.77%	
	ANN	86.47%	84.20%	
Toole and Boylan, 2017 [120]	KNN	96.20%	94.90%	Amplitude features, frequency features, Connectivity features, inter-burst features
	SVM	96.53%	95.33%	
	RF	93.40%	93.05%	
	ANN	94.88%	92.88%	
Park, Lee and Lee, 2018 [90]	Ensemble classifiers	71.61%	71.26%	Sub-band CSP
Bhatti et al., 2019 [18]	RBFNN	75.48%	75.90%	Sub-band CSP
Huang et al., 2020 [63]	KNN	71.95%	72.50%	Spectral Power, Absolute entropy, permutation entropy, Coherence, phase synchronization, clustering coefficient, average path length, small-worldness
	SVM	80.69%	80.10%	
	RF	77.56%	76.46%	
	ANN	83.66%	82.60%	

Holker and Susan, 2021 [59]	KNN	94.22%	94.89%	Amplitude, spectral, range and connectivity features
	SVM	95.71%	94.96%	
	RF	91.91%	92.53%	
	ANN	97.85%	98.90%	
Proposed QEEG Features	KNN	99.20%	98.75%	Band-wise absolute inter-electrode correlation features
	SVM	100.00%	99.58%	
	RF	97.20%	98.33%	
	ANN	98.84%	98.50%	

To assess the model's generalizability, we performed cross-validation by swapping the train and test sets. There are three versions of the open-source alcohol EEG dataset. Version 1 has only two alcoholics and two control subjects' EEG data. This dataset is very small in size. Version 2 of this EEG dataset has a separate train and test folder. Each of the train and test folders has 10 alcoholics with 300 samples and 10 control subjects with 300 samples. So, the train and test folders have 20 subjects' data with 600 samples each. Version 3 has a complete dataset with lots of missing and zero values. For this reason, we have used version 2, the large dataset, in our experiments. To test the model's generalizability, we consider the train and test data to be two different datasets because the test folder has 30 out-of-sample runs per subject compared to the train set. In our work, the validation accuracy is obtained using the test data, and cross-validation accuracy is achieved on the training data. Both cases follow the same trends in accuracy achieved. The highest classification accuracy is given by SVM, and the lowest accuracy is achieved by RF.

Some outcomes of our studies are mentioned here in detail over the selected 492 features. Rank one is associated with the highest average score feature, and the maximum rank has the minimum average score. All the features are arranged according to the maximum discrimination ability. So here, the top-20 top-ranked features are listed in Table 4.3, which summarizes the band, electrode name and position of the electrode on the scalp to which they belong. Out of the selected 492 features, the maximum number of features belong to the beta and gamma sub-bands, and the minimum number of features are selected from the delta sub-band, as illustrated in Figure 4.3 (a). From this statistic, it can be noted that beta and gamma are the most informative frequency sub-bands for classifying alcoholic data.

Table 4.3 Top-20 Ranked features on AUD dataset

Feature Rank	Band	Electrode 1	Brain lobe-Electrode 1	Electrode 2	Brain lobe-Electrode 2
1	5	PO1	Parietal	FT8	Frontal
2	5	CP3	Central	PO7	Parietal
3	4	PO1	Parietal	FPZ	Frontal
4	4	CP4	Central	YC	Reference
5	5	CP4	Central	YC	Reference
6	4	PO1	Parietal	FC3	Frontal
7	5	FPZ	Frontal	P6	Parietal
8	5	FP1	Frontal	TP7	Temporal
9	4	AFZ	Frontal	ND	Reference
10	5	PO1	Parietal	FC3	Frontal
11	5	FP2	Frontal	FC3	Frontal
12	5	AFZ	Frontal	P1	Parietal
13	4	FP2	Frontal	FC3	Frontal
14	4	P5	Parietal	C1	Parietal
15	5	FP1	Frontal	XC	EOG
16	5	P5	Parietal	C1	Central
17	5	C2	Central	FCZ	Frontal
18	5	AFZ	Frontal	ND	Reference
19	5	PZ	Parietal	F1	Frontal
20	5	F3	Frontal	FC4	Frontal

In the region-wise analysis of the 492 selected features shown in Figure 4.3 (b), the count was incremented by one for each of the two electrodes in a pair for evaluation purposes. The graph shows that the maximum number of electrodes are selected from the frontal brain region, and the minimum number of electrodes are selected from the temporal brain region. Figure 4.4 displays the electrode-wise analysis of the selected feature count employed in classification. The maximum number of selected features are from FP1 and CP4 electrodes, and minimum features are selected from the F7 electrode.

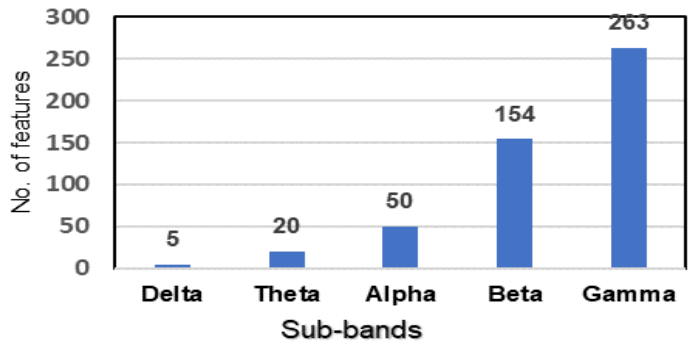

(a)

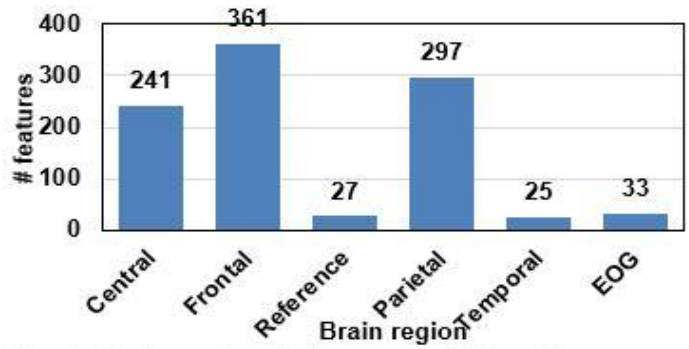

(b)

Figure 4.3. (a) Band-wise and (b) region-wise feature compilation for proposed QEEG for alcoholic and non-alcoholic/ control classification

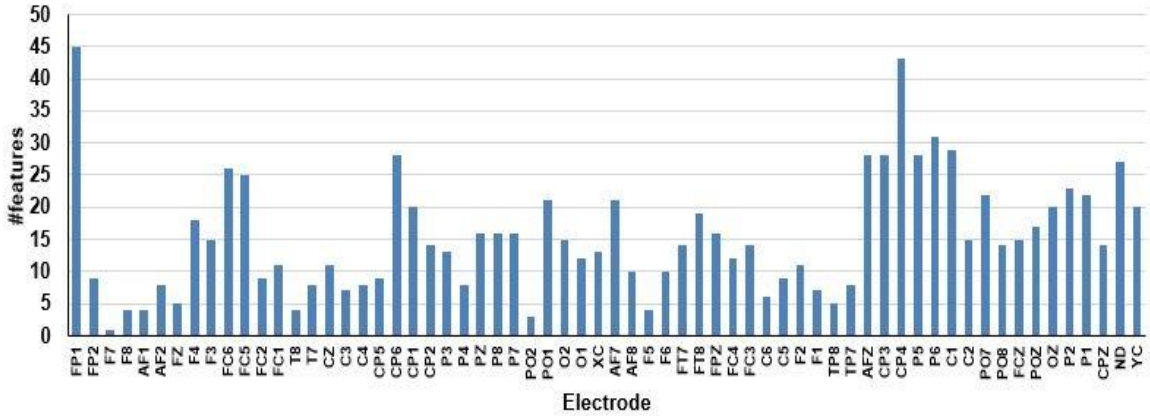

Figure. 4.4. Electrode-wise analysis of selected features for the classification

Table 4.4 categorizes the selected 492 absolute correlation coefficient values in terms of negligible, weak, moderate, strong and very strong correlation. When the absolute

value of Pearson's correlation coefficient is less than 0.10, it indicates a negligible correlation. When the value is greater than 0.90, it represents a very strong correlation between the pair of electrodes. Similarly, the correlation coefficient value in the range 0.10-0.39 indicates a weak correlation, 0.40-0.69 indicates a good correlation and 0.70-0.89 indicates a strong association between the electrodes. Among the 492 features, 11 features show a very strong correlation and 67 features have a strong correlation. Maximum selected features belong to moderate correlation with 265 features, and 149 features have weak correlation. None of the selected features have negligible correlation. The result is summarized in Table 4.4.

Table 4.4 Band-wise absolute value of inter-electrode correlation coefficient range and its interpretation

Interpretation	**Absolute value of Correlation coefficient**	**δ**	**θ**	**α**	**β**	**γ**	**Total**
Negligible Correlation	0.00 – 0.10	0	0	0	0	0	0
weak correlation	0.10 – 0.39	2	8	15	45	79	149
Moderate correlation	0.40 – 0.69	3	8	26	84	144	265
Strong correlation	0.70 – 0.89	0	4	7	23	33	67
Very Strong Correlation	0.90 – 1.00	0	0	2	2	7	11

Figure 4.5 displays the information flow between the selected electrodes in the gamma frequency sub-band. FP1 and CP4 electrodes from the frontal and central lobes are the most interconnected electrodes, with the most associated correlations. Our results confirm the literature findings that alcohol consumption affects the frontal, parietal, and central regions of the brain [82][126]. It is noticed that beta and gamma sub-bands are the most important frequency sub-bands for alcoholism diagnosis. The maximum number of selected features from the top-ranked 492 features belongs to these two frequency sub-bands.

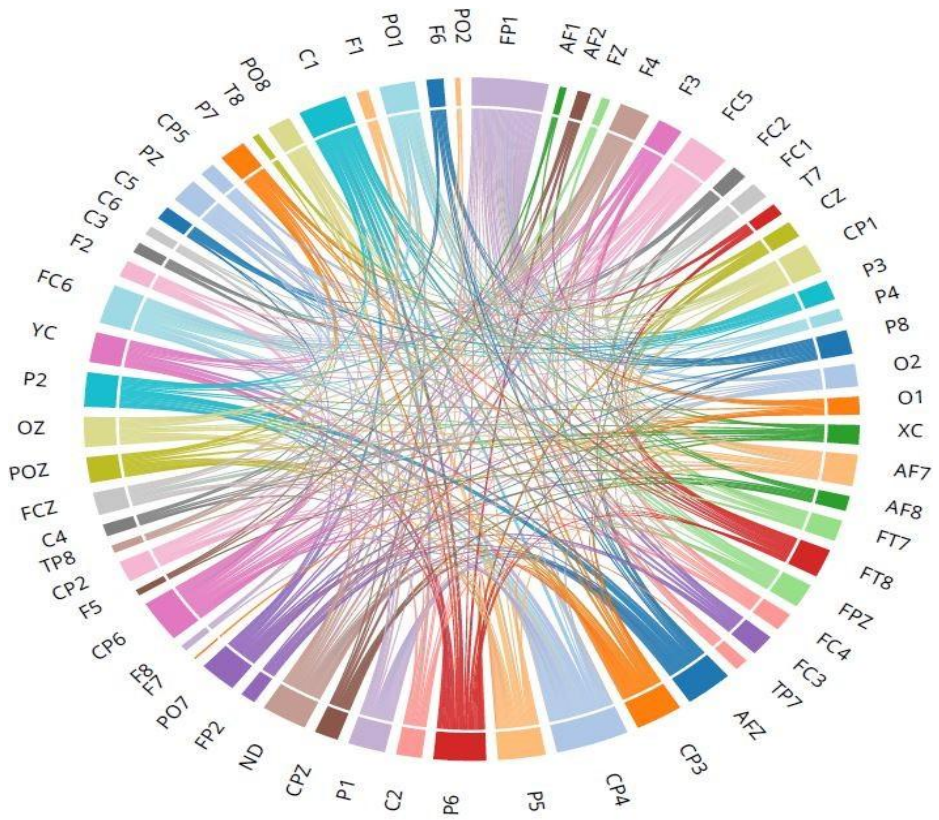

Figure. 4.5. Inter-relationships of selected electrodes in the gamma frequency sub-band

The proposed framework employed predefined filter-based techniques to decompose the signal in the delta, theta, alpha, beta, and gamma frequency bands instead of the adaptive filter bank techniques such as multivariate iterative filtering. The adaptive filter bank techniques are more suitable for subject-wise EEG data analysis and are high in computational cost [31-32]. Due to its iterative nature, the complexity of the framework for real-time application is increased. Instead, the predefined filter-based techniques extract and analyze the EEG signal's individual fixed frequency components associated with different cognitive processes. It has a lower computational cost, and the framework's complexity is also low as compared to the adaptive filter bank. The iterative filtering does not rely on predefined frequency bands, so it is not well applicable in cognitive tasks where fixed band-wise analysis is required.

4.2.2 Experiments on ADHD dataset

In this section, the proposed framework is employed on the ADHD dataset. The study involved 121 children between the ages of 7 and 12, consisting of both boys and girls. The clinical group included 61 children who had been formally diagnosed with ADHD by an expert psychiatrist using the DSM-IV criteria. All of these children had been taking Ritalin for a maximum of six months. The control group was composed of 60 children who were considered healthy, with no history of psychiatric disorders, epilepsy, or any reported high-risk behaviors.19 electrode (Fz, Cz, Pz, C3, T3, C4, T4, Fp1, Fp2, F3, F4, F7, F8, P3, P4, T5, T6, O1, O2) are used for the EEG recording based on 10-20 standard by at 128 Hz sampling frequency. The two electrodes A1 and A2 were the references located on the earlobes.

In the ADHD dataset, we have 19 channels and *N* time points. The number of samples in a single recording is not fixed because the response time of each child is different. The absolute value of the Pearson product-moment correlation coefficient is computed between all possible pairs of the 19 EEG channels in each of the five sub-bands. A 19×19 symmetric correlation matrix for each sub-band generates 171 unique features. These features are compiled across the five frequency sub-bands to yield a feature vector of 855 dimensions. ANOVA and Chi-square are employed to rank the features based on their relative importance; the two feature ranks are then averaged, and a wrapper algorithm (greedy forward selection) is employed to derive the *K* top-most ranked features, where *K* was determined to be 95 after ten-fold cross-validation on the train set. The most significant 95 features are then given as input to the four classifiers: SVM, RF, ANN and KNN to classify the alcoholic EEG signals.

This section compared the classification accuracy of the proposed band-wise inter-electrode QEEG features with existing QEEG features and discussed the main findings of the proposed framework. Table 4.5 lists the proposed and existing methods' classification accuracy on the open-source benchmark ADJD and non-ADHD EEG dataset. The proposed method achieves 83.47% accuracy with the ANN classifier and 81.60%, 77.69% and 76.86% accuracies with SVM, kNN, and RF classifiers, respectively. The experimental results establish the discriminative ability of the

proposed QEEG features for distinguishing between ADHD and non-ADHD subjects.

Table 4.5 Performance of various methods for ADHD diagnosis shown for 10-fold cross-validation on the train data

Study	EEG Channels	Features	Feature Selection	Classifiers	Accuracy (%)
Arns et al. [11]	1	Theta/Beta Ratio	-	kNN SVM RF ANN	78.12 63.58 53.95 58.99
Mumtaz et al. [83]	19	Absolute power, Relative power	t-test and PCA	kNN SVM RF ANN	69.16 73.31 72.20 69.90
Toole et al. [120]	19	Spectral, Amplitude, peak-to peak voltage features	-	kNN SVM RF ANN	73.68 76.02 81.46 81.38
Huang et al. [63]	19	Absolute power, Relative power, Permutation Entropy	-	kNN SVM RF ANN	71.01 68.57 73.38 63..92
Park et al. [18]	6	-	MIBIF	kNN SVM RF ANN	78.77 56.64 77.78 79.34
Vahid et al. [133]	19	-	-	EEGNet (deep)	77.14
Holker and Susan [59]	19	Spectral, Amplitude, peak-to-peak voltage, Connectivity	Majority voting scheme	kNN SVM RF ANN	71.25 72.60 75.88 71.73
Proposed method	19	Power, Spectral, Connectivity	Band-wise absolute inter-electrode correlation features	kNN SVM RF ANN	77.69 81.60 76.86 83.47

Some outcomes of our studies are mentioned here in detail over the selected 95 features. Rank one is associated with the highest average score feature, and the maximum rank has the minimum average score. All the features are arranged according to the maximum discrimination ability. Out of the selected features, the maximum number of features belong to the beta and gamma sub-bands, and the minimum number of features are selected from the delta sub-band, as illustrated in Figure 4.6 (a). From this statistic, it can be noted that beta and gamma are the most informative frequency sub-bands for classifying alcoholic data.

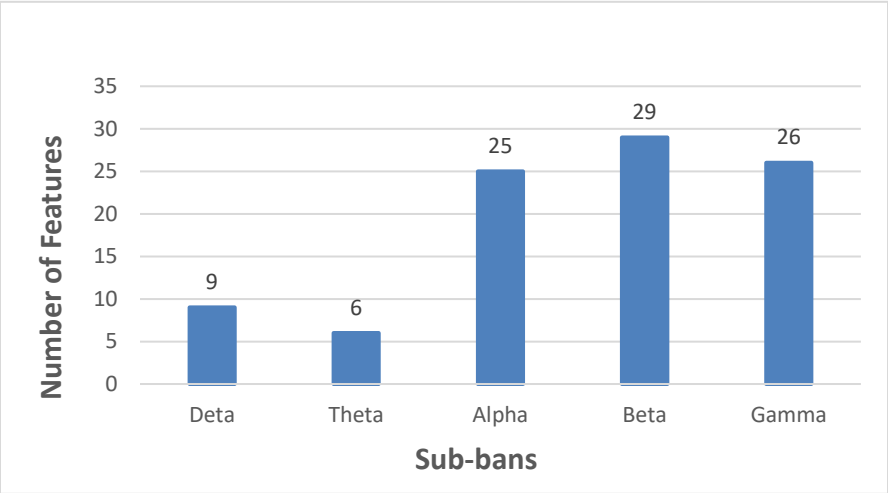

(a)

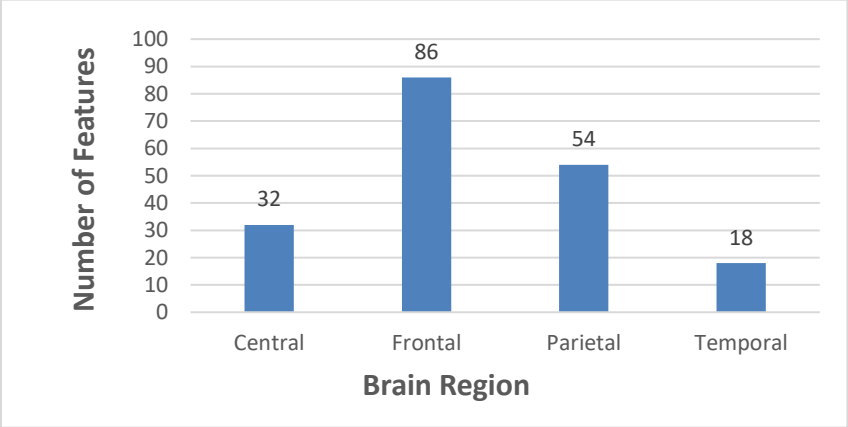

(b)

Figure 4.6. (a) Band-wise and (b) region-wise feature compilation for proposed QEEG for ADHD and non-ADHD/ control classification

In the region-wise analysis of the 95 selected features shown in Figure 4.6 (b), the count was incremented by one for each of the two electrodes in a pair for evaluation purposes. The graph shows that the maximum number of electrodes is selected from the frontal brain region, and the minimum number of electrodes is selected from the temporal brain region. Figure 4.7 displays the electrode-wise analysis of the selected feature count employed in classification. The maximum number of selected features is from F7 and FP2 electrodes, and the minimum features is selected from the P4 electrode.

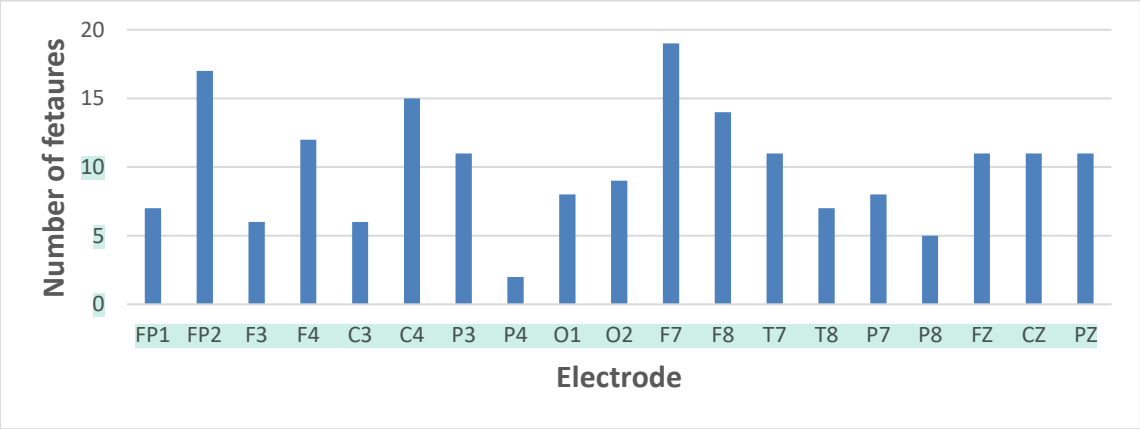

Figure. 4.7. Electrode-wise analysis of selected features for the classification

Table 4.6 categorizes the selected 492 absolute correlation coefficient values in terms of negligible, weak, moderate, strong and very strong correlation. When the absolute value of Pearson's correlation coefficient is less than 0.10, it indicates a negligible correlation. When the value is greater than 0.90, it represents a very strong correlation between the pair of electrodes. Similarly, the correlation coefficient value in the range 0.10-0.39 indicates a weak correlation, 0.40-0.69 indicates a good correlation, and 0.70-0.89 indicates a strong association between the electrodes. Among the 95 features, 5 have a strong correlation. The maximum selected features belong to moderate correlation, with 31 features, and 27 features have weak correlation. The result is summarized in Table 4.6.

Table 4.6 Band-wise absolute value of inter-electrode correlation coefficient range and its interpretation

Interpretation	**Absolute value of Correlation coefficient**	δ	θ	α	β	γ	**Total**
Negligible Correlation	0.00 – 0.10	0	0	3	10	19	32
weak correlation	0.10 – 0.39	7	1	8	8	3	27
Moderate correlation	0.40 – 0.69	2	3	12	10	4	31
Strong correlation	0.70 – 0.89	0	2	2	1	0	5
Very Strong Correlation	0.90 – 1.00	0	0	0	0	0	0

4.3 Conclusion

This chapter presents the design and implementation of a novel framework for measuring functional connectivity from EEG signals, to capture complex brain patterns to improve brain disorder classification. The proposed methodology focused on quantifying the functional relationships between different brain regions, which are known to be altered in conditions like Alcohol Use Disorder (AUD) and ADHD.

The core of this framework was the use of linear monotonic inter-electrode associations as the new Quantitative EEG (QEEG) features. A highly granular representation of brain functional connectivity was achieved by computing the absolute value of the Pearson product-moment correlation coefficient for time-series EEG data recorded from different electrode pairs and across multiple frequency sub-bands (delta, theta, alpha, beta, and gamma). This approach yielded a large number of potential features, reflecting the intricate network of neural interactions.

A key contribution of this framework was implementing a robust ensemble feature selection process. This step was crucial given the high dimensionality of the feature space created by computing correlations for all possible electrode pairs. By combining statistical filter methods with a greedy wrapper-based algorithm, we were able to identify an optimal, reduced subset of features that possessed maximum predictive

power. This strategic feature selection minimized the risk of overfitting and ensured that the final model was both computationally efficient and highly accurate.

In summary, the framework presented in this chapter provides a powerful and effective method for leveraging inter-electrode correlations to measure functional connectivity between different brain regions. The successful application of this framework, as evidenced by the high classification accuracy for behavioral disorders such as AUD and neurological disorders such as ADHD, validates its potential as a diagnostic tool that can be generalized across brain disorders. This work confirms that focusing on a refined subset of functional connectivity features is an effective strategy for enhancing the performance and reliability of EEG-based classification models.

Chapter 5

To determine a subset of relevant features from temporal, spectral, and spatial analysis of EEG signals for improved classification

In this chapter, we present two distinct methods for extracting multidomain QEEG features that encompass temporal, spectral, and spatial domains, and for identifying a subset of relevant features across these domains. Multi-domain early feature fusion improves model generalization and classification performance across brain disorders. The main focus of this work is to present a generalized framework that can determine the optimal subset of relevant features across temporal, spectral and spatial domains of EEG signal to enhance diagnostic performance. In the first approach, spectral-spatial filtered EEG data are used to extract the most relevant features for AUD classification. In the second approach, the temporal-spectral-spatial filtered EEG data are utilized to determine a subset of the most relevant EEG features for ADHD diagnosis.

5.1 Leveraging QEEG Neuro-Biomarkers of Alcohol-Related Visual Cognitive Impairment for Alcohol Abuse and Dependence Diagnosis

This section presents a novel approach for leveraging QEEG neuro biomarkers of alcohol-induced impairment of visual memory for alcohol abuse and dependence diagnosis. A spectral filter bank with a wide frequency range (0-100 Hz) is used in

conjunction with a spatial filter bank constructed using the Common Spatial Pattern algorithm. We extract a broad set of QEEG features from filtered EEG signals, including power, spectral distribution, and inter-hemisphere functional connectivity. A total of 1620 QEEG features are extracted from two independent cohorts to demonstrate the generalization ability of the proposed method. Further, Sequential Forward Selection (SFS) with stratified 10-fold cross-validation is used as a wrapper technique to select the subset of features with maximum predictive power, which is determined as 248 and 263 for the two cohorts. SFS was selected for its computational efficiency and effectiveness in optimizing feature subsets within a wrapper-based framework, while mitigating overfitting and preserving model interpretability. The proposed approach outperforms state-of-the-art models, achieving top diagnostic accuracies of 99.63% and 99.25% for the two cohorts using a Support Vector Machine classifier. Our findings reveal that features extracted from the lowest frequencies (delta, theta, and lower alpha bands) and the highest frequencies (higher gamma band) are most discriminative for identifying alcoholic individuals.

5.1.1 Materials and methods

This section describes the methodology for the experimentation. Firstly, we start by describing the dataset. This is followed by the main methodology that introduces the Spectro-spatial QEEG neuro-biomarkers used for alcohol use and dependence diagnosis. Ultimately, the sequential forward selection procedure is detailed, with a final note on the classification step.

Dataset preparation

The University of California has provided the EEG data of alcoholic and non-alcoholic patients (UCI). The data was originally donated by Dr. Henri Begleiter at the Neurodynamics Laboratory, State University of New York Health Centre, Brooklyn. The EEG data is available online. The details of the data collection procedure are elucidated by Zhang et al. in [129]. A total of 122 participants were shown 90 pictures

of diverse objects, and their EEG signals were recorded at the same time. All participants in the study were male. The alcoholic group comprised 77 individuals aged 20 to 50 years (mean age: 35.83), while the control group included 45 individuals aged 20 to 39 years (mean age: 25.81). Unfortunately, the dataset lacks additional demographic or clinical information, such as education levels or explicit inclusion/exclusion criteria. The subjects were shown either a single stimulus S1 ('matched' condition) or two different stimuli S1 and S2 ('unmatched' condition). The visual stimuli comprised of pictures from the 1980 Snodgrass and Vanderwart picture set which is a collection of 260 standardized images used for cognitive experiments on image agreement [112]. These picture sets contain a diverse collection of objects ranging from 'Accordion' to 'Zebra'. Examples of the visual stimuli S1 and S2 used for the cognitive test are illustrated in Figure 5.1 for the 'matched' and 'unmatched' conditions. As illustrated in Figure 5.1 (a) and Figure 5.1 (b), the experimental design included two trial types: matched and unmatched conditions. In matched trials (Figure 5.1 (a)), the second stimulus (S2) replicated the first (S1), eliciting recognition of repetition. In unmatched trials (Figure 5.1 (b)), S2 differed entirely from S1 including in semantic category, requiring participants to detect a novel stimulus. Trial types were randomized to minimize expectancy effects, with an equal distribution (50%) across both conditions to ensure balanced exposure. Matched trials represent lower-load cognitive processing and primarily assess recognition memory and perceptual matching. Individuals in the control group typically exhibit faster and more accurate responses on these trials, whereas alcoholic individuals demonstrate reduced speed and accuracy, reflecting deficits in attention and stimulus evaluation. In contrast, non-matched trials impose greater cognitive demands by engaging working memory, conflict monitoring, and executive decision-making. As a result, alcoholic participants tend to exhibit increased error rates and prolonged reaction times, attributable to alcohol related impairments in working memory function and disrupted inter-regional neural connectivity [125]. The subjects were instructed to press a mouse key held in one hand in case of a 'matched' condition, and press the mouse key on the other hand in case of an 'unmatched' condition. The EEG signal was acquired from 64 electrodes attached to the individuals' scalps, sampled at 256 Hz for 1 second. Only artifact-free

EEG responses were recorded. In real-world settings—such as clinical monitoring, or brain-computer interfaces—artifacts pose a significant challenge to the reliability and interpretability of EEG data. Artifacts can dominate the EEG, and overlap with frequency bands of interest, compromising signal integrity. Trials with excessive eye or body movements, indicated by peak-to-peak amplitudes greater than a voltage threshold (73.3 µV), were automatically excluded from further analysis. Figure 5.1 (c) presents the flowchart summarizing the task sequence.

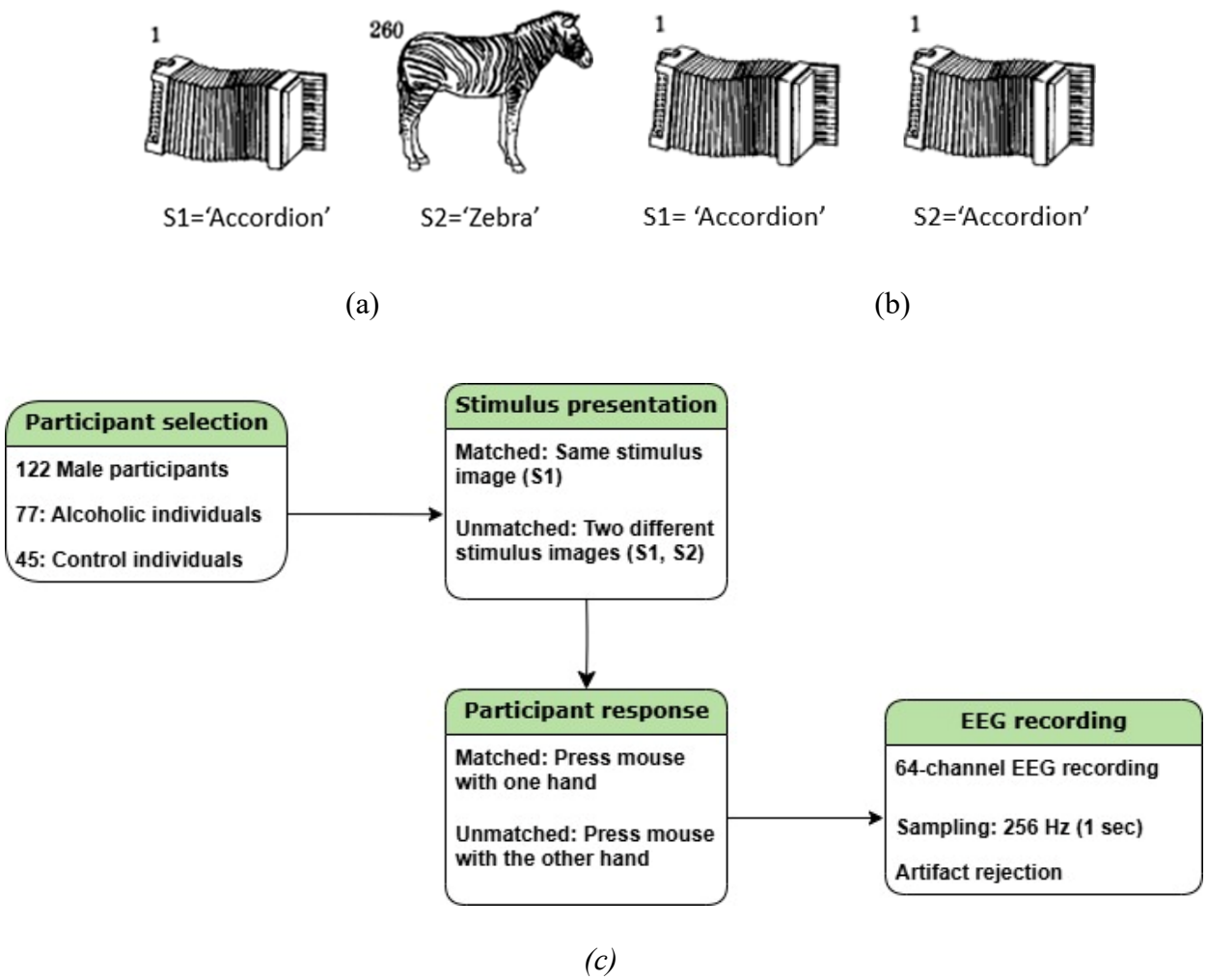

(c)

Figure 5.1. (a) Samples of matched stimulus images (b) Samples of unmatched stimulus images (from the 1980 Snodgrass and Vanderwart picture set) (c) Flowchart summarizing the task sequence.

Each participant completed 120 trials for a variety of stimuli. Each single trial yielded a 64 × 256 matrix that represents 64 channels and 256 time points. There are three

versions of this dataset. We have used the "Large" version of the dataset, which is the most popular version used by the majority of researchers in previous studies [34, 53, 59]. This version contains 300 samples belonging to 10 alcoholic individuals and 300 samples belonging to 10 control individuals in the training set, and likewise in the testing set. Two independent cohorts–validation (V) and cross-validation (CV) are used in the study, to test the generalization ability of the proposed approach. The validation cohort corresponds to the training set (600 samples), and the cross-validation cohort corresponds to the testing set (600 samples).

Process pipeline

The overall process flow is shown in Figure 5.2. In the proposed framework, the first step is to use a linear filter bank for decomposing each EEG signal into ten frequency sub-bands. A wide frequency range of (0-100) Hz is used in order to include the gamma frequencies (>30 Hz) that are excluded in most studies. Gamma band activity (>30 Hz) supports cognitive functions like attention, working memory, and perceptual binding areas often impaired by chronic alcohol use. Alcohol dependence is linked to disrupted gamma synchronization, indicating poor cortical communication and cognitive control [72-73]. Including gamma frequencies (up to 100 Hz) in our QEEG framework helps detect these deficits, improving sensitivity to alcohol-related cognitive impairment. Each filter has a bandwidth of 10 Hz. Specifically, the ten frequency sub-bands of the linear filter bank are B1 (0-10 Hz), B2 (11-20 Hz), B3 (21-30 Hz), B4 (31-40 Hz), B5 (41-50 Hz), B6 (51-60 Hz), B7 (61-70 Hz), B8 (71-80 Hz), B9 (81-90 Hz), and B10 (91-100 Hz).

In the next step, CSP is applied on each sub-band derived from the filter bank to identify the most discriminative EEG channels for alcoholism diagnosis. Spatial pattern filtering is accomplished by assigning weights to each electrode/channel based on its relevance to signal discrimination and its correlation with neighboring electrodes, effectively capturing spatially distinct neural activity across the scalp. Specifically, the CSP algorithm computes the spatial filter matrix W by solving a generalized eigenvalue problem based on the covariance matrices of the two classes—

control and alcoholic EEG in this case—with the objective of maximizing the variance for one class while minimizing it for the other. The spatial filter matrix W is used to project the multi-channel EEG signal into a new space where class-specific patterns are more distinct. Let Z denote the signal transformed by W. To derive the most discriminative channels from Z, we select d=3 rows each from the first and last rows, corresponding to three largest eigenvalues and three smallest eigenvalues. These correspond to the six electrodes or channels that provide the most discriminative information for differentiating between alcoholic and control individuals.

The EEG signal which is now spectrally-filtered (10 bands) and spatially-filtered (6 channels) is used in the next step to extract the twenty-seven QEEG features. In total, 1,620 QEEG features were extracted (10 bands × 6 channels × 27 features). SFS feature selection algorithm is applied for selecting the most discriminative QEEG features in the next step. Finally, five different classifiers: - RF, SVM, kNN, SVM and XGBoost are used for the classification of the top-ranked QEEG features in the two independent cohorts.

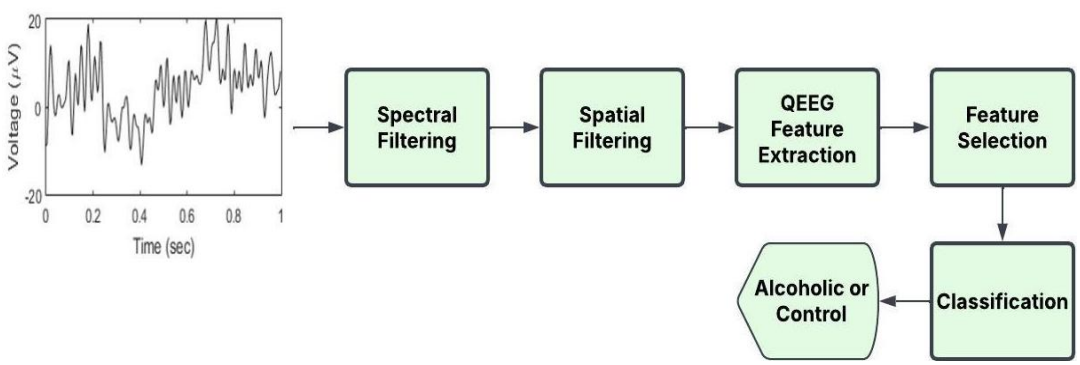

Figure 5.2. Process pipeline of the proposed approach.

QEEG feature extraction

Chronic alcohol use induces neurophysiological changes that disrupt the symmetry and distribution of EEG signals across temporal, spectral, and spatial domains. To capture these alterations, a comprehensive set of twenty-seven QEEG features is extracted from the spectrally- and spatially-filtered EEG data. These features are categorized into three groups: power (reflecting amplitude dynamics), spectral

distribution (characterizing frequency content), and inter-hemispheric functional connectivity. Together, they offer valuable insights into cortical activity and neural dysfunction associated with alcoholism, supporting its diagnosis and assessment. Table 5.1 summarizes the twenty-seven QEEG features utilized in this study (Table 3.1), detailing their definitions and significance. This Table outlines the clinical relevance of each feature in the context of alcoholism.

Table 5.1. Details of QEEG features used in the study with clinical relevance for Alcoholic individual

Feature	**Abbreviation**	**clinical relevance for Alcoholic individuals**
F1 (Power)	ATP (Amplitude Total power)	often reduced in alcoholic individuals indicating brain hypoactivity and possible long-term neurodegeneration
F2 (Power)	ASD (Amplitude Standard Deviation)	often reduced in alcoholic individuals in alpha and beta bands due to reduced responsiveness, while elevated in theta band due to cortical instability
F3 (Power)	ASKW (Amplitude Skewness)	higher positive skewness in alcoholic individuals indicating abnormally frequent bursts of excitatory activity leading to uneven amplitude distributions
F4 (Power)	AKR (Amplitude Kurtosis) [1]	increased kurtosis in alcoholic individuals indicating irregular or burst-like brain activity
F5 (Power)	AEM (Amplitude Envelop Mean)	often reduced in alcoholic individuals due to cognitive impairments and arousal deficits
F6 (Power)	AESD (Amplitude Envelop SD)	often reduced in alcoholic individuals due to blunted modulation capacity
F7 (power)	REM (rEEG Mean)	reduced mean peak-to-peak voltage in alcoholic individuals indicating cortical hypoactivity
F8 (power)	REMD (rEEG Median)	reduced median peak-to-peak voltage in alcoholic individuals indicating persistent underactivity in brain regions
F9 (Power)	RESD (rEEG SD)	Alcoholics show abnormal (either too high or too low) variation in peak-to-peak voltage across different time windows due

		to abnormal firing patterns alternated with cortical hypoactivity
F10 (Power)	RELM (rEEG Lower margin)	often reduced in alcoholic individuals due to persistent low-amplitude brain activity in alcoholic individuals
F11 (Power)	REUM (rEEG upper margin)	often reduced in alcoholic individuals due to suppression of strong neural responses because of reduced synaptic strength
F12 (Power)	REW (rEEG width)	often reduced in alcoholic individuals due to blunted neural dynamics
F13 (Power)	RCOV (rEEG Coefficient of variance)	higher coefficient of variation in alcoholic individuals due to unstable signal amplitude
F14 (Power)	REASY (rEEG Asymmetry)	high asymmetry in alcoholic individuals due to occasional extreme peaks
F15 (Spectral Distribution)	SPAP (Spectral absolute power)	Abnormal spectral profiles: high beta power due to anxiety and impulsivity; low alpha power due to cognitive deficits
F16 (Spectral Distribution)	SPRP (Spectral relative power)	increased relative beta power, and diminished relative alpha and theta powers in alcoholic individuals due to cortical disinhibition
F17 (Spectral Distribution)	SPF (Spectral Flatness- Winner Entropy) [34]	high spectral flatness in alcoholic individuals due to uniform spectrum reflecting disorganized brain activity
F18 (Spectral Distribution)	SPD (Spectral Difference)	high spectral difference observed in alcoholic individuals due to irregular brain rhythms
F19 (Spectral Distribution)	SPE (Spectral Entropy- Shannon entropy)	high spectral entropy in alcoholic individuals due to uniform frequency distribution reflecting cognitive dysfunction
F20 (Spectral Distribution)	SPEF (Spectral Edge Frequency)	high spectral edge frequency in alcoholic individuals due to power shift toward higher frequencies
F21 (Spectral Distribution)	FD (Fractal dimension)	high Katz fractal dimension in alcoholic individuals due to less regular, more chaotic signal indicating abnormal brain rhythms
F22 (Spectral Distribution)	PEEN (Permutation Entropy)	high permutation entropy in alcoholic individuals due to

		disordered eeg indicating chaotic brain activity
F23 (connectivity)	BSI (Brain symmetry index)	elevated Bsi in alcoholic individuals due to asymmetrical brain activity
F24 (connectivity)	CORR(Correlation)	low envelope correlation between channel pairs in alcoholic individuals due to the brain's loss of synchronized communication across regions
F25 (connectivity)	COHM (Mean coherence)	low coherence between channel pairs in alcoholic individuals due to poor functional connectivity between brain regions
F26 (connectivity)	COHMX (Connectivity coherence max)	elevated maximum coherence between channel pairs in alcoholic individuals due to abnormal over-coupling between brain regions, a sign of cognitive impairment
F27 (connectivity)	COHFMX (Frequency of maximum coherence)	shift of frequency of maximum coherence from (lower) alpha to (higher) beta band in alcoholic individuals indicating a state of hypervigilance and impulsivity

The power features used include Standard Deviation (SD), skewness and kurtosis, which measure the discontinuity of the signals. Another power feature is total amplitude power, which measures the EEG signal power. Additionally, two amplitude-based features are considered: envelope mean and envelope standard deviation (SD). The rEEG feature measures the peak-to-peak voltage of an EEG signal that is developed as an alternative to amplitude-integrated EEG. rEEG asymmetry measures the discontinuity of rEEG, and all the remaining rEEG features measure the EEG power. Similarly, the spectral features measure the spectral distribution of EEG signals. Only one spectral feature, the spectral difference, is used for analyzing the discontinuity of the signal. The inter-hemispheric functional connectivity features measure the connectedness between brain hemispheres, and are helpful for detecting various brain disorders.

To further condense the proposed feature set without causing a major drop in classification accuracy, smaller subsets of features from the three main categories: power (amplitude characteristics), spectral distribution (frequency characteristics), and

inter-hemispheric functional connectivity, are recommended. These subsets may include combinations of spectral features and connectivity measures, such as absolute and relative spectral power, entropy, permutation entropy, fractal dimension, spectral edge frequency, and coherence. Another effective combination is spectral power with coherence alone. Statistical measures derived from the time domain such as mean, standard deviation, median, entropy, skewness, and kurtosis can also be useful. The recommendation of these features is based on their popularity as identified through a literature survey.

Feature selection

The feature selection module comprises of two different concepts: a filter method that give a rank to each feature using ANOVA, chi-square, information gain and Gini index. Averaged ranked obtained by all the filter is then passed to a step-by-step wrapper technique called Sequential Feature Selection (SFS) to select the most significant QEEG features with maximum predictive power for AUD diagnosis. The rank of all features is determined using ten-fold stratified cross-validation with support vector machine as the core classifier. The SFS algorithm progresses in an incremental manner, starting from an empty set, incrementally adding more features till the criterion function does not decrease anymore. The criterion function used here is the average loss function represented by the mean squared error.

Classification

The QEEG features selected through SFS are classified using five different classifiers: - RF, SVM, kNN, SVM and XGBoost, and the performance scores are compared with that of baseline methods. Table 5.2 lists the hyperparameter selection for different classifiers. The selected features are then passed to the classification stage, which includes a Random Forest (RF) classifier with 500 trees and an Artificial Neural Network (ANN) consisting of two hidden layers with 130 and 40 neurons, respectively. Adam optimizer was used and the number of epochs was set to 200. The hyperparameters of various classifiers, selected through grid search are outlined in Table 5.2. Grid search is an exhaustive search in the hyperparameter space of the

learning algorithm [15].

Table 5.2: Hyperparameter selection for different classifiers.

Classifier	Hyperparameter
k-Nearest Neighbor (kNN)	Number of neighbors (k)=5 Distance='Manhattan'
Support Vector Machine (SVM)	Kernel=RBF C=1.0 γ= [1/number of features]
Random Forest (RF)	Number of estimators=500 Number of attributes for best split=11 Maximum depth=7 Number of records at a leaf node=5
Artificial Neural Network (ANN)	Number of hidden layers=2 Number of hidden units=130, 40 Number of epochs=200 Activation function=ReLu Optimizer=Adam
XGBoost	Maximum depth=6 Learning rate=0.3 Number of estimators=180 Minimum child weight=1

5.1.2 Results and Discussions

Experiments were performed on an Intel(R) Core (TM) i5-8265U CPU 1.80 GHz with 8 GB RAM. We used the MATLAB R2019a version software for the experiments and analysis. All methods have been implemented on the same dataset, i.e. UCI alcoholic EEG signal dataset. To encourage reproducibility of research, we have made our code available online[3]. The SFS wrapper technique with stratified 10-fold cross-validation was used for selecting the optimal subset of features. Here we applied the step forward technique to select the feature subset for classification. We employed a wrapper-based feature selection method using an SVM classifier as the core model. The highest accuracy during 10-fold cross-validation on the training set was obtained using the most significant feature subsets, consisting of 248 features for the validation

[3] https://github.com/ruchi-holker/QEEG-Neuro-Biomarkers-for-Alcohol-Abuse-and-Dependence-Diagnosis

cohort and 263 features for the cross-validation cohort, respectively.

12 The performance analysis and comparison of the proposed work with the state of the art is shown in Table 5.3 for the validation (V) and cross-validation (CV) cohorts. We compared our method with two primary conventions in AUD detection–those that use QEEG features and those that use filter banks. For the validation cohort, Mumtaz et al. [83] achieved 86.47% accuracy using an ANN using only two spectral power features-absolute power and relative power, with feature selection using t-test and PCA. Furthermore, QEEG features used by Toole et al. [120], for which the Support Vector Machine (SVM) classifier achieved 96.53% accuracy. The approach proposed by Huang et al. [63], which utilized spectral power, entropy, and coherence QEEG features, achieved an accuracy of 83.66%. Dorvashi et al. [34] and Al-Hadeethi et al. [6] achieved accuracies of 98.33% and 99.00%, respectively. Amplitude, frequency, rEEG, and functional connectivity features proposed in [59] achieved an accuracy of 97.6% for the top-3000 features. In contrast to this work, we select an even smaller subset of QEEG features (top-248 for validation cohort and top-263 for cross-validation cohort) and use the efficient SFS algorithm with stratified 10-fold cross-validation, thereby, achieving even higher accuracies for the classification task. In addition, the spectro-spatial decomposition of the EEG signal further optimizes the results. The highest accuracies (V: 99.63%; CV: 99.25%) are reported for the proposed method using the SVM classifier. The computational time involved was also less, in the order of a few seconds, since only six spatially-filtered channels are involved in contrast to the previous works that involve 64 EEG channels. In our current implementation, the average processing time was around 3.8 seconds on a standard machine (Intel i5 processor, 8 GB RAM) without GPU acceleration, highlighting the lightweight nature of our approach, which leverages a limited number of spatially filtered channels. The computational time of our approach was found comparable to other CSP-based methods [90, 18] and the method proposed by Mumtaz et al. [83], both of which required approximately 2 to 3 seconds to execute due to the smaller number of features involved. In contrast, other methods [34, 120, 63, 59] took around 1 to 3 minutes, primarily because they utilized a larger number of features and all 64

EEG channels. The highest execution time, approximately 7 minutes, was observed with the method by Al-Hadeethi et al. [6], which incorporated optimization via the Fruit Fly Optimization Algorithm.

Table 5.3. Performance comparison of the proposed QEEG framework with existing methods for AUD detection.

Author name & Ref.	**Classifier**	**Accuracy (V)**	**Accuracy (CV)**	**Feature extraction**	**Feature selection**	**No. of EEG channels**
Mumtaz et al. [83]	kNN	75.74%	74.64%	Absolute power, Relative power	t-test and principal component analysis	64
	SVM	84.32%	85.15%			
	RF	79.37%	78.77%			
	ANN	86.47%	84.20%			
Toole et al. (2017) [120]	kNN	96.20%	94.90%	Amplitude, rEEG, connectivity, burst and inter-burst intervals, and spectral QEEG	-	64
	SVM	96.53%	95.33%			
	RF	93.40%	93.05%			
	ANN	94.88%	92.88%			
Park et al. (2017) [90]	Ensemble classifier	71.61%	71.26%	CSP	Mutual information-based feature selection	6
Bhatti et al. (2019) [18]	Radial basis function neural networks	75.48%	75.90%	CSP	Sequential backward floating selection	6
Al-Hadeethi et al. (2022) [6]	SVM with Fruit-fly optimization	98.80%	98.25%	Ten statistical features extracted from eigenvalues of the covariance matrix integrated with a clustering	Kolmogorov–Smirnov test (KST)	64

				technique-based bootstrap		
Dorvashi et al. (2023) [34]	SVM kNN	98.30% 97.46%	98.70% 98.10%	Rhythm power, approximation and permutation entropies, Katz and Petrosion fractal dimension	Statistical analysis and Davis-Bouldin criterion	64
Huang et al. (2020) [63]	kNN	71.95%	72.50%	QEEG + All sub-bands	-	64
	SVM	80.69%	80.10%			
	RF	77.56%	76.46%			
	ANN	83.66%	82.60%			
Holker and Susan (2021) [59]	kNN	94.22%	94.89%	QEEG + All sub-bands	Majority-voting	64
	SVM	95.71%	94.96%			
	RF	91.91%	92.53%			
	ANN	97.85%	98.90%			
Proposed method	kNN	98.81%	98.90%	27 QEEG features comprising EEG power, discontinuity and spectral distribution features + CSP	Sequential Forward Selection (SFS)	6
	SVM	99.63%	99.25%			
	RF	99.01%	98.25%			
	XGBoost	98.26%	97.90%			
	ANN	97.25%	96.25%			

The spectral distribution of the selected QEEG features in Figure 5.3 for both cohorts reveals that the B1 (0–10 Hz), B6 (50–60 Hz), B9 (80–90 Hz), and B10 (90–100 Hz) sub-bands contribute more discriminative features for alcoholism diagnosis than the other sub-bands. B1 includes delta (0.5-4 Hz), theta (4-8 Hz), and lower alpha (8-10 Hz) bands, often linked to disrupted arousal and drowsiness [50]. B6, B9, and B10, on the other hand, span the high gamma range (>60 Hz), associated with higher-order cognitive processes and cortical communication [27]—functions known to be impaired in chronic alcohol use. Gamma oscillations are typically associated with higher-order cognitive processes such as attention, memory, and information

integration. In people with Alcohol Use Disorder (AUD), elevated gamma activity may suggest that the brain is overly active or "overstimulated" [96]. This often happens because long-term alcohol use disrupts the normal balance between calming (inhibitory) and stimulating (excitatory) brain signals, making the brain more excitable than usual. Features extracted from higher gamma frequencies (above 60 Hz) are particularly sensitive to these alcohol-related changes in brain function and contribute to the identification of AUD, making them valuable biomarkers for diagnosis.

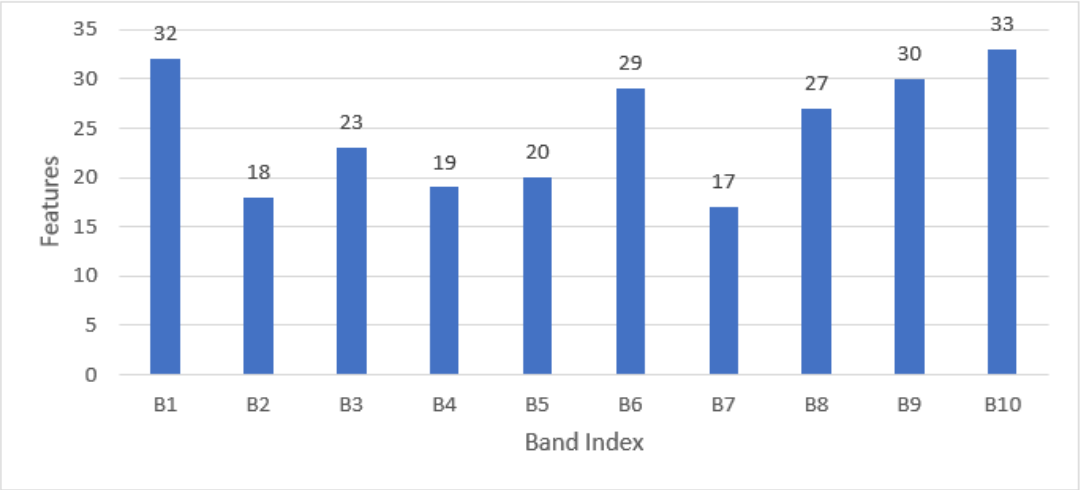

(a)

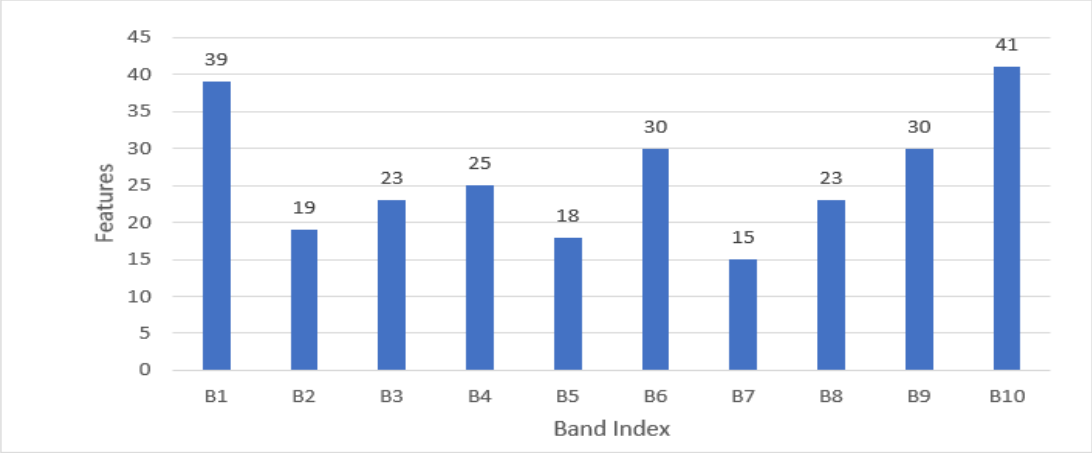

(b)

Figure 5.3. QEEG features selected from the ten sub-bands for (a) Validation cohort (b) Cross-validation cohort

A bootstrapping approach is used to understand data dependency of the discriminative

power of the proposed features and their associativity with different classifiers. Nine fractions varying from 10% to 90% of the complete dataset are selected in this approach. Ten training subsets are randomly selected for each fraction to avoid any dataset bias and provide statistically meaningful results. A total of 360 trials were carried out, with each trial comprising of one of the classifiers trained using smaller training subsets and tested using the complete testing dataset. The results of the experiments are summarized in Figure 5.4 for both cohorts, where each boxplot depicts the variation in classification accuracy for a varying fraction of the training dataset using different classifiers. In all cases, the variation in the classification accuracy decreases with the increasing fraction of the training dataset due to minimal variation in random subsets caused by higher fraction values. It can also be observed that SVM saturates faster for both cohorts (even at low training data) indicating it is more reliable than ANN. As the ratio increases, deviation decreases for SVM, unlike for ANN, XGBoost and kNN. The boxplots for the SVM classifier (Figure 5.4) clearly illustrate that the model's stability improves as the number of training samples increases, across both the validation and cross-validation cohorts. This trend is particularly evident from the progressive narrowing of the confidence intervals associated with the classification accuracy. Wider confidence intervals at lower sample sizes reflect higher variability in the model's performance, indicating that the classifier is more sensitive to fluctuations in the training data, a common sign of overfitting. However, as the training set grows, the boxplots exhibit reduced spread, and the confidence intervals become noticeably tighter. This narrowing suggests that the model's predictions are becoming more reliable and less dependent on specific subsets of the data, which is indicative of improved generalization. The convergence of validation and cross-validation accuracies, coupled with reduced variance, further supports the conclusion that overfitting is being mitigated. In essence, the consistent tightening of the confidence intervals demonstrates that the SVM model achieves more stable and reproducible performance as it is trained on larger datasets. The RF classifier performs second-best, and also shows a low variation in the box plots for the two independent cohorts.

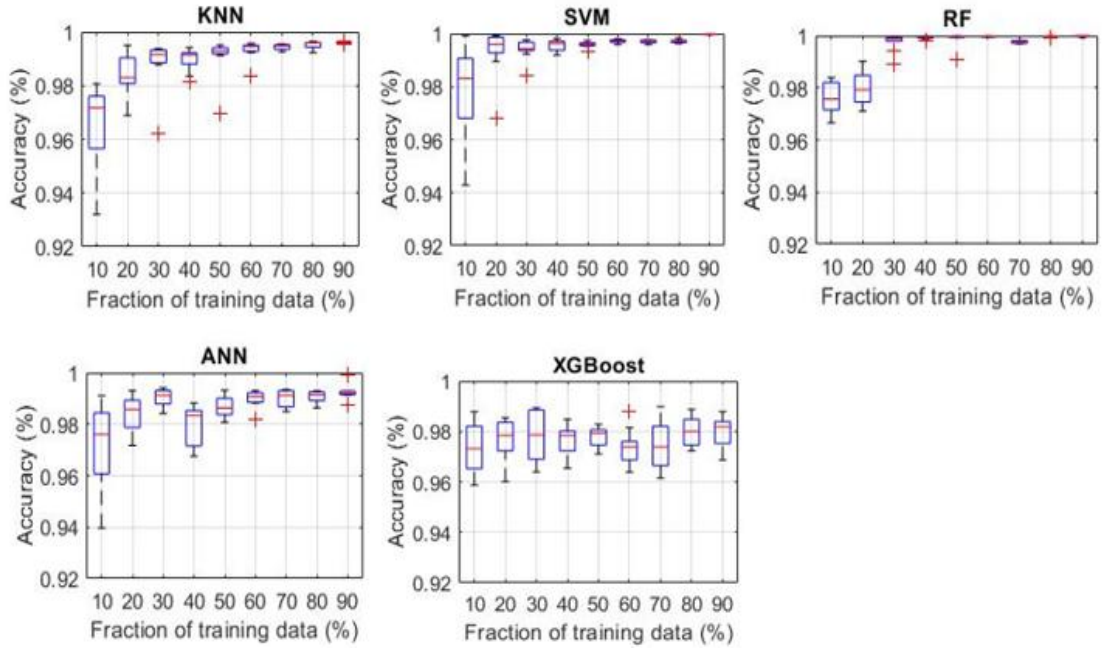

(a)

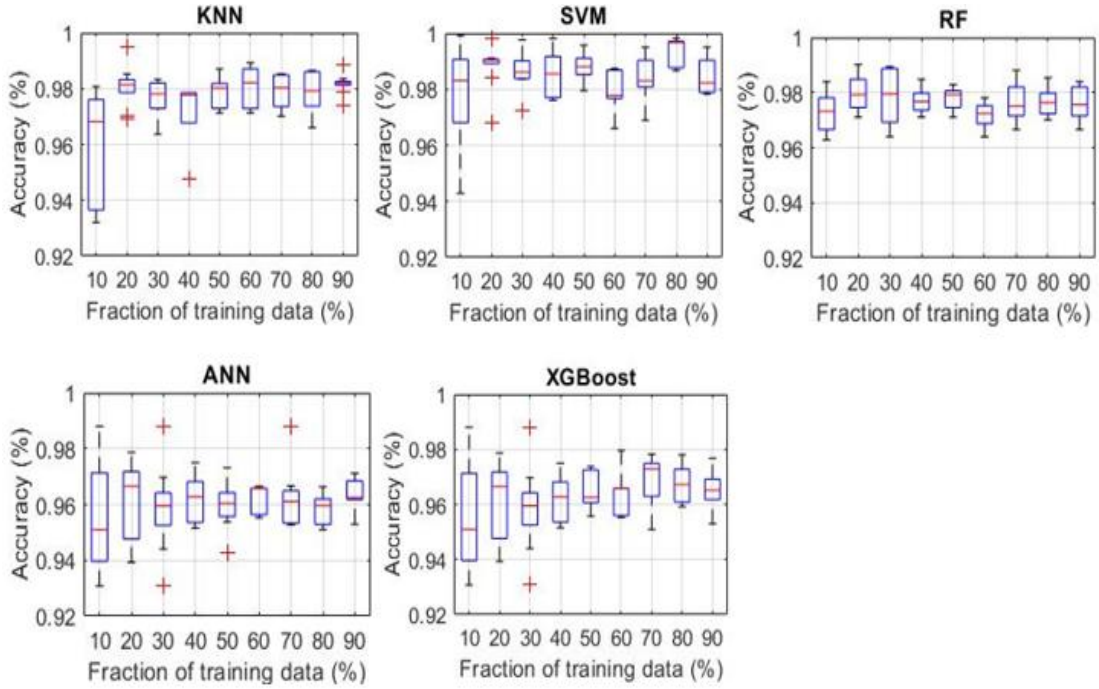

(b)

Figure 5.4. Boxplots showing variation in classification accuracy across different fractions of the training data for (a) Validation cohort (b) Cross-validation cohort

The proposed framework provides a non-invasive, objective tool for early diagnosis of alcohol-related cognitive impairment by analyzing EEG biomarkers during simple visual tasks. It complements traditional assessments by offering quantitative insights

for personalized treatment planning. This study has a few limitations. It addresses a binary classification task (alcoholic vs. control), but future work will aim to extend this to a multiclass classification problem. Additionally, the effectiveness of our approach could be better assessed using a larger dataset that includes participants of all genders, allowing for an analysis of how alcohol abuse and dependence may differ between males and females. Incorporating geographic and ethnic diversity in the dataset could also help capture variations in drinking behavior influenced by cultural factors. Key challenges for real-world implementation include the need for standardized EEG protocols, inter-individual variability, susceptibility to artifacts, addressing variability in equipment, and the need for integration into clinical workflows [73].

5.2 Generalizable Temporal-Spectral-Spatial Quantitative Electroencephalogram based Diagnosis of Attention Deficit Hyperactivity Disorder in Children

This section of the chapter proposes a novel diagnostic framework for ADHD, that quantifies cognitive ability through spectral, power and connectivity QEEG pooled across temporal, spectral and spatial dimensions of an EEG signal evoked by visual stimuli. The generalizability of this approach is proved using a subject-wise data splitting strategy. The spectral features represent the frequency characteristics of the EEG signal, while power features represent the amplitude characteristics. Connectivity refers to the inter-hemispheric brain region connectivity which is measured using averaged correlation and coherence statistics computed between all possible channel pairs in the left and right hemispheres. Ensemble-based feature selection is then employed for selection of optimal features from the concatenated feature list. Two ADHD datasets have been used for the evaluation. The first dataset is smaller and balanced, and involves 121 participants (ADHD:61, Healthy:60), while the second dataset is larger and imbalanced, and involves 144 participants (ADHD:23,773, Healthy:10,129). The results establish the diagnostic efficacy of the proposed method

and its potential for influencing future research.

5.2.1 Materials and Methods

This section details the methodology followed for the experiments conducted in this study. The raw EEG signal is subject to preprocessing to remove artifacts. The EEG signal is then segmented into time windows (temporal dimension), each time window is filtered into multiple frequency bands (spectral dimension), and in each frequency band, discriminative channels are identified (spatial dimension) for extracting QEEG features. The features concatenated across temporal, spectral and spatial dimensions are subject to rigorous feature selection to extract discriminatory features for classification. Figure. 5.5 illustrates the principal stages of the experimentation. Broadly, these are classified into datasets, preprocessing, sub-time segmentation, filter bank, common spatial pattern, QEEG feature computation, window averaging, feature selection ensemble, and classification. The steps are explained in more detail below.

Datasets

In this study, two ADHD EEG datasets were used for evaluating the performance of the proposed framework. The main difference between the two datasets is that they use different numbers of EEG channels and have different numbers of trials with different lengths of signals. Also, dataset-1[4] is a balanced dataset, while dataset-2[5] is an imbalanced dataset. Table 5.4 lists the characteristics of both datasets also referred to as D1 and D2.

[4] https://ieee-dataport.org/open-access/eeg-data-adhd-control-children
[5] https://osf.io/nceqv/?show=revision

106 ***Table 5.4: Details of the ADHD datasets used in the experiments***

Dataset	Number of participants	Age	channels	Samples	classes	Class Imbalance
Dataset-1 (D1)	Total=121 ADHD=61 Healthy=60	ADHD=9.62 ± 1.75 Healthy=9.85 ± 1.77	19	ADHD=61 Healthy=60	2	No
Dataset-2 (D2)	Total =144 ADHD=100 Healthy=44	ADHD= 10.6 ± 1.9 Healthy= 11.3 ± 2.2	56	ADHD= 23,773 Healthy= 10,129	2	Yes

127 In dataset-1, the 121 children enrolled in the study were divided into two groups in which ADHD group had 61 children and non-ADHD/control group had 60 children. In dataset-2, 144 children were included in the analysis. For the control group 10129 trials were conducted, and for the ADHD group 23773 trials were conducted. In both cases, prior to the EEG recording, the participant children were presented with visual stimuli (counting of characters in cartoons (dataset-1), recording time lapse of 1200ms after visual stimulus by pressing a button (dataset-2)), with the goal of capturing the cognitive ability of the participant.

We collected 256 samples per second, corresponding to 256 Hz sampling frequency. The sampling frequency is set to be at greater than twice the maximum possible frequency of an EEG signal which is around 100 Hz, with the highest frequency band (Gamma) lying in the range of 30 Hz to 100 Hz [104], and any frequencies above this range is labelled as noise.

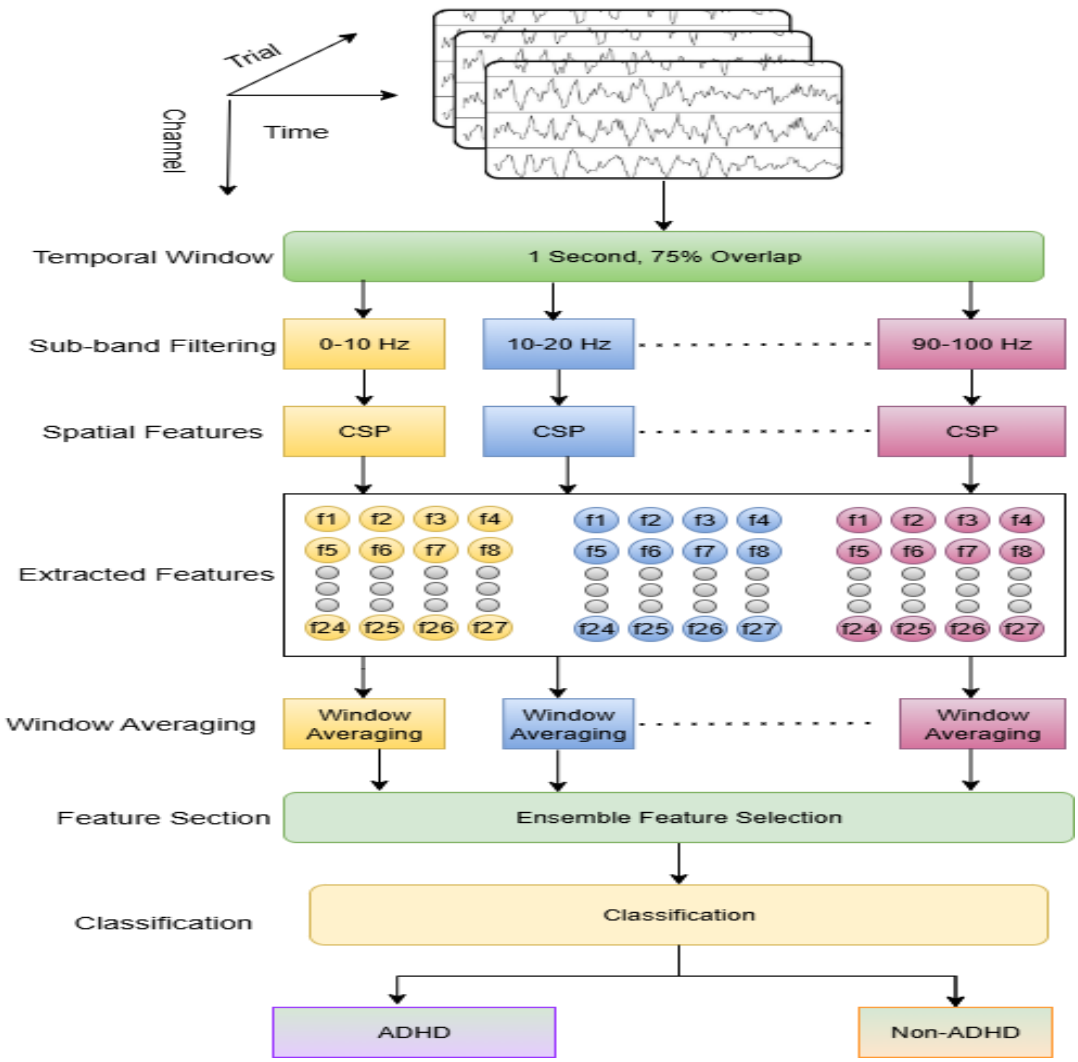

Figure 5.5. Process pipeline of the proposed method

Preprocessing of EEG Measurements

The multi-channel EEG signal is recorded by electrodes placed on the scalp, and subjected to a preprocessing stage comprising of signal processing steps to extract useful information from noisy EEG recordings. For all the datasets used in our work, technical artifacts caused due to eye or muscle movements were removed at the source itself through raw data inspection. Furthermore, Independent Component Analysis (ICA) was employed to remove any remaining artifacts. Line noise was eliminated using the notch filter. This is the cleaned multi-channel EEG signal used in all the experiments reported in this chapter. The number of EEG electrodes or channels vary

for different datasets. Bipolar montage reference system is used for all the experiments, wherein each electrode is linked and compared with the electrode behind it.

Feature Extraction

Dividing the EEG signal into multiple sub-time segments or windows using a sliding window technique allows for the analysis of changes in the signal over time. We have followed the precedence of previous works on EEG segmentation followed by multiple-band filtering of each time window [74,76]. EEG signal can vary with time, and this variation can be gauged by analyzing the signal in smaller time windows. So, in the proposed scheme, a temporal sliding window technique is used to capture continuous changes in the signal over time. Consider that S is a raw EEG signal that is divided into n overlapping sub-time window segments of duration t seconds each, denoted by $S = \{S_1, S_2, S_3, \ldots S_n\}$. The number of windows (n) is variable since the EEG signals used in the experiment are of varying length (in the order of several seconds), hence we retained the original length of signals without any truncation. To determine the size of the sliding window, we test various window sizes (such as 0.5 s,1.0 s and 1.5 s) in order to identify the optimal window size for ADHD detection. Empirical trials established that the window size of 1 second was optimal for the experiments conducted in our study.

Filter bank

To analyze the ADHD signal in different frequency sub-bands we apply the filter bank on each sub-time window. A filter bank is a collection of band-pass filters that divide the input signal into several components, each one carrying a single frequency sub-band of the original signal. We construct a linear filter bank with ten sub-bands, with frequencies ranging from 0 to 100 Hz, using ten fifth-order Butterworth Infinite Impulse Filter (IIR) bandpass filters, each with a passband of 10 Hz; these filters are known for their maximally flat frequency response in the passband. The frequency ranges of the ten filters are: (0-10) Hz, (10-20) Hz, (20-30) Hz,….,(90-100) Hz. The spectrally filtered signal obtained from each sub-time window is now subjected to

spatial filtering.

Common Spatial Pattern

The temporally-segmented and spectrally-filtered multi-variate EEG signal x is now spatially filtered by applying CSP [116] to each frequency sub-band. The aim of spatial filtering is to detect specific signal components of interest in the multi-variate EEG signal. CSP is an adaptive spatial filtering technique that combines the information from different channels to improve the discrimination between ADHD and non-ADHD classes. In the first step, the average sample covariance matrix C is computed for ADHD and non-ADHD classes using Eq. *(5.1)* and Eq. *(5.2),* respectively.

$$C_1 = \frac{x_1 \times x_1^T}{trace(x_1 \times x_1^T)} \tag{5.1}$$

$$C_2 = \frac{x_2 \times x_2^T}{trace(x_2 \times x_2^T)} \tag{5.2}$$

Here, the superscript T denotes the transpose of a matrix. x_1 and x_2 denote the time-varying EEG signals for classes 1 (ADHD) and 2 (non-ADHD), respectively, that are mean centred, i.e. the mean is subtracted from the EEG signals prior to the computation of covariance. The $trace(\cdot)$ operator in the denominator of Eq. *(5.1)* and Eq. *(5.2)* denotes the trace of the matrix obtained by multiplying the EEG signal with its transpose; its function is to normalize the covariance matrix. Next, we estimate the spatial filters by solving the generalized eigenvalue problem [116] given by Eq. *(5.3).*

$$C_1 \boldsymbol{\omega} = \boldsymbol{\lambda} C_2 \boldsymbol{\omega} \tag{5.3}$$

Here, $\boldsymbol{\lambda}$ is the set of all eigenvalues $\{\lambda_i\}$, and the matrix $\boldsymbol{\omega}$ is the set of all eigenvectors $\{\omega_i\}$ also known as spatial filters, where λ_i is the eigenvalue corresponding to the ith spatial filter ω_i corresponding to the ith column vector of the CSP matrix $\boldsymbol{\omega}$. Finally, the temporally-segmented and spectrally-filtered EEG signal x is projected onto the CSP matrix $\boldsymbol{\omega}$ to obtain the reduced dimension feature matrix y, as shown below

$$y = \boldsymbol{\omega}^T x \tag{5.4}$$

A total of $2d$ columns are selected from the transformed feature matrix y (first d

columns and last d columns of y, in order to maximize the variance between the two classes). In our experiments $d=3$, thus a total of 2d=6 spatially filtered signals are obtained as the outcome of this stage.

QEEG features

The EEG signal can be objectively and consistently examined by using quantitative EEG analysis, which entails collecting numerous statistical and signal-processing properties from the EEG. Quantitative EEG analysis is preferable to visual interpretation because it is a mathematical way to analyze a signal. The complete list of the twenty-seven QEEG features employed in this study is given in Table 5.5. This chapter proposes a framework that measures twenty seven QEEG features spread across three broad categories: power (amplitude characteristics), spectral (frequency characteristics), and inter-hemispheric connectivity; these three categories are chosen since they capture the inherent characteristics of a multi-channel EEG signal across multiple domains, unlike previous works in literature that have concentrated on fewer features. The power features are solely based on the signal power, signal envelope, and peak-to-peak voltage measurements. The spectral features are computed after transforming the signal into the frequency domain using FFT. Inter-hemispheric connectivity measures the interaction between the left and right brain hemispheres in terms of neural activity. The total number of features that are extracted from each time window is 1620=10×6×27. Here 10 is the number of sub-bands obtained after spectral filtering, 6 is the total number of channels that are selected after spatial filtering, and 27 is the number of QEEG features.

Window-based averaging of QEEG features

As explained in previous subsection, the EEG signal of duration $n \times t$ seconds is divided into n sub-time windows, each of duration t seconds, using the sliding window concept. The size of the sliding window t is set to 1.0 second with 75% overlap between successive sub-time windows. The QEEG signals computed from each time window are averaged to yield the final feature set for an EEG signal. Window-based averaging helps to reduce the variability of features over time as proved in earlier

works [44].

5.2.2 Classification of controls and patients with ADHD

Feature selection

For the next stage, we propose an ensemble of two feature selection approaches: a step-by-step wrapper technique and a filter method to select the most distinct QEEG features for ADHD identification. In the proposed framework, we ensemble two feature selection techniques named filter and wrapper. The filter technique is independent of the machine learning algorithm, and a rank is associated with each feature according to feature intrinsic properties that are measured via univariate statistics. In the ensemble feature selection approach, we use four methods- ANOVA, Information Gain Ratio, Gini index (GI) and chi-square that assign a rank to each of the 1620 features according their discrimination criteria. Then all the four ranks are averaged to obtain the new rank, the features are re-arranged as per the new rank, and after that feed-forward selection approach is employed to select the top-ranked features (233 features for dataset-1 and 241 features for dataset-2 after applying feed-forward selection). The obtained features are now passed to the four supervised machine learning algorithms to classify ADHD and non-ADHD children.

Table 5.5: A comprehensive list of the 27 QEEG features used in this study, with detailed descriptions of each feature's clinical relevance for children with ADHD

Feature	**Abbreviation**	**clinical relevance for children with ADHD**
F1 (Power)	ATP(Amplitude Total power)	Increased time-domain amplitude power due to delayed brain maturation and sensitivity to background noise, making focused attention difficult
F2 (Power)	ASD(Amplitude Standard Deviation)	Elevated standard deviation due to higher EEG variability corresponding to behavioral inconsistencies and attention fluctuations
F3 (Power)	ASKW(Amplitude Skewness)	Fluctuates between high positive skew (due to intermittent hyperarousal) and high negative skew (due to occasional lapses in attention)

F4 (Power)	AKR (Amplitude Kurtosis)	Elevated kurtosis due to short, high-amplitude bursts surrounded by low activity.
F5 (Power)	AEM (Amplitude Envelop Mean)	Low mean envelope level due to hypoarousal and cortical disengagement
F6 (Power)	AESD (Amplitude Envelop SD)	High standard deviation in the signal envelope due to inconsistent cognitive engagement
F7 (power)	REM (rEEG Mean)	Fluctuates between high peak-to-peak amplitude (due to intermittent hyperexcitability) and low peak-to-peak amplitude (due to reduced neural responsiveness)
F8 (power)	REMD (rEEG Median)	Fluctuates between high median value (due to intermittent hyperexcitability) and low median value (due to attention deficits)
F9 (Power)	RESD (rEEG SD)	High standard deviation due to erratic signal amplitude corresponding to alternating periods of overactivation and underactivation
F10 (Power)	RELM (rEEG Lower margin)	Low value of 5th percentile peak-to-peak voltage due to periods of minimal neural engagement
F11 (Power)	REUM (rEEG upper margin)	High value of 95th percentile peak-to-peak voltage due to intense spikes in cortical activity corresponding to restlessness and impulsivity
F12 (Power)	REW (rEEG width)	Larger inter-percentile range due to frequent shifts between hypo- and hyper-activation.
F13 (Power)	RCOV (rEEG Coefficient of variance)	High coefficient of variation due to high EEG variability and fluctuation
F14 (Power)	REASY(rEEG Asymmetry)	Fluctuates between negative symmetry (lapses of attention) and positive symmetry (hyperactivity or impulsivity)
F15 (Spectral Distribution)	SPAP (Spectral absolute power)	Increased theta power (due to immature cortical development) and reduced beta power (due to impaired cognitive control)
F16 (Spectral Distribution)	SPRP (Spectral relative power)	Increased theta to beta power ratio due to cortical hypoarousal and reduced cognitive engagement
F17 (Spectral Distribution)	SPF (Spectral Flatness- Winner Entropy)	Fluctuates between higher flatness (due to noise-like EEG spectrum) and lower flatness (due to abnormal oscillations in

		certain bands) reflecting dysfunctional brain network activity
F18 (Spectral Distribution)	SPD (Spectral Difference)	Increased spectral difference due to fluctuating levels of cortical arousal
F19 (Spectral Distribution)	SPE (Spectral Entropy- Shannon entropy)	Elevated spectral entropy due to disorganized, chaotic, and inefficient brain activity
F20 (Spectral Distribution)	SPEF (Spectral Edge Frequency)	Reduced spectral edge frequency due to increased slow-wave activity and cortical underarousal (increased theta and reduced beta activity)
F21 (Spectral Distribution)	FD (Fractal dimension)	Higher fractal dimension due to rougher EEG waveform with greater fluctuations indicating a brain that is overly reactive or struggling to maintain focus
F22 (Spectral Distribution)	PEEN (Permutation Entropy)	Increased permutation entropy corresponding to high brain signal irregularity caused due to variable attention, impulsivity, and unstable brain activity.
F23 (connectivity)	BSI(Brain symmetry index)	Elevated brain symmetry index due to abnormal hemispheric balance, linked to attention and control deficits
F24 (connectivity)	CORR(Correlation)	Low median envelope correlation between channel pairs in the left and right brain hemispheres due to poor inter-regional coordination
F25 (connectivity)	COHM (Mean coherence)	Reduced median of mean coherence between channel pairs in the left and right brain hemispheres due to weakened overall brain connectivity, linked to poor attention and control
F26 (connectivity)	COHMX (Connectivity coherence max)	Fluctuates between elevated (median of) maximum coherence in fronto-parietal regions and reduced (median of) maximum coherence in some slow-wave bands due to underconnectivity and over-synchronization, respectively.
F27 (connectivity)	COHFMX (Frequency of maximum coherence)	Lower median frequency of maximum coherence indicating dominance of slower rhythms in functional connectivity

Classification and Generalizability Test

After extracting the features, we used several machine learning algorithms to classify the EEG signal into ADHD and non-ADHD/control samples. The algorithms used include Support Vector Machine (SVM), k-Nearest Neighbor (kNN), Random Forest (RF), Artificial neural network (ANN) and eXtreme Gradient Boosting (XGBoost). Grid search was employed for hyperparameter tuning of all classifiers. The best values of the hyperparameters across all grids are specified in Table 5.6. To prove the generalizability of the proposed method, and to test its performance on unseen test samples, we implemented the Leave-One-Subject-Out (LOSO) experiment for both datasets. We acknowledge that LOSO evaluation can offer valuable insights into the model's generalization performance. The objective is to assess how effectively the model captures individual variability and generalizes to new cases.

Table 5.6: Hyperparameters of classifiers used in the experiment

SVM	kNN	RF	ANN	XGBoost
C=30 eps=0.1 kernal=RBF	K=14, manhattan distance	Trees=500 depth=6 10 feature/ node	[90,10] ReLu, Adam	Trees=180 depth=6 min. child weight=1

Algorithm 1: Proposed method for ADHD diagnosis

Input: Raw EEG signal
Output: Predicted class of EEG signal: ADHD or non-ADHD
Step1: Sub-time segmentation
The raw EEG signal is divided into n overlapping sub-time window segments of duration t seconds each, denoted by $S = \{S_1, S_2, S_3, \ldots, S_n\}$.
***Step 2*: Spectral filter**
Linear filter bank $\{b_i\}$ divides each time window segment S_i into ten sub-bands: $b_1, b_2, b_3, \ldots, b_{10}$.
***Step 3*: Spatial Filter**
For j=1 to the *number of spatial filters* do
3.1 Find the covariance matrix as per Eq. (5.1), Eq. (5.2)
3.2 Obtain spatial filter following Eq. (5.3)
3.3 Obtain the spatially filtered signal using Eq. (5.4)
End
***Step 4*: QEEG Feature Extraction**
Extract 1620=10×6×27 QEEG features from each sub-time window S_i.

***Step 5*: Window averaging**
The QEEG signals computed from different time windows are averaged to yield the final feature set for an EEG signal.
***Step 6:* Ensemble-based feature selection**

6.1 V is a vector of all the features such that $V = \{v_1, v_2, v_3, v_4, \ldots, v_f\}$ where f is the number of features (=1620)

6.2 R is a set of rankers defined as $R=\{r_1, r_2, r_3, \ldots\ldots, r_m\}$ where m is the total number of rankers.

For j in 1 to n do

Rank_order (j)=mean (Rank [$1: m, j$])

End

6.3 Select top-D features with the highest Rank_order

***Step 7*: Classification**

7.1 Train the classifiers: SVM, kNN, RF, ANN and XGBoost using top-D features

7.2 Classify the test EEG signal using trained model

5.2.3 Results and discussions

All experiments were conducted in MATLAB. We extracted the twenty-seven QEEG features from the spectral-spatial filtered EEG signal using the Neural Toolbox [120]. So, the total number of features that are extracted from each time window is 1620=10×6×27. Here, 10 is the number of sub-bands obtained after spectral filtering, 6 is the total number of channels that are selected after spatial filtering, and 27 is the number of QEEG features. Now, to minimize the temporal variance in the obtained features, we apply a window averaging technique on all the features so that the obtained features can provide a more consistent estimate of the signal.

In this section, we discuss the main findings of the work done in this work. The performance of the proposed framework is compared with the existing methods listed in Table 5.7 for both the datasets. We used 10-fold cross-validation to evaluate the proposed framework. The spectral-spatial filter bank with the unique set of twenty-seven features gives the best accuracy of 98.75±0.98% on dataset-1 and 98.68±0.52% on dataset-2 (with kNN classifier), respectively. The low values of standard deviation over the 10 folds prove that the proposed framework is fairly robust. We have compared our method with primary conventions in ADHD detection: - those that use conventional EEG features such as Theta/Beta Ratio (TBR) [11] and absolute and

relative power [83], and those that use spatial filter banks [18][90]. We have also compared with EEGNet a deep learning approach [133]. However, the traditional feature-based approaches [4][24] are not effective enough for ADHD detection as proved from the lower accuracies achieved. Bhati et al. [18] and Park et al. [90] are two other baseline comparison approaches. They used the spectral and spatial filter bank for EEG signal classification. However, they did not include any QEEG features and sub-time segmentation in their framework. On comparison with all other methods, our proposed framework performed better for both datasets. One of the factors causing the lower accuracy for the D1 dataset is that all the samples have varied lengths of longer duration. The shortest duration is 15.591 sec, while the largest duration is 84.476 sec. Whereas, for D2 dataset, all the sample size is fixed and short in length (1 sec duration). Considering our proposed method, we first segmented all the samples using a short time window. Therefore, our proposed method gives higher accuracy as compared to dataset 1. For the D1 dataset, due to fixed size of the short windows of each signal in the proposed framework, higher accuracies were achieved as compared to all other existing techniques.

Table 5.7 shows the results of LOSO validation on both datasets. The proposed method achieves the highest accuracy of 98.18±0.98% for dataset D1 and 97.69±0.52% for dataset D2 with the kNN classifier. We note that the LOSO accuracy is only marginally lower than the k-fold accuracy by 1-2%, thereby proving the generalizability of the proposed framework to unseen test samples.

Since, dataset-2 is imbalanced, we employed various sampling strategies: SMOTE, NRSB_SMOTE, MWMOTE and ADASYN to augment the minority class. The results are shown in Figure 5.6. SMOTE gives the best classification accuracy for the imbalanced dataset as compared to the other sampling strategies. The results in Table 5.7 show the results of SMOTE for the imbalanced dataset-2. SMOTE is applied to the training data to generate synthetic samples of the minority class to balance the class distribution. This can help improve the performance of classifiers when dealing with imbalanced datasets.

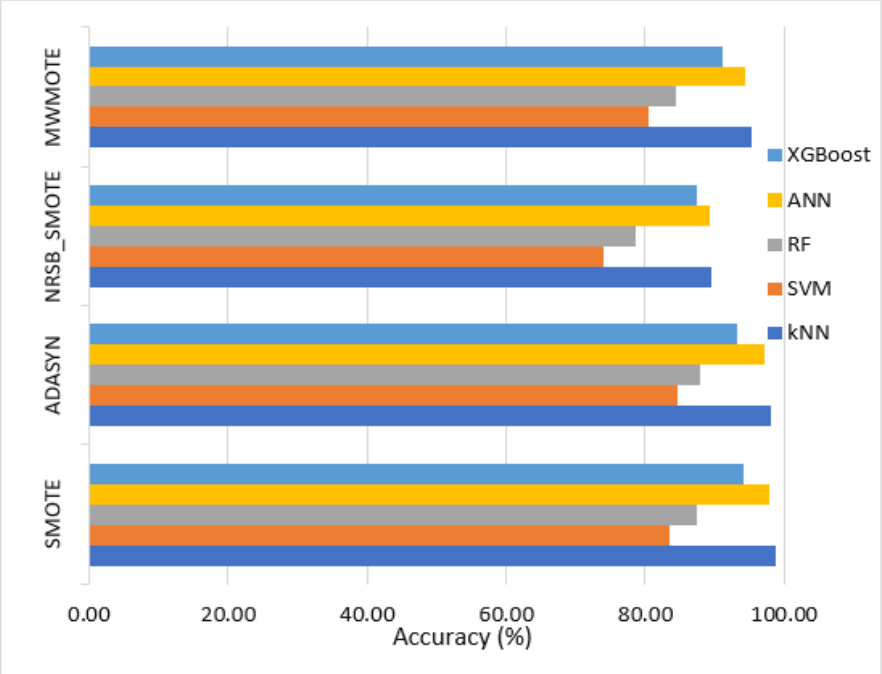

Figure. 5.6. Classification accuracy (%) of different sampling strategies–SMOTE, ADASYN, NRSB_SMOTE and MWMOTE, for the imbalanced dataset D2.

Table 5.7: Implementation details and performance comparison of the proposed method and the existing methods for the two ADHD datasets (D1: Dataset-1, D2: Dataset-2)

Study	EEG Channels		Features	Feature extraction	Feature selection method	Classifier	Accuracy (%)			
Study	D1	D2					LOSO (D1)	10-Fold CV (D1)	LOSO (D2)	10-Fold CV (D2)
TBR [11]	1	1	Theta/Beta Ratio	Cz electrode	-	kNN SVM RF ANN	75.65 59.49 51.21 54.27	78.12 63.58 53.95 58.99	80.12 57.43 48.59 52.96	83.46 62.42 54.63 57.56
Mumtaz et al. [83]	19	56	Absolute power, Relative power	All sub-bands	t-test and PCA	kNN SVM RF ANN	67.78 73.02 70.10 67.80	69.16 73.31 72.20 69.90	94.30 78.86 77.77 92.39	94.49 80.14 79.36 95.25

Toole et al. [120]	19	56	Spectral, Amplitude, peak-to peak voltage features	All sub-bands	-	kNN SVM RF ANN	73.39 73.13 79.50 78.94	73.68 76.02 81.46 81.38	91.31 76.14 70.26 88.52	96.52 79.31 74.11 93.38
Huang et al. [63]	19	56	Absolute power, Relative power, Permutation Entropy	All sub-bands	-	kNN SVM RF ANN	69.87±3 67.34 72.21 62.90	71.01 68.57 73.38 63..92	91.21 77.27 71.46 90.16	97.03 78.21 74.44 94.90
Bhatti et al. [18]	6	6	Linear Discriminant Analysis (LDA) Matrix	Sub-band CSP	Sequential Backward Floating Selection	kNN SVM RF ANN	96.19 80.39 84.97 94.12	98.56 82.71 86.53 97.84	91.76 77.79 85.02 91.59	93.44 80.53 85.36 94.23
Park et al. [90]	6	6	-	Sub-band CSP	MIBIF	kNN SVM RF ANN	78.45 54.49 76.69 77.75	78.77 56.64 77.78 79.34	94.39 85.23 87.95 93.24	96.12 87.51 90.11 93.43
Vahid et al. [133]	19	56	-	-	-	EEGNet (deep)	76.24	77.14	73.89	74.90
Holker and Susan [59]	19	56	Spectral, Amplitude, peak-to-peak voltage, Connectivity	All sub-bands	Majority voting scheme	kNN SVM RF ANN	70.11 71.02 74.67 69.58	71.25 72.60 75.88 71.73	95.65 ±0.79 78.34 75.55 82.66	97.01 81.43 77.09 85.57
Hamadicharef et al. [55]	18	18	-	Sub-band CSP	Mutual Information	FLD	91.23	94.21	94.89	97.53
Proposed method	6	6	Power, Spectral, Connectivity	Sub-time segmentation + Sub-band CSP	Feature selection Ensemble	kNN SVM RF ANN XGBoost	98.18 85.22 88.71 95.21 92.39	98.57 86.08 89.07 97.75 94.02	97.69 83.21 86.29 94.17 93.67	98.68 83.54 87.52 97.89 94.21

To evaluate the performance of all classifiers, the ROC-AUC receiver operating characteristic curves are shown in Figure. 5.7 with a 95% confidence interval. The ROC curve is a graph representation of the false positive rate and the true positive rate, and the maximum surface under the curve represents the best performance. In Figure 5.7 (a) and Figure 5.7 (b), the ROC curves of kNN, SVM, RF, ANN and XGBoost classifiers are shown for dataset-1 and dataset-2, respectively. The kNN classifier demonstrates consistently good performance in accordance with the trends in Table 5.7. We also conclude from the boxplots in Figures. 5.8 (a) and 5.8 (b) that kNN

classifier achieves the best classification accuracy as compared to the ANN, SVM and RF classifiers for both datasets.

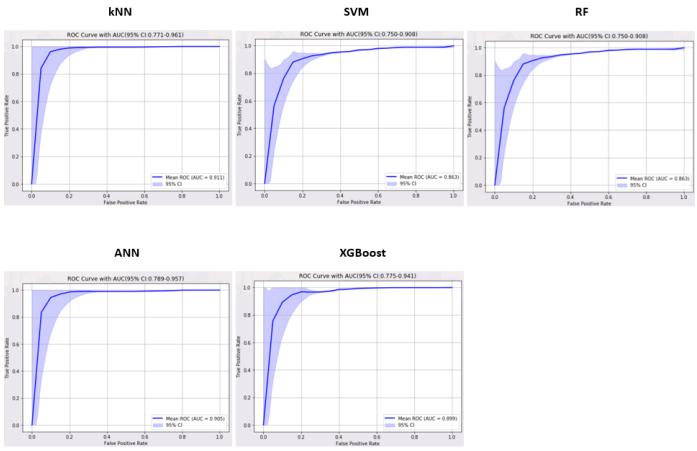

(a)

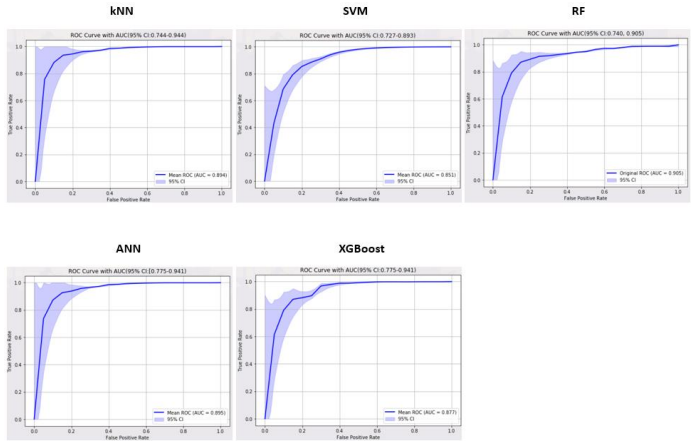

(b)

Figure. 5.7. ROC curves of kNN, SVM, RF, ANN and XGBoost classifiers for (a) dataset-1 and (b) dataset-2 shown for 95% confidence interval.

To plot the box-plots in Figure 5.8, nine parts of a complete set, from 10% to 90%, are selected. Ten training subgroups are randomly selected for each number to avoid biases in the database and provide statistically significant results. A total of 360 trials were conducted, each of which consisted of four classifications trained using a small training subgroup and tested using the complete test dataset. The results of the experiment are summarized in Figure 5.8, each box plot showing the variation in accuracy using four different classifiers for different fractions of the training dataset. On dataset-1, kNN and RF exhibit minimal variation in classification accuracy at lower fractions, indicating greater reliability compared to ANN and SVM for smaller training

subsets. For dataset-2, classification accuracy variation decreases as the training dataset fraction increases due to reduced variation in random subsets at higher fraction values across all five classifiers. The specificity and sensitivity scores for the proposed method are illustrated in Table 5.8. The kNN classifier demonstrates the best performance for both datasets in terms of both specificity and sensitivity indicating a high value of accuracy with low false negatives (high sensitivity), and a low value of false alarm rate (high specificity), as compared to all other classifiers. A comparison of the execution times of different models proves that the kNN classifier takes minimal time for execution, establishing its overall efficacy of the proposed approach.

To plot the box-plots in Figure 5.8, nine parts of a complete set, from 10% to 90%, are selected. Ten training subgroups are randomly selected for each number to avoid biases in the database and provide statistically significant results. A total of 360 trials were conducted, each of which consisted of four classifications trained using a small training subgroup and tested using the complete test dataset. The results of the experiment are summarized in Figure 5.8, each box plot showing the variation in accuracy using four different classifiers for different fractions of the training dataset. On dataset-1, kNN and RF exhibit minimal variation in classification accuracy at lower fractions, indicating greater reliability compared to ANN and SVM for smaller training subsets.

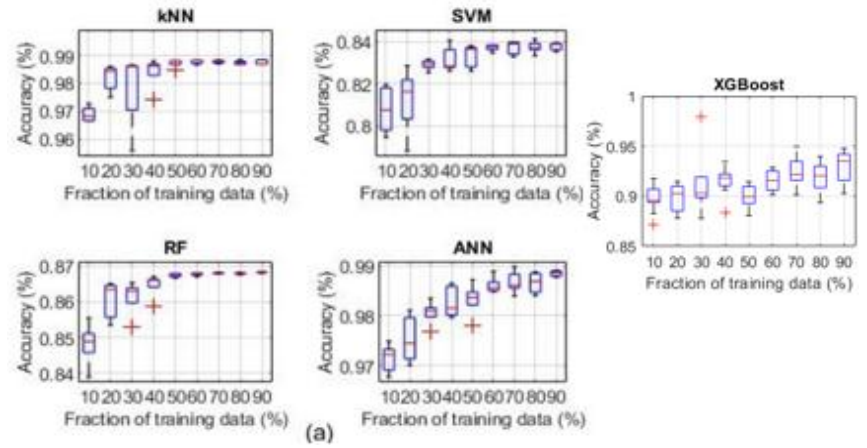

(a)

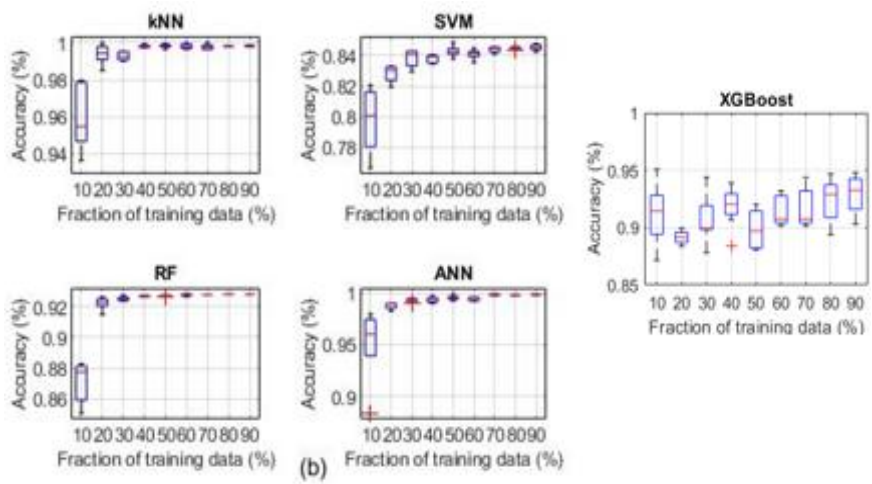

(b)

Figure 5.8. Boxplot representing the variation in accuracy for a varying fraction of the training set for (a) dataset-1 (b) dataset-2.

For dataset-2, classification accuracy variation decreases as the training dataset fraction increases due to reduced variation in random subsets at higher fraction values across all five classifiers. The specificity and sensitivity scores for the proposed method are illustrated in Table 5.8 The kNN classifier demonstrates the best performance for both datasets in terms of both specificity and sensitivity, indicating a high value of accuracy with low false negatives (high sensitivity), and a low value of false alarm rate (high specificity), as compared to all other classifiers. A comparison of the execution times of different models in Table 5.8 proves that the kNN classifier takes minimal time for execution, establishing its overall efficacy.

Table 5.8 Sensitivity and specificity values for the proposed method with execution time

Classifiers	Sensitivity		Specificity		Execution time (secs)
	D1	D2	D1	D2	
kNN	0.9899	0.9884	0.9831	0.9847	4.5
SVM	0.9078	0.8773	0.7939	0.7594	9.2
RF	0.9088	0.8865	0.8723	0.8658	10.4
ANN	0.9738	0.9756	0.9790	0.9806	18.3
XGBoost	0.9482	0.9572	0.9323	0.9268	109.2

We also analyze the total number of features selected from the different sub-bands in Figure 5.9 An analysis of the number of features selected per sub-band in Figure 5.9 reveals that for dataset-1, sub-bands 1, 4, 7 and 10 are important, while for dataset-2, sub-bands 1, 4, 6 and 10 are important for ADHD diagnosis. The range of the first sub-band which contributes the maximum number of features is 0-10 Hz, which implies that delta (0.5-4 Hz), theta (4-7 Hz) and alpha (7-13Hz) bands are more reliable for the diagnosis of ADHD in children; these findings are in agreement with neurobiological findings that inattentive symptoms are associated with the delta, alpha and gamma bands [70]. From gamma band (30-100 Hz), two sub-bands 30-40 Hz and 90-100 Hz show more significance than the other sub-bands. These high-frequency components in the gamma waves (> 30 Hz) have been less explored in the context of ADHD. However, recent research suggests that gamma activity could be associated with various cognitive functions, including perception, attention, and memory, which are impaired in individuals with ADHD [78]. The importance of the last few frequency bands (30-40Hz) and (90-100Hz), which are less recognized for ADHD detection, is indeed an intriguing finding of this research.

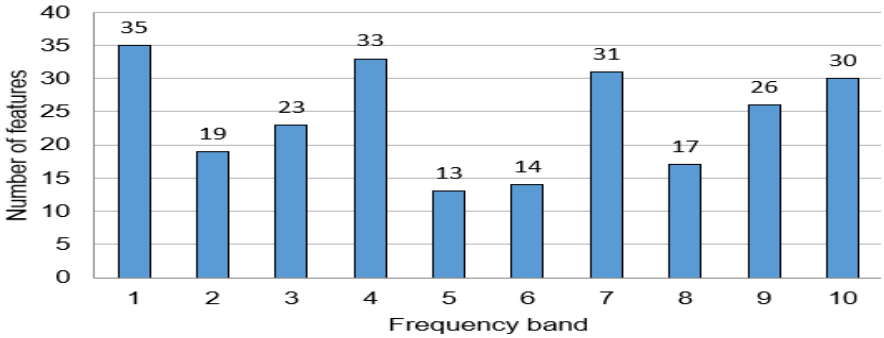

(a)

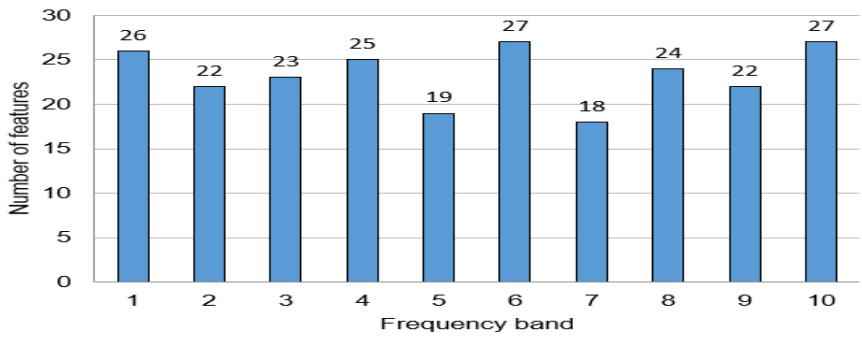

(b)

Figure 5.9 Selected feature distribution across all ten sub-bands for (a) dataset-1 (b) dataset-2.

One limitation of our approach is that kNN, which is the best performing classifier model, becomes computationally expensive when the feature space is very large. The problem may be mitigated by using efficient feature selection methods for dimensionality reduction. Additionally, feature selection strategies based on evolutionary or meta-heuristic optimization techniques such as genetic algorithm, particle swarm optimization, and differential evolution algorithms [4, 104], that advocate globally-optimal solutions in a large feature space, are expected to further boost the performance of the proposed diagnostic framework.

5.3 Conclusion

This chapter successfully demonstrated a comprehensive methodology for determining an optimal subset of relevant features from the temporal, spectral, and spatial domains of EEG signals. This is the first EEG-based ADHD early diagnosis study to integrate spectral-spatial filtering with sub-time segmentation for selecting discriminative QEEG features, broadly categorized into power, spectral, and connectivity groups. The main objective is to enhance classification performance and ensure the generalizability of diagnostic models for behavioral and neurodevelopmental disorders. The research presented here, based on studies into both AUD and ADHD, highlights the limitations of relying on a limited number of QEEG features. By employing a multi-domain approach, we were able to extract a rich and diverse set of neuro-biomarkers that comprehensively captured the neurological

underpinnings of these disorders. Specifically, our analysis included a wide range of QEEG features, such as: Spectral features captured the frequency characteristics of the EEG signal. Spatial/Connectivity features quantified the functional relationships between different brain regions, while Temporal features provided insights into the signal's statistical properties in the time domain. Another key finding of this chapter is the critical role of feature selection. Due to the large number of features extracted, a systematic feature selection process was essential to eliminate redundant or irrelevant data. The successful application of methods like Sequential Forward Selection (SFS) and ensemble-based feature selection effectively identified a smaller, highly predictive subset of features. This not only prevented model overfitting but also significantly improved the overall classification accuracy and reduced computational complexity.

Chapter 6

Conclusion

The primary objective of this thesis is to design and validate a robust and generalizable framework for the diagnosis of behavioral and neurological disorders, using a multi-domain features analysis of Electroencephalogram (EEG) signals. This work aimed to identify a subset of highly discriminative Quantitative EEG (QEEG) features that could be applied effectively across multiple brain disorders. The research presented in this thesis has successfully accomplished this objective.

6.1 Contributions of the Study

The first proposed framework (Chapter 3) demonstrated the statistical analysis of EEG signals to identify a novel discriminative set of Quantitative EEG (QEEG) features that exhibit generalizability across multiple brain disorders. The research highlighted the importance of a comprehensive feature set, incorporating power, spectral, and functional connectivity features to capture the diverse neurological patterns associated with conditions like Attention-Deficit Hyperactivity Disorder (ADHD) and Alcohol Use Disorder (AUD).

We next extracted the novel set of twenty-seven QEEG features from the spectrally- and spatially-filtered EEG signal for improved classification of brain disorders like

AUD (Chapter 5.1). CSP was applied for spatial filtering, while spectral filtering was performed using a linear filter bank. In a departure from normal, a wide frequency range (0 – 100 Hz) is considered for designing the spectral filter bank for the raw EEG signal. A linear filter bank is designed using a stack of ten non-overlapping filters of frequency band 10 Hz, with cut-off frequencies in the range 10-100 Hz. The aim is to capture the variation in brain electrical activity in the gamma frequency band (>30 Hz) which is typically ignored by most researchers, as compared to the delta (0.5-4 Hz), theta (4-8 Hz), alpha (8-12 Hz), and beta (12-30 Hz) frequency bands. In individuals with various brain disorders, deviations in these bands reflect underlying neural dysfunction and cognitive impairment. The spectrally-filtered signal is subject to spatial filtering using Common Spatial Pattern (CSP) algorithm, which is another highlight of this work. Spectro-spatial filtering enables the extraction of QEEG features from the most informative EEG channels in specific frequency sub-bands.

The proposed method surpasses state-of-the-art models, attaining peak diagnostic accuracies of 99.63% and 99.25% for the two cohorts using a Support Vector Machine classifier. Our results indicate that features from the lowest (delta, theta, and lower alpha) and highest (high gamma) frequency bands are the most effective for distinguishing alcoholic individuals.

Chapter 5.2 presents the first EEG-based approach for early ADHD diagnosis that integrates spectral-spatial filtering with sub-time segmentation to identify discriminative QEEG features spanning power, spectral, and connectivity categories. Generalizability is validated through subject-wise data splitting. Spectral features capture frequency patterns, power features reflect amplitude, and connectivity measures inter-hemispheric correlations and coherence. Ensemble-based feature selection identifies the most relevant features. Evaluated on two ADHD datasets—one small and balanced (121 participants) and one large and imbalanced (144 participants)—the method achieves peak accuracies of 98.57% and 98.68% (kNN, 10-fold CV), and 98.18% and 97.69% (LOSO), demonstrating strong diagnostic performance and subject-level generalizability.

Another achievement of this thesis is the implementation of functional connectivity analysis between different brain regions (Chapter 4), which are known to be significantly altered in various brain disorders. For this, we utilized the linear monotonic inter-electrode associations as the primary Quantitative EEG (QEEG) features in the time domain signal. By systematically computing the absolute value of the Pearson product-moment correlation coefficient between pairs of EEG electrodes across multiple frequency sub-bands, we were able to create a highly comprehensive map of brain functional connectivity. This approach generated a high-dimensional feature space, reflecting the intricate network of neural interactions.

Another contribution of this work is the wrapper-based sequential forward feature selection algorithm that leverages ten-fold stratified cross-validation for selecting the most significant QEEG biomarkers for AUD and ADHD diagnosis. The use of multiple feature ranking methods, such as ANOVA, Chi-square, Gini Index, and Information Gain ratio, in conjunction with sequential forward feature selection algorithm, proved to be a powerful strategy. This ensemble approach effectively filtered out irrelevant and redundant features, thereby reducing model complexity and preventing overfitting.

To validate the generalizability and predictive power of the identified feature subsets, a range of classification algorithms was employed in all the experiments conducted in this study. The use of multiple classifiers, specifically Support Vector Machine (SVM), K-Nearest Neighbours (KNN), Artificial Neural Network (ANN), Random Forest and XGBoost, proved that the success of the framework was not dependent on a single algorithm, but rather on the quality of the selected features.

6.2 Summary of Key Findings

This thesis makes several significant contributions to the fields of neuroinformatics and biomedical signal processing, which are summarized as follows.

- A novel feature set of twenty seven QEEG features is introduced for EEG signal classification, which effectively diagnoses various brain disorders.
- A generalizable framework applicable to the diagnosis of both behavioral and neurological brain disorders, including AUD and ADHD.
- Ensemble-based advanced feature selection techniques, integrating filter and wrapper techniques, to identify the most discriminative feature set in all experiments conducted in this thesis.
- Design and validation of a comprehensive generalizable multi-domain features framework that integrates temporal, spectral, and spatial domains for enhanced diagnostic performance.
- A novel framework for extracting functional connectivity QEEG features by computing band-wise absolute inter-electrode correlations. The EEG signal is first decomposed into five frequency sub-bands, and within each, the absolute Pearson correlation is calculated between electrode pairs across different brain regions.

The implications of this research are substantial. By providing a more objective and accurate diagnostic tool, this work has the potential to support clinicians in making more informed decisions, ultimately leading to earlier intervention and improved patient outcomes.

6.3 Future Work and Social Impact

While this thesis establishes a strong foundation, the following limitations and future research offer significant potential. Designing a generalizable framework for the diagnosis of various brain disorders is challenging. Thus, further, various deep learning algorithms can be explored. Also, new feature selection techniques could be utilized to find the discriminative features for classification.

The research presented in this thesis has the potential to generate significant social impact by transforming the diagnostic landscape for neurodevelopmental disorders. By providing an objective, data-driven diagnostic tool, it can reduce the reliance on subjective clinical assessments, which can sometimes lead to misdiagnosis or delayed

intervention. This can be particularly beneficial in low-resource settings where access to specialist clinicians is limited.

Future work can focus on integrating the enhanced accuracy and efficiency of the proposed diagnostic framework into clinical environments to enable earlier and more precise diagnoses. Such integration will facilitate timely interventions, which are critical for improving long-term outcomes and quality of life for individuals with ADHD, AUD, and related conditions. By supporting faster and more accurate diagnosis within real-world healthcare settings, this research has the potential to reduce stigma around these disorders and promote better patient care, ultimately contributing to a healthier society.

The framework lays the groundwork for the development of portable, real-time diagnostic systems. The computational efficiency achieved by identifying a minimal feature subset makes such tools feasible, enabling accurate diagnosis to be more accessible in low-resource settings and remote areas where specialist clinicians are not readily available.

Bibliography

[1] American Psychiatric Association, D. S., and American Psychiatric Association. Diagnostic and statistical manual of mental disorders: DSM-5. Vol. 5. Washington, DC: American psychiatric association, 2013.

[2] Acharya, U. Rajendra, Sumitha Adeli, and Hojjat Adeli. "Computer-aided diagnosis of alcoholism-related EEG signals." Epilepsy & Behavior 41 (2014): 257-263.

[3] Acharya U. Rajendra, Shu Lih Oh, Yuki Hagiwara, Jen Hong Tan, and Hojjat Adeli. "Deep convolutional neural network for the automated detection and diagnosis of seizure using EEG signals." Computers in biology and medicine 100 (2018): 270-278.

[4] Agrawal, Prachi, Hattan F. Abutarboush, Talari Ganesh, and Ali Wagdy Mohamed. "Metaheuristic algorithms on feature selection: A survey of one decade of research (2009-2019)." Ieee Access 9 (2021): 26766-26791.

[5] Aydın, Serap, Fatih Hilmi Cetin, Merve Çıkılı Uytun, Zehra Babadagi, Ahmet Sami Gueven, and Yasemen Işık. "Comparison of domain specific connectivity metrics for estimation brain network indices in boys with ADHD-C." Biomedical Signal Processing and Control 76 (2022): 103626.

[6] Al-Hadeethi H, Abdulla S, Diykh M, Deo RC, Green JH. An Eigenvalues-Based Covariance Matrix Bootstrap Model Integrated With Support Vector Machines for Multichannel EEG Signals Analysis. Front Neuroinform. 2022;15:808339.

[7] Al-Hadeethi, Hanan Ali Hammoodi. "Developing artificial intelligence models for classification of brain disorder diseases based on statistical techniques."

PhD diss., University of Southern Queensland, 2021.

[8] Allahverdy, Armin, Alireza Khorrami Moghadam, Mohammad Reza Mohammadi, and Ali Motie Nasrabadi. "Detecting adhd children using the attention continuity as nonlinear feature of eeg." Frontiers in Biomedical Technologies 3, no. 1-2 (2016): 28-33.

[9] Anuragi, Arti, Dilip Singh Sisodia, and Ram Bilas Pachori. "Automated alcoholism detection using Fourier-Bessel series expansion based empirical wavelet transform." IEEE Sensors Journal 20, no. 9 (2020): 4914-4924.

[10] Anuragi, Arti, and D. Singh Sisodia. "Alcohol use disorder detection using EEG Signal features and flexible analytical wavelet transform." Biomedical Signal Processing and Control 52 (2019): 384-393.

[11] Arns, Martijn, C. Keith Conners, and Helena C. Kraemer. "A decade of EEG theta/beta ratio research in ADHD: a meta-analysis." Journal of attention disorders 17, no. 5 (2013): 374-383.

[12] Barttfeld, Pablo, Agustín Petroni, Sandra Báez, Hugo Urquina, Mariano Sigman, Marcelo Cetkovich, Teresa Torralva et al. "Functional connectivity and temporal variability of brain connections in adults with attention deficit/hyperactivity disorder and bipolar disorder." Neuropsychobiology 69, no. 2 (2014): 65-75.

[13] Bavkar, Sandeep, Brijesh Iyer, and Shankar Deosarkar. "Rapid Screening of Alcoholism: An EEG Based Optimal Channel Selection Approach." IEEE Access 7 (2019): 99670-99682.

[14] Bavkar, Sandeep, Brijesh Iyer, and Shankar Deosarkar. "Optimal EEG channels selection for alcoholism screening using EMD domain statistical features and harmony search algorithm." Biocybernetics and Biomedical

Engineering 41, no. 1 (2021): 83-96.

[15] Belete DM, Huchaiah MD. Grid search in hyperparameter optimization of machine learning models for prediction of HIV/AIDS test results. International Journal of Computers and Applications. 2022 Sep 2;44(9):875-86.

[16] Bernardin, F., A. Maheut-Bosser, and F. Paille. "Cognitive Impairments in Alcohol-Dependent Subjects." Frontiers in psychiatry 5 (2014): 78.

[17] Berry, M.S. and Pentreath V.W(1980): The neurophysiology of alcohol. In: Sandler, M(Ed.) Psychopharmacology of Alcohol. Raven press, New York, pp.43-72.

[18] Bhatti, Muhammad Hamza, Javeria Khan, Muhammad Usman Ghani Khan, Razi Iqbal, Moayad Aloqaily, Yaser Jararweh, and Brij Gupta. "Soft computing-based EEG classification by optimal feature selection and neural networks." IEEE Transactions on Industrial Informatics 15, no. 10 (2019): 5747-5754.

[19] Bhatti, Muhammad Iqbal, A. Pervaiz, and Mirza Haris Baig. "EEG signal decomposition and improved spectral analysis using wavelet transform." In 2001 Conference Proceedings of the 23rd Annual International Conference of the IEEE Engineering in Medicine and Biology Society, vol. 2, pp. 1862-1864. IEEE, 2001.

[20] Bonita, J. D. et al. "Time domain measures of inter-channel EEG correlations: a comparison of linear, nonparametric and nonlinear measures." Cognitive Neurodynamics 8, no. 1 (2014): 1-15.

[21] Bragard, E, Giorgi S, Juneau P, Curtis BL. Loneliness and daily alcohol consumption during the COVID-19 pandemic. Alcohol and Alcoholism (Oxford, Oxfordshire). 2022; 57(2):198.

[22] Campanella, S., G. Petit, P. Maurage, C. Kornreich, P. Verbanck, and X. Noël. "Chronic alcoholism: Insights from neurophysiology." Neurophysiologie Clinique/Clinical Neurophysiology 39, no. 4-5 (2009): 191-207.

[23] Çetin, Fatih Hilmi, Miraç Barış Usta, Serap Aydın, and Ahmet Sami Güven. "A case study on EEG analysis: embedding entropy estimations indicate the decreased neuro-cortical complexity levels mediated by methylphenidate treatment in children with ADHD." Clinical EEG and Neuroscience 53, no. 5 (2022): 406-417.

[24] Chakladar, D. D., and S. Chakraborty. "EEG based emotion classification using “Correlation Based Subset Selection”." Biological Inspired Cognitive Architecture 24 (2018): 98-106.

[25] Chen, He, Yan Song, and Xiaoli Li. "A deep learning framework for identifying children with ADHD using an EEG-based brain network." Neurocomputing 356 (2019): 83-96.

[26] Clarke, Adam R., Robert J. Barry, Rory McCarthy, and Mark Selikowitz. "EEG analysis of children with attention-deficit/hyperactivity disorder and comorbid reading disabilities." Journal of learning disabilities 35, no. 3 (2002): 276-285.

[27] Crone NE, Korzeniewska A, Franaszczuk PJ. Cortical gamma responses: searching high and low. International Journal of Psychophysiology. 2011 Jan 1;79(1):9-15.

[28] Cura, Ozlem Karabiber, Sibel Kocaaslan Atli, and Aydin Akan. "Attention deficit hyperactivity disorder recognition based on intrinsic time-scale decomposition of EEG signals." Biomedical Signal Processing and Control 81 (2023): 104512.

[29] Das, K., V. K. Singh, and R. B. Pachori. "Introduction to EEG Signal Recording and Processing." In Artificial Intelligence Enabled Signal Processing based Models for Neural Information Processing, pp. 1-19. CRC Press.

[30] Das, K., and R. B. Pachori. "Schizophrenia detection technique using multivariate iterative filtering and multichannel EEG signals." Biomedical Signal Processing and Control 67 (2021): 102525.

[31] Das, K., and R. B. Pachori. "Multivariate Iterative Filtering-Based SSVEP Detection in Mobile Environment for Brain–Computer Interface Application." IEEE Sensors Letters (2024).

[32] Das, K., and R. B. Pachori. "Electroencephalogram-based motor imagery brain–computer interface using multivariate iterative filtering and spatial filtering." IEEE Transactions on Cognitive and Developmental Systems 15, no. 3 (2022): 1408-1418.

[33] Deshmukh, Manjusha, Mahi Khemchandani, and Paramjit Mahesh Thakur. "Contributions of brain regions to machine learning-based classifications of attention deficit hyperactivity disorder (ADHD) utilizing EEG signals." Applied Neuropsychology: Adult (2024): 1-15.

[34] Dorvashi M, Behzadfar N, Shahgholian G. An efficient method for classification of alcoholic and normal electroencephalogram signals based on selection of an appropriate feature. J Med Signals Sens. 2023;13(1):11.

[35] Ebrahimi, A., U. K. Wiil, T. Schmidt, A. Naemi, A. S. Nielsen, G. M. Shaikh, and M. Mansourvar. "Predicting the Risk of Alcohol Use Disorder Using Machine Learning: A Systematic." IEEE Access 9 (2021): 151697-151712.

[36] Ekhlasi, Ali, Ali Motie Nasrabadi, and Mohammad Reza Mohammadi. "Direction of information flow between brain regions in ADHD and healthy children based on EEG by using directed phase transfer entropy." Cognitive Neurodynamics 15, no. 6 (2021): 975-986.

[37] Ekhlasi, Ali, Ali Motie Nasrabadi, and Mohammadreza Mohammadi. "Analysis of EEG brain connectivity of children with ADHD using graph theory and directional information transfer." Biomedical Engineering/Biomedizinische Technik 68, no. 2 (2023): 133-146.

[38] Ekhlasi, Ali, Ali Motie Nasrabadi, and Mohammad Reza Mohammadi. "Analysis of effective connectivity strength in children with attention deficit hyperactivity disorder using phase transfer entropy." Iranian Journal of Psychiatry 16, no. 4 (2021): 374.

[39] Ekhlasi, Ali, Ali Motie Nasrabadi, and Mohammadreza Mohammadi. "Classification of the children with ADHD and healthy children based on the directed phase transfer entropy of EEG signals." Frontiers in Biomedical Technologies (2021).

[40] Einizade, Aref, Mohsen Mozafari, Mohammadreza Rezaei-Dastjerdehei, Elnaz Aghdaei, Amir Mohammad Mijani, and Sepideh Hajipour Sardouie. "Detecting adhd children using the attention continuity as nonlinear feature of eeg." Frontiers in Biomedical Technologies 3, no. 1-2 (2016): 28-33.

[41] Farsi, L., S. Siuly, E. Kabir, and H. Wang. "Classification of alcoholic EEG signals using a deep learning method." IEEE Sensors Journal 21, no. 3 (2020): 3552–3560.

[42] Fattah, S. A., K. Fatima, and C. Shahnaz. "An approach for classifying alcoholic and non-alcoholic persons based on time domain features extracted from EEG signals." In 2015 IEEE International WIE conference on Electrical

and Computer Engineering (WIECON-ECE), pp. 479-482. IEEE, 2015.

[43] Fira, M., H.N. Costin, L. Goraș. "On the classification of ECG and EEG signals with various degrees of dimensionality reduction." Biosensors 11, no. 5 (2021): 161.

[44] García-Ponsoda, Sandra, Alejandro Maté, and Juan Trujillo. "Refining ADHD diagnosis with EEG: The impact of preprocessing and temporal segmentation on classification accuracy." Computers in Biology and Medicine 183 (2024): 109305.

[45] Garn, H., C. Coronel, M. Waser, G. Caravias, and G. Ransmayr. "Differential diagnosis between patients with probable Alzheimer's disease, Parkinson's disease dementia, or dementia with Lewy bodies and frontotemporal dementia, behavioral variant, using quantitative electroencephalographic features." J. Neural Transm. (Vienna) 124, no. 5 (2017): 569–581.

[46] Gaur, Pramod, Harsh Gupta, Anirban Chowdhury, Karl McCreadie, Ram Bilas Pachori, and Hui Wang. "A sliding window common spatial pattern for enhancing motor imagery classification in EEG-BCI." IEEE Transactions on Instrumentation and Measurement 70 (2021): 1-9.

[47] Gaur, P., K. McCreadie, R. B. Pachori, H. Wang, and G. Prasad. "An automatic subject specific channel selection method for enhancing motor imagery classification in EEG-BCI using correlation." Biomedical Signal Processing and Control 68 (2021): 102574.

[48] Ghassemi, Farnaz, Mohammad Hassan Moradi, Mehdi Tehrani-Doost, and Vahid Abootalebi. "Using nonlinear features of EEG for ADHD/normal participants' classification." Procedia-Social and Behavioral Sciences 32 (2012): 148-152.

[49] Ghassemi, Farnaz, Mohammad Hassan Moradi, Mehdi Tehrani-Doost, and Vahid Abootalebi. "Classification of ADHD/normal participants using frequency features of ERP's Independent Components." In 2010 17th Iranian Conference of Biomedical Engineering (ICBME), pp. 1-4. IEEE, 2010.

[50] Gibbings A, Ray LB, Gagnon S, Collin CA, Robillard R, Fogel SM. The EEG correlates and dangerous behavioral consequences of drowsy driving after a single night of mild sleep deprivation. Physiology & Behavior. 2022 Aug 1;252:113822.

[51] González, Julián J., Guzmán Alba, Soledad Mañas, Almudena González, and Ernesto Pereda. "Assessment of ADHD through electroencephalographic measures of functional connectivity." ADHD-New Dir. Diagnosis Treat (2017): 35-54.

[52] Greenblatt, Milton and Sidney Levin. "The electroencephalogram associated with chronic alcoholism, alcoholic psychosis and alcoholic convulsions." Archives of Neurology & Psychiatry 52, no. 4 (1944): 290-295.

[53] Guntaka R, Tcheslavski G. On the EEG-based automated detection of alcohol dependence. International Journal Bioautomation. 2013;17(3):167.

[54] Hakim, N., E. Awh, E. K. Vogel, and M. D. Rosenberg. "Inter-electrode correlations measured with EEG predict individual differences in cognitive ability." Current Biology 31, no. 22 (2021): 4998-5008.e6.

[55] Hamadicharef, Brahim, Haihong Zhang, Cuntai Guan, Chuanchu Wang, Kok Soon Phua, Keng Peng Tee, and Kai Keng Ang. "Learning EEG-based spectral-spatial patterns for attention level measurement." In 2009 IEEE International Symposium on Circuits and Systems (ISCAS), pp. 1465-1468. IEEE, 2009

[56] Hasin D. Classification of alcohol use disorders. Alcohol Research & Health. 2003;27(1):5.

[57] Hettich, S. and Bay, S. D. The UCI KDD Archive [http://kdd.ics.uci.edu], Irvine, CA: University of California, Department of Information and Computer Science. 1999.

[58] Hjorth B. EEG analysis based on time domain properties. Electroencephalography and clinical neurophysiology. 1970 Sep 1;29(3):306-10.

[59] Holker, Ruchi, and Seba Susan. "Quantitative EEG Feature Selection by MajorityVoting for Alcohol Use Disorder Detection." In 2021 IEEE EMBS International Conference on Biomedical and Health Informatics (BHI), pp. 1-4. IEEE, 2021.

[60] Holker, Ruchi, and Seba Susan. "Computer-Aided Diagnosis Framework for ADHD Detection Using Quantitative EEG." In Brain Informatics: 15th International Conference, BI 2022, Padua, Italy, July 15–17, 2022, Proceedings, pp. 229-240. Cham: Springer International Publishing, 2022.

[61] Holker R, Susan S. Linear Monotonic Inter-electrode Associations as Quantitative EEG for Alcoholism Diagnosis. International Journal of Computational Intelligence Systems. 2024 Sep 30;17(1):250.

[62] Holker, Ruchi, and Seba Susan. "Neuroscience-Inspired Parameter Selection of Spiking Neuron Using Hodgkin Huxley Model." International Journal of Software Science and Computational Intelligence (IJSSCI) 13, no. 2 (2021): 89-106.

[63] Huang, Huijin, Zikang Niu, Gang Liu, Mengdi Jiang, Qingxia Jia, Xiaoli Li, and Yingying Su. "Early consciousness disorder in acute large hemispheric

infarction: an analysis based on quantitative EEG and brain network characteristics." Neurocritical Care 33, no. 2 (2020): 376-388.

[64] Ildar, R. "Deep learning and machine learning for EEG signal processing on the example of recognizing the disease of alcoholism." bioRxiv, medRxiv (2021).

[65] Jiajie L, Narasimhan K, Elamaran V, Arunkumar N, Solarte M, Ramirez-Gonzalez G. Clinical decision support system for alcoholism detection using the analysis of EEG signals. IEEE Access. 2018 Oct 14;6:61457-61.

[66] Kaur, Simranjit, Priti Arun, Sukhwinder Singh, and Damanjeet Kaur. "EEG Based Decision Support System to Diagnose Adults with ADHD." In 2018 IEEE Applied Signal Processing Conference (ASPCON), pp. 87-91. IEEE, 2018.

[67] Khare, S. K., V. Bajaj, and G. R. Sinha. "Adaptive tunable Q wavelet transform-based emotion identification." IEEE transactions on instrumentation and measurement 69, no. 12 (2020): 9609–9617.

[68] Khaleghi N, Hashemi S, Peivandi M, Ardabili SZ, Behjati M, Sheykhivand S, Danishvar S. EEG-based functional connectivity analysis of brain abnormalities: A review study. Informatics in Medicine Unlocked. 2024 Mar 21:101476.

[69] Khoshnoud, Shiva, Mohammad Ali Nazari, and Mousa Shamsi. "Functional brain dynamic analysis of ADHD and control children using nonlinear dynamical features of EEG signals." Journal of integrative neuroscience 17, no. 1 (2018): 17-30.

[70] Kiiski, Hanni, Laura M. Rueda-Delgado, Marc Bennett, Rachel Knight, Laura Rai, Darren Roddy, Katie Grogan, Jessica Bramham, Clare Kelly, and Robert

Whelan. "Functional EEG connectivity is a neuromarker for adult attention deficit hyperactivity disorder symptoms." Clinical Neurophysiology 131, no. 1 (2020): 330-342.

[71] Li, Y., T. Zhang, B. Wang, and M. Nakamura. "EEG and related physiological signals investigation under the condition of +Gz accelerations." In 2012 ICME International Conference on Complex Medical Engineering (CME), Kobe, Japan, 2012.

[72] Liu, H., Y. Gao, J. Zhang, and J. Zhang. "Epilepsy EEG classification method based on supervised locality preserving canonical correlation analysis." Math. Biosci. Eng. 19, no. 1 (2022): 624–642.

[73] Liu Y, Chen Y, Fraga-González G, Szpak V, Laverman J, Wiers RW, Richard Ridderinkhof K. Resting-state EEG, substance use and abstinence after chronic use: a systematic review. Clinical EEG and Neuroscience. 2022 Jul;53(4):344-66.

[74] Luo, Tian-jian. "Selective multi–view time–frequency decomposed spatial feature matrix for motor imagery EEG classification." Expert Systems with Applications 247 (2024): 123239.

[75] Mahato, A., K. Das, and R. B. Pachori. "A Multivariate Approach for Drowsiness Detection Using Empirical Fourier Decomposition." Authorea Preprints (2023).

[76] Malan, Nitesh Singh, and Shiru Sharma. "Time window and frequency band optimization using regularized neighbourhood component analysis for Multi-View Motor Imagery EEG classification." Biomedical Signal Processing and Control 67 (2021): 102550.

[77] Maniruzzaman, Md, Jungpil Shin, Md Al Mehedi Hasan, and Akira Yasumura.

"Efficient Feature Selection and Machine Learning Based ADHD Detection Using EEG Signal." Computers, Materials & Continua 72, no. 3 (2022).

[78] Mateos, Diego M., Gabriela Krumm, Vanessa Arán Filippetti, and Marisel Gutierrez. "Power spectrum and connectivity analysis in EEG recording during attention and creativity performance in children." NeuroSci 3, no. 2 (2022): 347-365.

[79] Mehla, V. K., A. Singhal, and P. Singh. "A novel approach for automated alcoholism detection using Fourier decomposition method." J. Neurosci. Methods 346 (2020): 108945.

[80] Mikola, A., I. Ratsep, M. Sarkela, and T. Lipping. "Prediction of outcome in traumatic brain injury patients using long-term qEEG features." In 2015 37th Annual International Conference of the IEEE Engineering in Medicine and Biology Society (EMBC), Milan, 2015.

[81] Mohammadi, Mohammad Reza, Ali Khaleghi, Ali Moti Nasrabadi, Safa Rafieivand, Moslem Begol, and Hadi Zarafshan. "EEG classification of ADHD and normal children using nonlinear features and neural network." Biomedical Engineering Letters 6, no. 2 (2016): 66-73.

[82] Moselhy, H. F., G. Georgiou, and A. Kahn. "Frontal lobe changes in alcoholism: a review of the literature." Alcohol Alcohol 36, no. 5 (2001): 357–368.

[83] Mumtaz, Wajid, Pham Lam Vuong, Likun Xia, Aamir Saeed Malik, and Rusdi Bin Abd Rashid. "Automatic diagnosis of alcohol use disorder using EEG features." Knowledge-Based Systems 105 (2016): 48-59.

[84] Mumtaz, Wajid, Pham Lam Vuong, Likun Xia, Aamir Saeed Malik, and Rusdi Bin Abd Rashid. "An EEG-based machine learning method to screen alcohol

use disorder." Cognitive neurodynamics 11, no. 2 (2017): 161-171.

[85] Neeraj, V. Singhal, and J. Mathew. "A deep learning architecture for spatio-temporal feature extraction and alcoholism detection." in 2021 IEEE EMBS International Conference on Biomedical and Health Informatics (BHI), Athens, Greece, 2021.

[86] Ong, Kok-Meng, K-H. Thung, Chong-Yaw Wee, and Raveendran Paramesran. "Selection of a subset of EEG channels using PCA to classify alcoholics and non-alcoholics." In 2005 IEEE Engineering in Medicine and Biology 27th Annual Conference, pp. 4195-4198. IEEE, 2006.

[87] O'Reilly, Deirdre, Michael A. Navakatikyan, Marcia Filip, Deirdre Greene, and Linda J. Van Marter. "Peak-to-peak amplitude in neonatal brain monitoring of premature infants." Clinical neurophysiology 123, no. 11 (2012): 2139-2153.

[88] Park, Y., and W. Chung. "A novel EEG correlation coefficient feature extraction approach based on demixing EEG channel pairs for cognitive task classification." IEEE Access 8 (2020): 87422–87433.

[89] Park, Y., and W. Chung. "Optimal channel selection using correlation coefficient for CSP based EEG classification." IEEE Access 8 (2020): 111514–111521.

[90] Park, S.-H., D. Lee, and S.-G. Lee. "Filter bank regularized common spatial pattern ensemble for small sample motor imagery classification." IEEE Trans. Neural Syst. Rehabil. Eng. 26, no. 2 (2018): 498–505.

[91] Pei, Z., H. Wang, A. Bezerianos, and J. Li. "EEG-based multiclass workload identification using feature fusion and selection." IEEE Trans. Instrum. Meas. 70 (2021): 1–8.

[92] Peng, G., M. Nourani, J. Harvey, and H. Dave. "Personalized Feature Selection for Wearable EEG Monitoring Platform." In 2020 IEEE 20th International Conference on Bioinformatics and Bioengineering (BIBE), pp. 380-386. IEEE, 2020.

[93] Peng, G., M. Nourani, J. Harvey and H. Dave. "Feature Selection Using F-statistic Values for EEG Signal Analysis." In 42th Annual International Conference of the IEEE Engineering in Medicine & Biology Society (EMBC), 2020, pp 5963-5966.

[94] Peng, G., M. Nourani, H. Dave and J. Harvey. "SEEG-Based Epileptic Seizure Network Modeling and Analysis for Pre-surgery Evaluation." Computers in Biology and Medicine 167 (2023): 107692.

[95] Priya, Anchala, Pooja Yadav, Shweta Jain, and Varun Bajaj. "Efficient method for classification of alcoholic and normal EEG signals using EMD." The Journal of Engineering 2018, no. 3 (2018): 166-172.

[96] Ramlakhan JU, Ma M, Zomorrodi R, Blumberger DM, Noda Y, Barr MS. The role of gamma oscillations in the pathophysiology of substance use disorders. Journal of personalized medicine. 2020 Dec 28;11(1):17.

[97] Rezaeezadeh, Maryam, Sina Shamekhi, and Mousa Shamsi. "Attention Deficit Hyperactivity Disorder Diagnosis using nonlinear univariate and multivariate EEG measurements: a preliminary study." Physical and engineering sciences in medicine 43, no. 2 (2020): 577-592.

[98] Robinson, N., K. P. Thomas, and A. P. Vinod. "Canonical correlation analysis of EEG for classification of motor imagery." in 2017 IEEE International Conference on Systems, Man, and Cybernetics (SMC), Banff, AB, 2017.

[99] Rodrigues JD, Rebouças Filho PP, Peixoto Jr E, Kumar A, de Albuquerque VH. Classification of EEG signals to detect alcoholism using machine learning techniques. Pattern Recognition Letters. 2019 Jul 1;125:140-9.

[100] Rodrak, Supassorn, and Yodchanan Wongsawat. "EEG brain mapping and brain connectivity index for subtypes classification of attention deficit hyperactivity disorder children during the eye-opened period." In 2013 35th annual international conference of the IEEE engineering in medicine and biology society (EMBC), pp. 7400-7403. IEEE, 2013.

[101] Saby, Joni N., and Peter J. Marshall. "The utility of EEG band power analysis in the study of infancy and early childhood." Developmental neuropsychology 37, no. 3 (2012): 253-273.

[102] Sadiq MT, Siuly S, Almogren A, Li Y, Wen P. Efficient novel network and index for alcoholism detection from EEGs. Health Information Science and Systems. 2023 Jun 17;11(1):27.

[103] Saddam, M., H. Tjandrasa, and D. A. Navastara. "Classification of alcoholic EEG using wavelet packet decomposition, principal component analysis, and combination of genetic algorithm and neural network." in 2017 11th International Conference on Information & Communication Technology and System (ICTS), IEEE, 2017, pp. 19–24.

[104] Sanei, Saeid, and Jonathon A. Chambers. EEG signal processing and machine learning. John Wiley & Sons, 2021.

[105] Shaw, J. C. "Correlation and coherence analysis of the EEG: a selective tutorial review." International Journal of Psychophysiology 1, no. 3 (1984): 255–266.

[106] Sharma, Manish, Dipankar Deb, and U. Rajendra Acharya. "A novel three-

band orthogonal wavelet filter bank method for an automated identification of alcoholic EEG signals." Applied Intelligence 48, no. 5 (2018): 1368-1378.

[107] Shooshtari, M. Alavash, and S. Kamaledin Setarehdan. "Selection of optimal EEG channels for classification of signals correlated with alcohol abusers." In IEEE 10th INTERNATIONAL CONFERENCE ON SIGNAL PROCESSING PROCEEDINGS, pp. 1-4. IEEE, 2010.

[108] Shri, T. K. Padma, and Natarajan Sriraam. "Pattern recognition of spectral entropy features for detection of alcoholic and control visual ERP's in multichannel EEGs." Brain informatics 4, no. 2 (2017): 147-158.

[109] Siuly, S., and Y. Li. "Improving the separability of motor imagery EEG signals using a cross correlation-based least square support vector machine for brain-computer interface." IEEE Trans. Neural Syst. Rehabil. Eng. 20, no. 4 (2012): 526–538.

[110] Siuly, S., Bajaj, V., Sengur, A. and Zhang, Y., 2019. An advanced analysis system for identifying alcoholic brain state through EEG signals. International Journal of Automation and Computing, 16(6), pp.737-747.

[111] Singh, Ajay, Chia Jung Yeh, Nidhi Verma, and Ajay Kumar Das. "Overview of attention deficit hyperactivity disorder in young children." Health psychology research 3, no. 2 (2015).

[112] Snodgrass JG, Vanderwart M. A standardized set of 260 pictures: norms for name agreement, image agreement, familiarity, and visual complexity. Journal of experimental psychology: Human learning and memory. 1980 Mar;6(2):174.

[113] Sohn, Hansem, Wonhye Lee, Inhye Kim, and Jaeseung Jeong. "Approximate entropy (ApEn) analysis of the EEG in attention-deficit/hyperactivity disorder

(AD/HD) during cognitive tasks." In *World Congress on Medical Physics and Biomedical Engineering 2006: August 27–September 1, 2006 COEX Seoul, Korea "Imaging the Future Medicine"*, pp. 1083-1086. Berlin, Heidelberg: Springer Berlin Heidelberg, 2007.

[114] Stancin, I., M. Cifrek, and A. Jovic. "A review of EEG signal features and their application in driver drowsiness detection systems." Sensors (Basel) 21, no. 11 (2021): 3786.

[115] Susan, Seba, Aishwary Kumar, and Anmol Jain. "Evaluating Heterogeneous Ensembles with Boosting Meta-Learner." In Inventive Communication and Computational Technologies, pp. 699-710. Springer, Singapore, 2021.

[116] TaghiBeyglou, Behrad, Navid Hasanzadeh, Fatemeh Bagheri, and Mehran Jahed. "ADHD diagnosis in children using Common spatial pattern and Nonlinear Analysis of Filter banked EEG." In 2020 28th Iranian Conference on Electrical Engineering (ICEE), pp. 1-5. IEEE, 2020.

[117] Taran, S., and V. Bajaj. "Rhythm-based identification of alcohol EEG signals." IET Science, Measurement & Technology 12, no. 3 (2018): 343–349.

[118] Teplan, M. "Fundamentals of EEG measurement." Measurement Science Review 2 (2002): 2.

[119] Tcheslavski, G. V., and F. F. Gonen. "Alcoholism-related alterations in spectrum, coherence, and phase synchrony of topical electroencephalogram." Computers in Biology and Medicine 42, no. 4 (2012): 394–401.

[120] Toole, J. M., and G. B. Boylan. NEURAL: quantitative features for newborn EEG using Matlab. 2017.

[121] Tor, Hui Tian, Chui Ping Ooi, Nikki SJ Lim-Ashworth, Joel Koh En Wei, V.

Jahmunah, Shu Lih Oh, U. Rajendra Acharya, and Daniel Shuen Sheng Fung. "Automated detection of conduct disorder and attention deficit hyperactivity disorder using decomposition and nonlinear techniques with EEG signals." Computer Methods and Programs in Biomedicine 200 (2021): 105941.

[122] Tosto, Maria Grazia, Sukhleen Kaur Momi, Philip Asherson, and Karim Malki. "A systematic review of attention deficit hyperactivity disorder (ADHD) and mathematical ability: current findings and future implications." BMC medicine 13, no. 1 (2015): 1-14.

[123] Upadhyay, R., P. K. Padhy, and P. K. Kankar. "Alcoholism diagnosis from EEG signals using continuous wavelet transform." In 2014 annual IEEE India Conference (INDICON), pp. 1-5. IEEE, 2014.

[124] Wang, Z. et al. "Spatial-temporal feature fusion neural network for EEG-based emotion recognition." IEEE Trans. Instrum. Meas. 71 (2022): 1–12.

[125] Wang Y, Zhao Y, Nie H, Liu C, Chen J. Disrupted brain network efficiency and decreased functional connectivity in multi-sensory modality regions in male patients with alcohol use disorder. Frontiers in human neuroscience. 2018 Dec 21;12:513.

[126] Waszkiewicz, N. et al. "Neurobiological effects of binge drinking help in its detection and differential diagnosis from alcohol dependence." Dis. Markers 2018 (2018): 1–9.

[127] Yeh PY, Sun CK, Sue YR. Predicting the Risk of Driving Under the Influence of Alcohol Using EEG-Based Machine Learning. Computers in Biology and Medicine. 2025 Jan 1;184:109405.

[128] Yu, X., M. Z. Aziz, M. T. Sadiq, Z. Fan, and G. Xiao. "A new framework for automatic detection of motor and mental imagery EEG signals for robust BCI

systems." IEEE Trans. Instrum. Meas. 70 (2021): 1–12.

[129] Zhang, Xiao Lei, Henri Begleiter, Bernice Porjesz, and Ann Litke. "Event related potentials during object recognition tasks." *Brain research bulletin* 38, no. 6 (1995): 531-538.

[130] Zhang R, Dong X, Zhang L, Lin X, Wang X, Xu Y, Wu C, Jiang F, Wang J. Quantitative Electroencephalography in Term Neonates During the Early Postnatal Period Across Various Sleep States. Nature and Science of Sleep. 2024 Dec 31:1011-25.

[131] Zhang, Huiwen, Jiahui Yao, Cheng Xu, and Chengyu Wang. (2023). Targeting electroencephalography for alcohol dependence: A narrative review. CNS Neuroscience & Therapeutics 29, no. 5: 1205-1212.

[132] van Putten MJ. The revised brain symmetry index. Clinical neurophysiology. 2007 Nov 1;118(11):2362-7.

[133] Vahid, Amirali, Annet Bluschke, Veit Roessner, Sebastian Stober, and Christian Beste. "Deep learning based on event-related EEG differentiates children with ADHD from healthy controls." Journal of clinical medicine 8, no. 7 (2019): 1055.